ERASMUS MUNDUS MSc PROGRAMME

COASTAL AND MARINE ENGINEERING AND MANAGEMENT
CoMEM

HYDRODYNAMIC LOADS ON BUILDINGS CAUSED BY OVERTOPPING WAVES

Delft University of Technology
June 2011

Xuexue CHEN
4055195

The Erasmus Mundus MSc Coastal and Marine Engineering and Management
is an integrated programme organized by five European partner institutions,
coordinated by Delft University of Technology (TU Delft).
The joint study programme of 120 ECTS credits (two years full-time) has been
obtained at three of the five CoMEM partner institutions:

- Norges Teknisk- Naturvitenskapelige Universitet (NTNU) Trondheim, Norway
- Technische Universiteit (TU) Delft, The Netherlands
- City University London, Great Britain
- Universitat Politècnica de Catalunya (UPC), Barcelona, Spain
- University of Southampton, Southampton, Great Britain

The first year consists of the first and second semesters of 30 ECTS each, spent at
NTNU, Trondheim and Delft University of Technology respectively.
The second year allows for specialization in three subjects and during the third semester
courses are taken with a focus on advanced topics in the selected area of specialization:
- Engineering
- Management
- Environment
In the fourth and final semester an MSc project and thesis have to be completed.
The two year CoMEM programme leads to three officially recognized MSc diploma
certificates. These will be issued by the three universities which have been attended by
the student. The transcripts issued with the MSc Diploma Certificate of each university
include grades/marks for each subject. A complete overview of subjects and ECTS
credits is included in the Diploma Supplement, as received from the CoMEM coordinating
university, Delft University of Technology (TU Delft).

Information regarding the CoMEM programme can be obtained from the programme
coordinator and director

Prof. Dr. Ir. Marcel J.F. Stive
Delft University of Technology
Faculty of Civil Engineering and geosciences
P.O. Box 5048
2600 GA Delft
The Netherlands

HYDRODYNAMIC LOADS ON BUILDINGS CAUSED BY OVERTOPPING WAVES

Flume Experiments

Hydrodynamic loads on buildings caused by overtopping waves

Master thesis of

X. CHEN

4055195

Xuexue.cheung@gmail.com

June 2011

The Graduation Committee

Prof.dr.ir. W.S.J. Uijttewaal (Chairman)	Delft University of Technology
Ir. H.J. Verhagen	Delft University of Technology
Dr.ir. S.N. Jonkman	Delft University of Technology /Royal Haskoning
Ir. T. Verwaest	Flanders Hydraulics Research
Dr.ir. W. Hassan	Flanders Hydraulics Research
Dr.ir. T. Suzuki	Flanders Hydraulics Research/Ghent University

TUDelft

flanders HYDRAULICS RESEARCH

This publication must be cited as follows:

Chen, X. (2011) *Hydrodynamic loads on buildings caused by overtopping waves*. Master thesis for Delft University of Technology, Delft, Netherlands; Project number: 770_59 for Flanders Hydraulics Research, Antwerp, Belgium.

Preface

This study is performed in order to obtain the degree of Master of Science at Delft University of Technology. It has been carried out at Flanders Hydraulics Research Laboratory in Antwerp, Belgium.

In this master thesis, a large variety of work was included; from practical work, like calibrating the instruments, to academic work, e.g. by deriving the relationship between the overtopping wave force and incident wave characteristics. It was interesting to see what physically happens when waves overtop on the dike crest and hit the vertical plane.

First of all, I want to thank my graduation committee for their supervision and guidance during my master thesis. For the graduation committee members from TU Delft, I am grateful for the advice from Wim Uijttewaal and Henk Jan Verhagen and, last but not least, Bas Jonkman for his kind advice and encouragement even though he was working in the US during the whole period of my thesis. For the graduation committee members from Flanders Hydraulics Research, in particular I want to thank Wael Hassan and Tomohiro Suzuki for their advice and support; I want to thank Toon Verwaest for his smart words and his ideas. Furthermore I also want to thank the lab personnel for supporting me during my work in the laboratory: William for helping me with my thesis review, Sam for his help with the installation and calibrating the instruments, Tim for encouraging me when I worked in the laboratory.

Lastly, I want to thank my friends: Xiaoyan Pang, Hua Zhong, Xuefei Mei, Mingliang Li, Xu Zhang, Gensheng Zhao and many other friends who offered me accommodation and food when I was on my way from London to Delft, from Delft to Antwerp and back, and their kind encouragement, advice for Matlab and suggestions for my presentation.

Apart from my thesis, I want to thank the CoMEM Program, especially Prof. Marcel Stive, Mariette van Tilburg and Madelon Burgmeijer, without whose encouragement and help, I could not have finished my study in the CoMEM program successfully within these two years. Above all, I want to thank my family for their unconditional support throughout my entire study.

Xuexue Chen

Delft, June 2011

Summary

There is a chance that storm surges occurring in coastal areas cause overtopping over wide crested dikes. The overtopping water results in a hydrodynamic load on the structures built on top of the crest. This is for example the case at the Belgian coast where houses and hotels are constructed on top of the dike crest.

In this study, physical model tests were executed on a schematized model scaled 1/30. The aim was to come up with a relationship describing the force on a vertical plane exerted by the overtopping water as a function of wave parameters and geometrical characteristics. Due to time constraints the number of tests had to be restricted so only a limited number of parameters could be varied. Despite these restrictions, the experiments revealed the most important mechanism of the impact process under the two dike configurations included: the dike side case with dike crest width of 0 m and the inland case with dike crest of width 0.5 m in model scale.

The overtopping wave force could directly be related to the overtopping wave momentum flux, resulting in a simple formulation for the prediction of the wave force. Thus, the overtopping wave force is proportional to the overtopping wave momentum flux, obtained by integrating the maximum water depth in front of the vertical plane for the inland case and the dike side case. The coefficients of these two cases are almost the same, namely around 0.33.

When building the relationship between the overtopping wave force and the incident wave and dike geometrical characteristics, three other approaches were also applied. Firstly, the concept of overtopping wave tongue thickness was introduced into the relationship between the overtopping wave force and incident wave characteristics; secondly, overtopping flow velocity and water layer thickness at the beginning crest of the sea dike were also added into the analysis of overtopping wave force and finally, a new dimensionless overtopping wave force was developed. This dimensionless overtopping wave force is also proportional to the dimensionless freeboard: the least scatter for this parameter gave a rather good potential suitability for force prediction, especially with the conditions of large incident wave height impacts on the relatively low freeboard. The coefficient related to the two dimensionless parameters could also be dimensionless with a form of crest width divided by wave length, however due to the limited configurations, this dimensionless coefficient still needs to be explored further in future study.

The reduction effect for crest width of 0.5 m is about 65%. Due to the fact that only two widths crest were tested in the present study, the relationship between the width and overtopping wave force could not be presented. Therefore, in future study, variation of the width of the crest should be increased, and the effect of the crest width could be further researched.

Contents

List of tables

List of figures

List of symbols

Roman Symbols

a	Constant coefficient	[-]
b	Constant coefficient	[-]
B	Dike crest width	[m]
C_1	Coefficient	[-]
C_2	Coefficient	[-]
C_3	Coefficient	[-]
d	Water depth in wave flume	[m]
$d(t)$	Time series of overtopping wave surface elevation	[m]
$d_1(t)$	The time series of overtopping wave surface elevation tested by wave probe 1 at the beginning of the dike crest	[m]
$d_2(t)$	The time series of overtopping wave surface elevation tested by wave probe 2 in front of the building	[m]
D	Lowest overtopping wave surface elevation	[m]
D_2	Lowest overtopping wave surface elevation tested by wave probe 2 in front of the building	[m]
E	Wave energy	[N/m]
f_p	Cut-off frequency	[Hz]
F	Maximum overtopping wave load	[N/m]
F_{max}	Maximum overtopping wave load	[N/m]
g	Gravity acceleration	[m/s^2]
h	Highest overtopping wave surface elevation	[m]
h_A	Overtopping flow thickness at the seaward slope of dike	[m]
h_0	Overtopping flow thickness at the beginning edge of dike	[m]
h_1	Highest overtopping wave surface elevation at the edge of dike crest tested by wave probe 1	[m]
h_2	Highest overtopping wave surface elevation in front of the building tested by wave probe 2	[m]
h_{in}	Tsunami inundate water depth	[m]
H	Incident wave height near toe	[m]

H_2	Overtopping wave height	[m]
H_m	Average value of incident wave height for regular test	[m]
H_{m0}	Spectral incident wave height for irregular waves	[m]
n	Cotangent of dike slope	[-]
P_1	Pressure value obtained by pressure sensor 1	[mbar]
P_2	Pressure value obtained by pressure sensor 2	[mbar]
P_3	Pressure value obtained by pressure sensor 3	[mbar]
P_4	Pressure value obtained by pressure sensor 4	[mbar]
q	Mean overtopping discharge rate	[m^3/m/s]
q_0	Mean overtopping discharge rate with 0 m width of crest	[m^3/m/s]
q_1	Mean overtopping discharge rate with 15 m width of crest	[m^3/m/s]
R_c	Crest freeboard relative to SWL	[m]
R_u	Wave run-up height (regular waves)	[m]
$R_{u2\%}$	Wave run-up height of the two percent largest incoming waves (irregular waves)	[m]
$R_{ux\%}$	Wave run-up height of the x percent largest incoming waves (irregular waves)	[m]
s	Wave steepness	[-]
S_0	Overtopping wave tongue thickness at the edge of crest	[m]
t_0	Start time of each event	[s]
t_t	End time of each event	[s]
T	Wave periods	[s]
T_p	Peak wave period	[s]
T_m	Average wave period (regular waves)	[s]
$T_{m-1,0}$	Spectral wave period (irregular waves)	[s]
V_A	The overtopping flow velocity on the slope near crest	[m/s]
V_0	The overtopping flow velocity at the beginning of the crest	[m/s]
W	Water weight	[N/m^3]
X_Z	Remaining overtopping run-up length	[m]
X_A	The length of crest edge to the still water line	[m]

| X^* | $X_Z - X_A$ | [m] |

Greek Symbols

α	Dike slope angle	[°]
β	Coefficient	[-]
ρ	Water density	$[kg/m^3]$
ξ	Breaker parameter	[-]
ξ_0	Breaker parameter based on local wave height near toe and wave period in deep water	[-]
ξ_d	Breaker parameter based on local wave height near toe and wave period in deep water	[-]
ξ_{gr}	Limit of breaker type	[-]

Abbreviations

$2D$	Two dimensions
ARC	Active Reflection Compensation
SWL	Still water level
TAW	Water elevation level measurement base line for Belgium
WL	Water level

1 Introduction

1.1 Background

1.1.1 Coastal flooding disasters and storm surge

Natural disasters such as earthquakes, tsunamis, and floods have occurred frequently in the past decades. For example, the catastrophic flooding in Japan caused by a tsunami on 11 March 2011, swept away boats, homes and cars along the north-eastern Japanese coast. In late August 2005, flooding due to hurricane Katrina, the most damaging hurricane in U.S. history, also left more than 204,000 homes in Louisiana uninhabitable, damaged, or destroyed *(FEMA, 2006).* And in 2004, the tsunami wave caused by an earthquake in Indonesia, one of the biggest natural disasters in recent human history, killed at least 290,000 people and affected the livelihood of millions of people in over ten countries. Coastal flooding caused by a storm surge is especially important for low-lying areas.

Storm surges are caused primarily by high winds pushing on the ocean's surface. The wind causes the water to "pile up" higher than the ordinary sea level. Along the coast, a storm surge is often the greatest threat to life and property. Figure 1.1 (a) shows the definition of a storm surge and its threat to buildings. In the past high death tolls were the results from the rise of the ocean associated with many of the major hurricanes that have made landfall *(National Hurricane Centre, 2010)*. A five floor hotel was destroyed in hurricane Katrina in 2005, refer to Figure 1.1 (b).

Existing building codes, design practices and disaster planning methods pay little attention to flood impacts, related to earthquakes and wind loads acting on buildings. For example, ASCE/SEI 7–05 *(ASCE 2005)* introduces many building design methods for engineers for a variety of loading conditions. In this publication there are 60 pages detailing wind loading and more than 100 pages on earthquake loading, while only two pages deal specifically with wave loading *(Wilson, et al, 2009).*
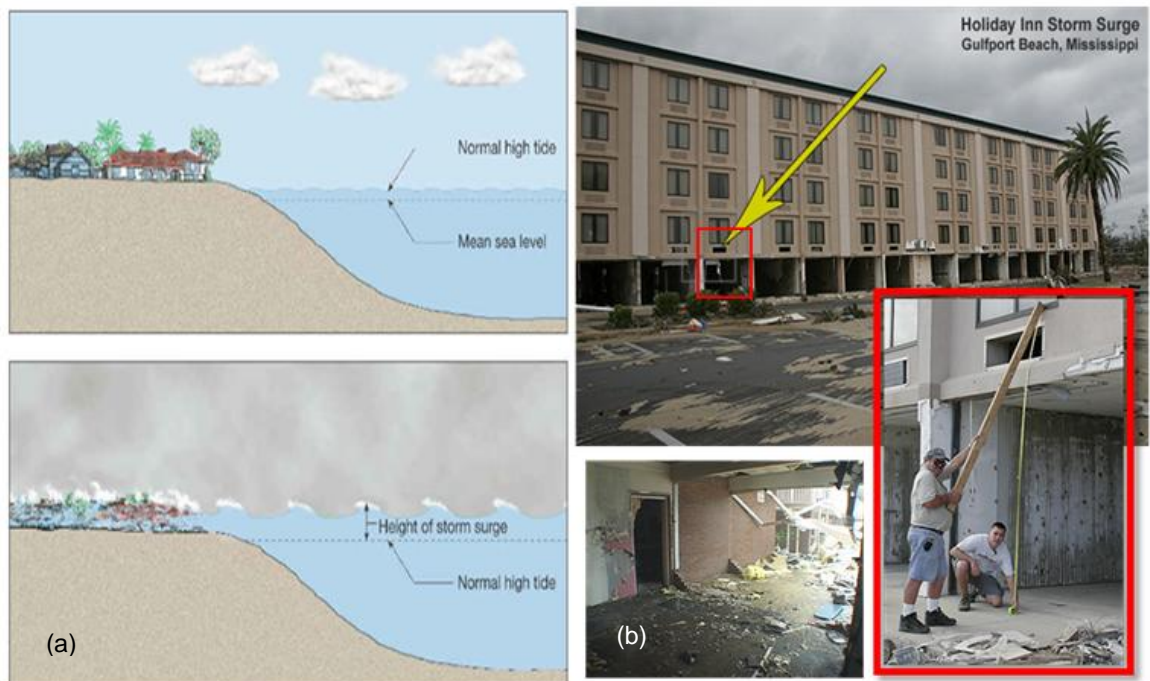
Figure 1.1   (a) Schematic of storm surge and (b) building damage due to Hurricane Katrina

1.1.2 Sea dikes for low-lying area

Different types of coastal structures are built worldwide to protect inland areas from coastal flooding. A sea dike is a common coastal structure found in low-lying land areas. The primary function of sea dikes is to protect low-lying coastal areas from inundation by the sea under extreme wave conditions by a separation of the shoreline from the hinterland with a highly impermeable structure. Figure 1.2 shows a typical dike cross-section and a photo of a typical Dutch sea dike. It is a predominantly earthen structure consisting of a sand core, a watertight outer protection layer, toe protection and a drainage channel. These structures are designed to resist wave action and to prevent or minimize overtopping.
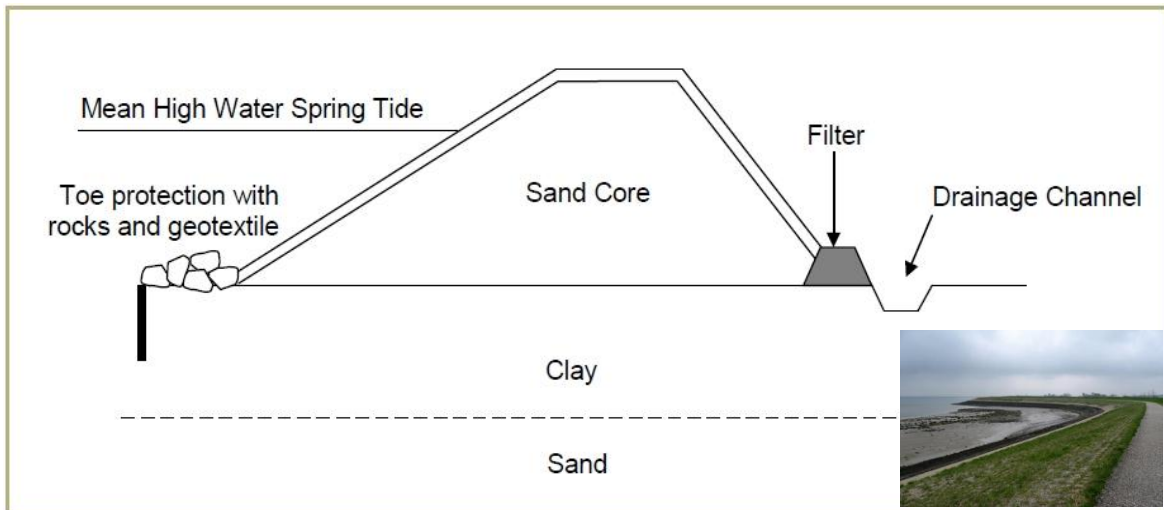
Figure 1.2   (a) Typical sea dike cross section (Linham and Nicholls, 2010) and (b) typical dutch sea dike photo.

Dikes have been utilized as flood defenses in the Netherlands over the past several hundred years. As such, the Dutch have extensive experience in their design, and many countries apply the Dutch design practice in dike construction.

Typically, the Dutch practice employs the following design guidelines, extracted from *Linham and Nicholls (2010)*:

- Sloped seaward face at a gradient of between 1:3 to 1:6 – to reduce wave loadings
- Sloped landward face at a gradient of between 1:2 to 1:3 – to minimize land take and maximizes stability
- Impermeable cover layer – this is usually composed of clay but is sometimes supplemented by asphalt. It serves to protect the sand core.
- Toe protection – used as supplemental armor for the beach and prevents waves from scouring and undercutting the structure.
- Dike core usually composed of sand to ensure that water that does enter can drain away. The core provides support for the cover layer and gives the structure sufficient volume and weight to resist high water pressures.
- Drainage channel – allows any water which does enter the structure to drain away, therefore ensuring the structure is not weakened by water saturation.

1.2 Belgian coastal sea dikes

The Belgian coastal zone is 67 km long. It consists of a low-lying area, with an average width of 15 km and located at an average level of 2 m below the surge level of an annual storm *(Verwaest, 2006)* as shown in Figure 1.3. The natural sea defenses are sandy beaches and dunes. However, hard defense structures, such as dikes and sea-walls, have replaced the dunes almost everywhere in coastal towns and ports, and hence represent approximately two thirds of the Belgian coastal defense.
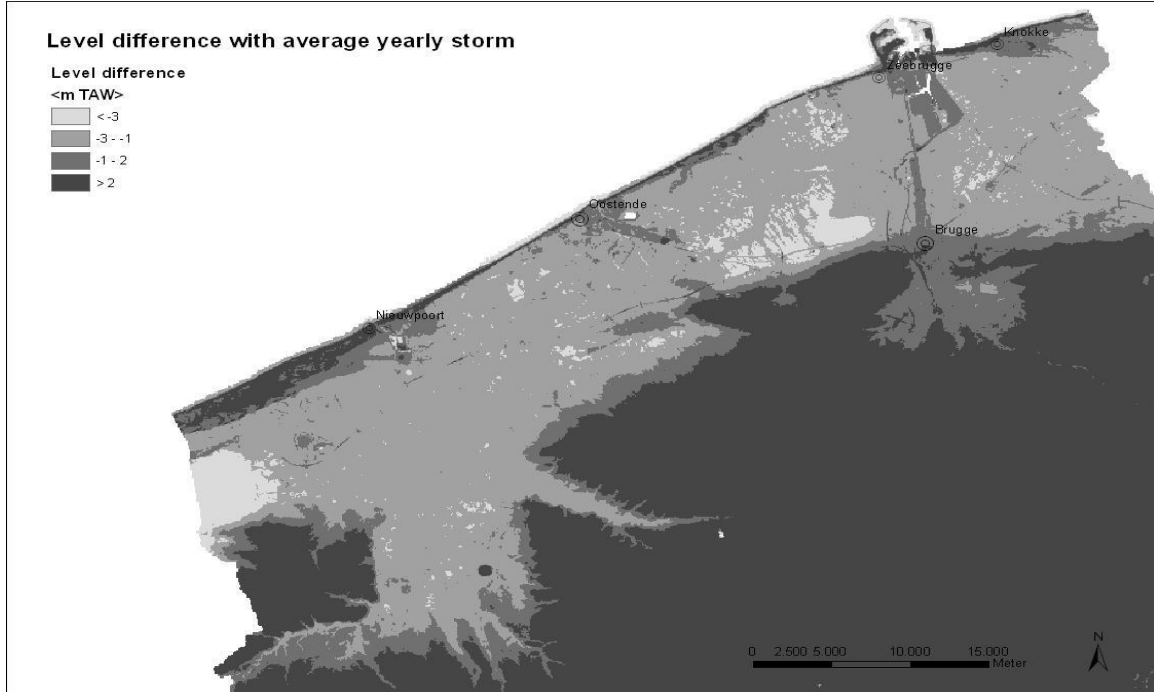
Figure 1.3 Level difference between the coastal land and the surge level of an annual storm (Verwaest, 2006)

Figure 1.4 Coastal town, Oostende, Belgium (GKVP, 2011)

In the Netherlands buildings are not commonly constructed close to sea dikes. However, in the Belgian region, coastal defenses typically exhibit a crest up to several tens of meters wide in front of apartment buildings. The Belgian coastal sea dike has a wide crest which is often built on former dune belts. Today the function of these dikes is not only used as coastal protection but also as a recreational promenade of high importance for tourism (*Verwaest and Vanpoucke, et al, 2010*). This situation generates a densely populated low-lying coastal zone in Belgium which is under a relatively high risk of coastal flooding. Also, many buildings have been built very close to the existing dikes and are at high risk from coastal flooding, as depicted in Figure 1.4.

Figure 1.5   Picture of a typical Flemish coastal dike during moderate storm conditions with a little bit of overtopping occurring (Verwaest, et al, 2010).

1.3 Research objectives and methodology

In the winter storm season, there is a risk that storm surges occurring in the Belgian coastal area may cause overtopping of the dikes (refer to Figure 1.5). The overtopping wave may threaten buildings and even lead to damage and casualties in extreme cases. The research related to overtopping waves on a wide crested Belgian dike and the wave impact loading on buildings and structures on the dike is limited.

Therefore, the primary objective of this study is to investigate the relationship between the overtopping wave characteristics and its hydrodynamic loading on buildings set back from the edge of the sea dike, using a 1:30 scale physical hydraulic model. In order to study the loading caused by overtopping waves, the following processes relevant to wave run-up and wave overtopping flow on the dike crest will be addressed:

- Wave parameters at the toe of the sea dike,
- Wave transformation on the seaward slope up to the breaking point,
- Wave run-up and wave run-down on the seaward slope,
- Wave overtopping on the dike crest,
- Wave overtopping loadings on the building.

These processes are described in more detail in the following chapters. Figure 1.6 gives an overview of the objectives and the methodology of the present study, following a similar outline given in *(Schüttrumpf and Oumeraci, 2005).*
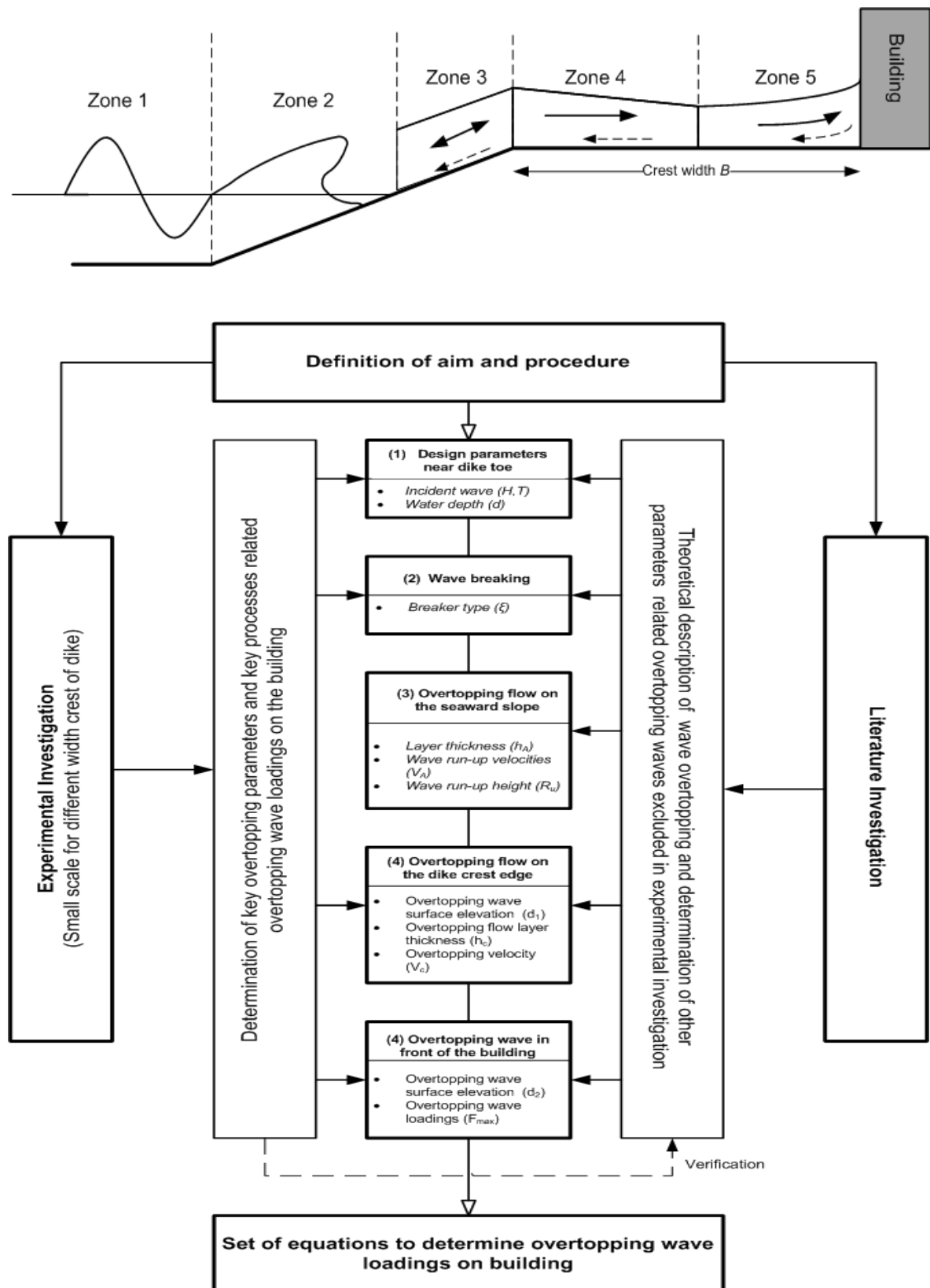
Figure 1.6   Research objective and methodology (adapted from Schüttrumpf and Oumeraci, 2005).

1.4 Report outline

The current report contains the following chapters:

Chapter 2 is a literature study in which the existing methods and processes related to overtopping waves are presented. In Chapter 3, the physical model set-up is described including a detailed presentation of the scale model used in this study. In Chapter 4, the data processing methods are discussed. Presentation and analysis of the results can be found in Chapter 5. In Chapter 6, a discussion based on the findings of Chapter 5 is given. Finally, the report closes with Chapter 7 where the main conclusions and recommendations are presented.

2 Literature Study

2.1 Introduction

The following sections provide a review of the existing literature into wave overtopping of dikes investigations. The physical dimensions and hydraulic parameters are defined in section 2.2. In section 2.3, a selection of recent research relating to overtopping behavior on the crest is presented. Finally, in section 2.4, Tsunami wave force on the dike crest or inland induced force on buildings and the behaviors of overtopping waves are explored.

2.2 Physical dimensions and hydraulic parameters
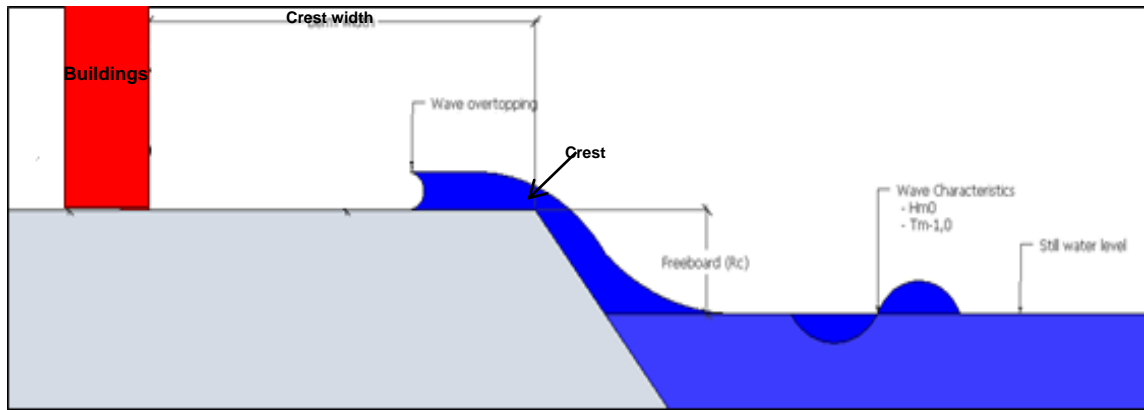
Figure 2.1   Schematic of a typical sea dike for the Belgian coast

2.2.1   Physical dimensions

The following sections discuss and define the physical dimensions of a sea dike. A schematic of a typical sea dike for the Belgian coast is given in Figure 2.1. The key geometric parameters for the dike are explained as follows.

- **Crest freeboard (R_c)**

The crest freeboard (R_c) is defined as the height of the dike crest to the still water level (SWL)

- **Crest width (B)**

For this study, the crest width (B) is defined as the width for the crest of the dike to the edge of buildings, sea-wall or other forms of structure.

- **Roughness**

Roughness can decrease wave run-up and consequently overtopping as it can dissipate wave energy. Roughness is created by irregular shaped block revetments, artificial ribs or blocks on a smooth slope. In common overtopping design formulae, it is characterized by the roughness reduction factor. *(Lioutas, 2010)*

2.2.2   Hydraulic parameters

The following sections describe hydraulic parameters that characterize wave overtopping. Most of these definitions are referred from EurOTop Manual *(EurOTop, 2007).*

- **Wave height (H_{m0}, H)**

For irregular wave condition, the wave height used in the wave run-up and overtopping formulae is the incident significant wave height H_{m0} at the toe of the structure, called the spectral wave height. Another definition of significant wave height is the average of the highest third of the waves, $H_{1/3}$.

For regular wave (in this study), *H* is used to describe the incident wave height of each waves.

- **Wave period (*T_p*, *T_m*, *T*)**

For irregular wave condition, various wave periods can be defined for a wave spectrum or wave record. Conventional wave periods are the peak period T_p (the period that gives the peak of the spectrum), the average period T_m (calculated from the spectrum or from the wave record) and the significant period $T_{1/3}$ (the average of the highest 1/3 of the waves). The relationship T_p/T_m usually lies between 1.1 and 1.25, and T_p and $T_{1/3}$ are almost identical.

The wave period used for some overtopping formulae is the spectral period $T_{m-1.0}$. This period gives more weight to the longer periods in the spectrum than an average period and, independent of the type of spectrum, gives similar wave run-up or overtopping for the same values of $T_{m-1,0}$ and the same wave heights. In this way, wave run-up and overtopping can be easily determined for double-peaked and 'flattened' spectra, without the need for other difficult procedures. Vertical and steep seawalls often use the $T_{m-1,0}$ or T_m wave period. For regular wave condition, *T* is used to describe the incident wave period.

- **Wave steepness (*s*)**

Wave steepness (*s*) is defined as the ratio of wave height to wave length. Wave length depends on the used wave period, different wave lengths can be calculated resulting in different wave steepness. This number can give some information about the wave's generation and characteristics. Generally a steepness of 0.01 indicates a typical swell wave and a steepness of 0.04 to 0.06 a typical wind wave. Swells will often be associated with long period waves where it is the period that becomes the main parameter that affects the overtopping.

Wind sea conditions can also lead to low steepness waves if the wave breaks on a gentle foreshore. When wave breaking occurs, the period does not change significantly *(EurOTop, 2007)*, but the wave height decreases resulting in lower steepness. Generally, low wave steepness in deep water means swells while for depth limited conditions it often means broken waves on a gentle foreshore *(Lioutas, 2010)*.

- **Breaker parameter (ξ)**

The beaker parameter (ξ) is also known as surf similarity parameter or Iribarren number. Originally it was introduced as an indicator for whether a wave would break on a plane slope. Apart from whether or not breaking will occur, it also describes the way a wave will break. It is widely used for the modeling of many phenomena related to waves in shallow waters such as wave breaking, run-up and overtopping. The breaker parameter is basically a ratio of the bed slope (α) or wave steepness (*s*).

$$\xi = \frac{\tan(\alpha)}{\sqrt{s}} = \frac{\tan(\alpha)}{\sqrt{\dfrac{H}{L}}} \qquad\qquad \textbf{2.1}$$

Depending again on the used wave period (T_p , T_m or $T_{m-1,0}$) and thus steepness (s_{op} , s_{om} or $s_{m-1,0}$), different breaker parameters can be calculated (ξ_{op} , ξ_{om} and $\xi_{m-1,0}$). The main types of breaking are surging, collapsing, plunging and spilling. Figure 2.2 shows those different types of breaking for characteristic values of $\xi_{m-1,0}$. The classification of breaker type in Figure 2.2 is robust, and *Schüttrumpf (2001)* gives a breaker type limits table of ξ_0 (based on local incident wave height and period in deep water) in which the classification is according to differernt dike slope (Figure 2.3). Note ξ_d in Figure 2.3 has the same meaning with ξ_0 .
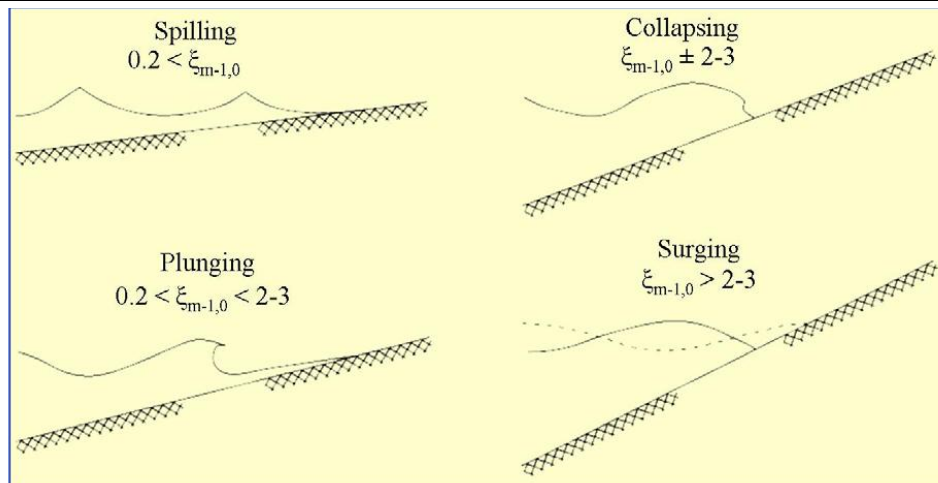
Figure 2.2   Different types of breaker parameter

Deichneigung 1:n =	Sturzbrecher	Collapsing-Brecher	Reflexionsbrecher
1:6	$\xi_d < 2{,}1$	$2{,}1 < \xi_d < 2{,}8$	$\xi_d > 2{,}8$
1:4	$\xi_d < 2{,}4$	$2{,}4 < \xi_d < 3{,}1$	$\xi_d > 3{,}1$
1:3	$\xi_d < 2{,}6$	$2{,}6 < \xi_d < 3{,}3$	$\xi_d > 3{,}3$
gemittelt	$\xi_d < 2{,}3$	$2{,}3 < \xi_d < 3{,}0$	$\xi_d > 3{,}0$

Figure 2.3   Limits of breaker type (Schüttrumpf, 2001)
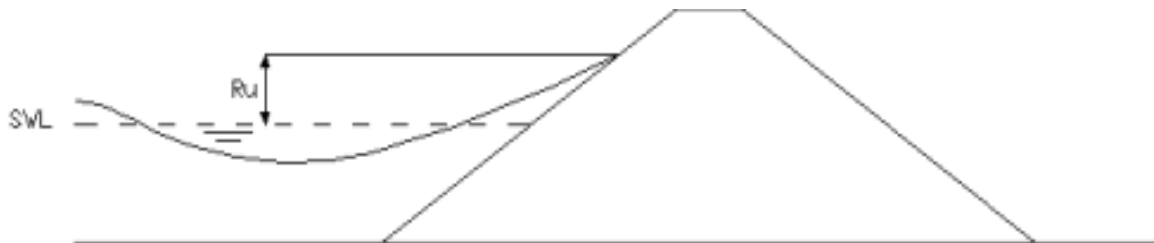
Figure 2.4   Sketch definition of wave run-up height

- **Wave run-up height (R_u)**

The run-up height R_u is defined as the vertical distance between maximum wave run-up on an infinite, smooth and impermeable slope and still water level (SWL), see Figure 2.4.

Granthem (1953), *Saville (1955, 1956, 1958)* and *Savage (1958)* contributed to the earlier investigation of wave run-up. These researchers measured wave run-up caused by regular wave trains impinging on various types of smooth and rough sloping structures, composite slope structures and other variations (stepped, recurred, etc.) (*Hughes, 2004*).

Early practical formulas for regular wave run-up on smooth and rough plane slopes and composite slopes were presented by *Hunt (1959)*. Hunt recognized that different formulas would be needed to differentiate run-up caused by non-breaking waves that surge up steeper slopes from run-up caused by waves that break on milder slopes as plunging or spilling breakers (*Hughes, 2004*). *Schüttrumpf (2001)* gives a hyperbolic function for regular wave (Equation 2.2) to have a smoother transition between the different breaker types.

$$\frac{R_u}{H} = 2.25 \tanh(0.5\xi_0)$$

2.2

For irregular waves, the wave run-up height is given by $R_{u2\%}$. This is the wave run-up level, measured

vertically from the still water line, which is exceeded by 2% of the number of incident waves. The number of waves exceeding this level is hereby related to the number of incoming waves and not to the number that run-up. For the wave-up is not the research objective, therefore, here is just given a general formula for irregular wave run-up by EurOTop Manual (Equation 2.3). Details about the wave run-up theory can refer to other researcher's findings such as *Hughes (2004)*.

$$R_{u2\%} = H_{m0}(4 - \frac{1.5}{\sqrt{\xi_0}})$$ **2.3**

2.3   Overtopping and overtopping wave bore

2.3.1   Overview

Wave overtopping occurs when the barrier (such as sea dike, breakwater, or other format structures) crest height is lower than the potential run-up level; waves running up the face of a barrier reach and pass over the barrier crest.

There are three physical forms of overtopping *(FEMA, 2005):*

- Green water overtopping occurs when waves break onto or over the barrier and the overtopping volume is relatively continuous.

- Splash overtopping occurs when wave break seaward of the face of the structure, or where the barrier is high in relation to the wave height, and overtopping is a stream of droplets. Splash overtopping can be carried over the barrier under its own momentum or may be driven by on-shore wind.

- Spray overtopping is generated by the action of wind on the wave crests immediately offshore of the barrier. Without the influence of a strong onshore wind, this spray does not contribute to significant overtopping volume.

The first type is the key objective of this study, so the literature investigation will be focused on green water overtopping type. According to the objective of this study, little information is available on the dynamic loadings of wave after overtopping; therefore, literature survey presented here is focused primarily on behavior of post-overtopping wave, as represented by generation of overtopping bore, its height and its bore front velocity.

2.3.2   Bore propagation

Cox & Machemehl (1986) firstly interpreted the character of the bore of water propagating from a green water overtopping wave. The preceding analysis was an extremely simplified approach to analyzing the overland propagation of a bore. Figure 2.5 shows a sketch of overtopping wave bore propagation, where h_0 is the initial bore height, which is also named as overtopping wave layer thickness in other literature. For simplification, h_0 is named as overtopping wave layer thickness in this study.

Schüttrumpf (2005) descript that at the transition line from the seaward slope to the dike crest the wave run-up divides into two flow fields. The water passing this line flows over the crest of the dike (overtopping wave bore is generated) and results in wave overtopping. The remaining water in the wave run-up tongue flows on the seaward slope and runs back as wave run-down. During the model tests, it was visually observed that some water flows back from the dike crest to the seaward slope. Wave run-down is disregarded in his analysis of the layer thicknesses and overtopping velocities on the dike crest. In his study, he proposed a mathematical form of the formula for the layer thickness (h_0) and layer speed (V_0) for narrow-crested dikes, see Equation 2.4 and Equation 2.5:

$$h_0 = a \cdot (R_u - R_c)$$ **2.4**

$$v_0 = b \cdot \sqrt{g} \cdot \sqrt{(R_u - R_c)}$$ **2.5**

in which *a* and *b* are constants which can be determined by calibration in experiment according to different exceedance probability for R_u.
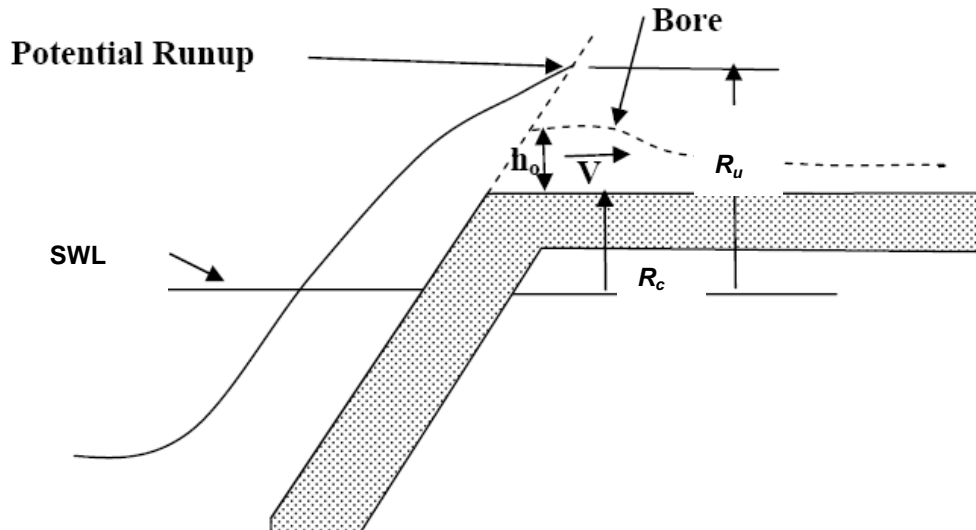
Figure 2.5   Bore propagation of overtopping wave (FEMA, 2005)

For exploring the overtopping wave layer thickness and velocity at the beginning of crest, *Schüttrumpf (2001)* derived his formula by different breaker types, one is plunging breaker, and the other is surging breaker. Figure 2.6 shows the definition sketches of two type breakers, where ξ_d is the breaker number in deep water (using local wave height near toe) and ξ_{gr} is the limit of breaker type, see Figure 2.3. Note that the reason of applying different breaker type to estimate layer thickness is that *Schüttrumpf (2001)* applied the wave run-up estimated method of *Hunt (1959)* which depends on the breaker type to determine his mathematical formula then using experimental tests to verify his derivation. Here list his main findings for regular wave condition, see Equation 2.6 and Equation 2.7, as for x_z, which is the remaining overtopping run-up length and can be determined by the formula in Figure 2.6, where c1 equals 1 for regular waves, x_A is the horizontal length between the crest edge and the interface point of slope and still water level.

$$h_0 = 0.071(x_Z - x_A) \cdot \cos\alpha \qquad \qquad \textbf{2.6}$$

$$\frac{V_0}{\left(\dfrac{\pi H}{T}\right)} = 0.75 \cdot n \cdot \xi_d \sqrt{\frac{R_u - R_c}{H}} \qquad \qquad \textbf{2.7}$$

(a)Plunging breaker ($\xi_d < \xi_{gr}$)   (b)Surging breaker ($\xi_d \geq \xi_{gr}$)
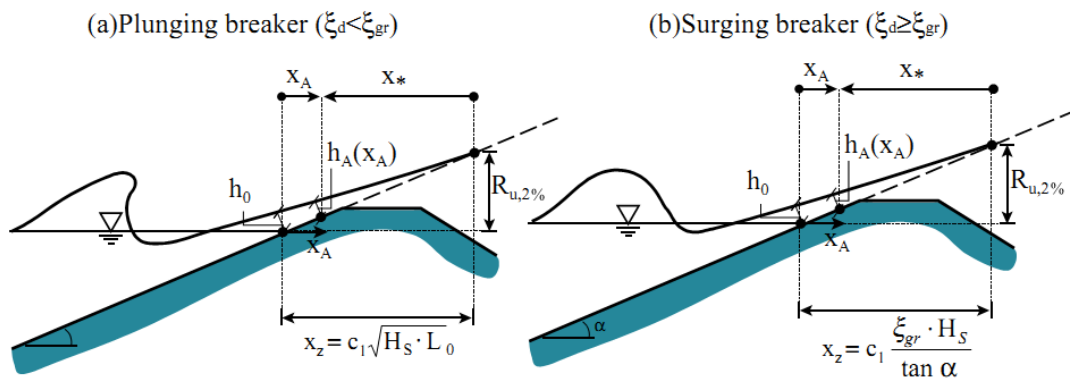
Figure 2.6   Layer thickness on the seaward slope for plunging and surging breakers (definition sketch) (Schüttrumpf & Oumeraci, 2005).

Lowe (2006) used a numerical ANEMONE model which was developed to compute wave overtopping in the highly energetic and nonlinear regime at and near to the shoreline to simulate height and velocity

of the overtopping bore. The result showed that bore height was decaying quickly over the first 6 m, but then much more slowly, the velocity had little change over relatively flat hinterlands, although more complex methods may be needed to calculate down-slope velocities for the rear face of embankment seawalls.

2.3.3 Wave overtopping discharge rate (*q*)

Wave overtopping is the mean discharge per linear meter of width, q, for example in m^3/s/m or in l/s/m.

Due to the complexity of overtopping processes and the wide variety of structures over which overtopping can occur, wave overtopping is highly empirical and generally based on laboratory experimental results and on relatively few field investigations *(FEMA, 2005).*

There are many methods that can describe overtopping discharge rates and for details we refer to the EuroTOp manual for the calculation of overtopping discharges in m^3/s/m unless otherwise stated. It is, however, often more convenient to multiply by 1000 and quote the discharge in l/s/m.

Schüttrumpf (2001) gives an estimation method to determine the maximum overtopping discharge rate on the crest, using the overtopping wave layer thickness Equation 2.6) and its velocity (Equation 2.7), see Equation 2.8.

$$q_{max} = h_0 V_0 \qquad\qquad \textbf{2.8}$$

Verwaest and Vanpoucke, et al, (2010) give an experimental exploration for overtopping discharge on the wide crest dike for a Belgian coastal town in a 1/30 scale model, which can be seen as the preceding research for this study. In their study, the mathematical formulas are based on Equation 2.4 and Equation 2.5 by *Schüttrumpf (2001)*, which they applied to a series of experiments to calibrate the coefficients **a** and **b** in these two equations. **q₀** in Figure 2.7 means the overtopping discharge with 0 m width of crest while **q** is the discharge measured on 15 m crest width crest (prototype scale). Figure 2.7 shows that the wide crest in Flemish coastal towns can reduce small overtopping events to zero or almost zero, but on the other hand very large overtopping discharges are only reduced in a relatively limited way by the wide crest. It is obvious that both the width of the crest and the seaward slope of the crest have an important effect on the reduction of the overtopping.
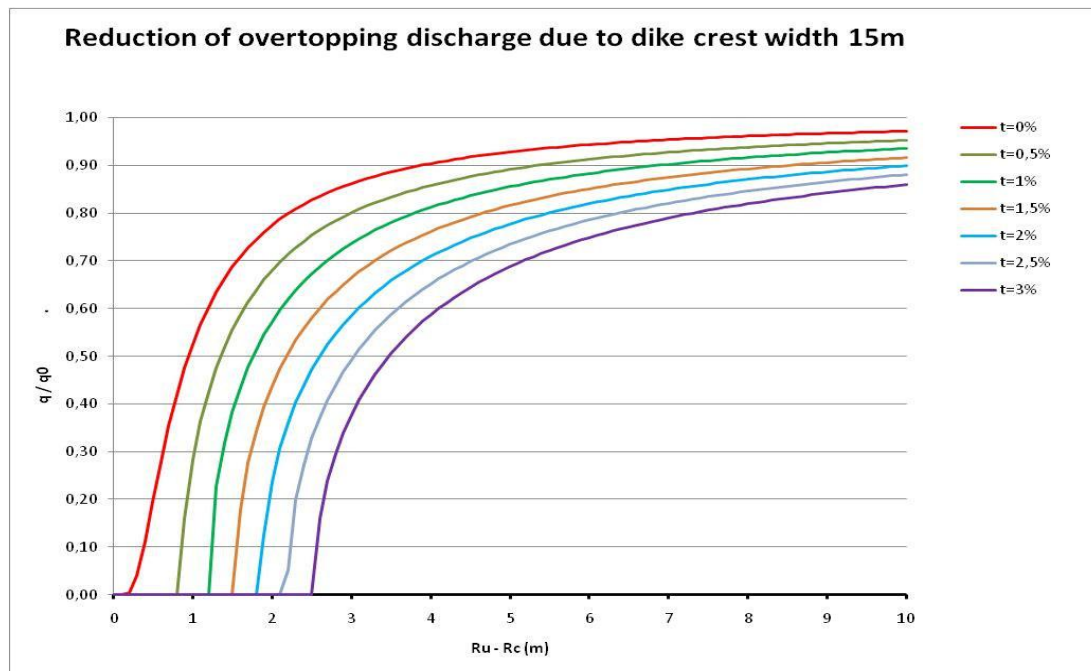
Figure 2.7   Reduction of overtopping discharge due to dike crest width with 15 m *(Verwaest and Vanpoucke, et al, 2010)*

2.4 Overtopping wave loadings and Tsunami wave

As a wave overtops a berm it could be considered a breaking wave propagating across the dike. In general, wave breaking occurs as the result of kinematic instability as the fluid velocity at the crest exceeds the wave speed. On flat slopes the usual mode of wave breaking is by spilling. In spilling, the breaker's turbulence is primarily contained between the crest-trough region, which at least qualitatively resembles the processes of a bore *(Cox & Machemehl, 1986).*

There may be some common characters to a wave bore in an overtopping flow and the tsunami wave bore. Compared with the little information related to overtopping wave loading on buildings, there are a lot of studies done for Tsunami waves (refer to Figure 2.8). Therefore, within this section, the first part concerns the literature study on Tsunami-induced forces which give a better understanding of the behaviour of overtopping wave on the wide crest; in the second part limited research work about overtopping wave loadings is introduced.
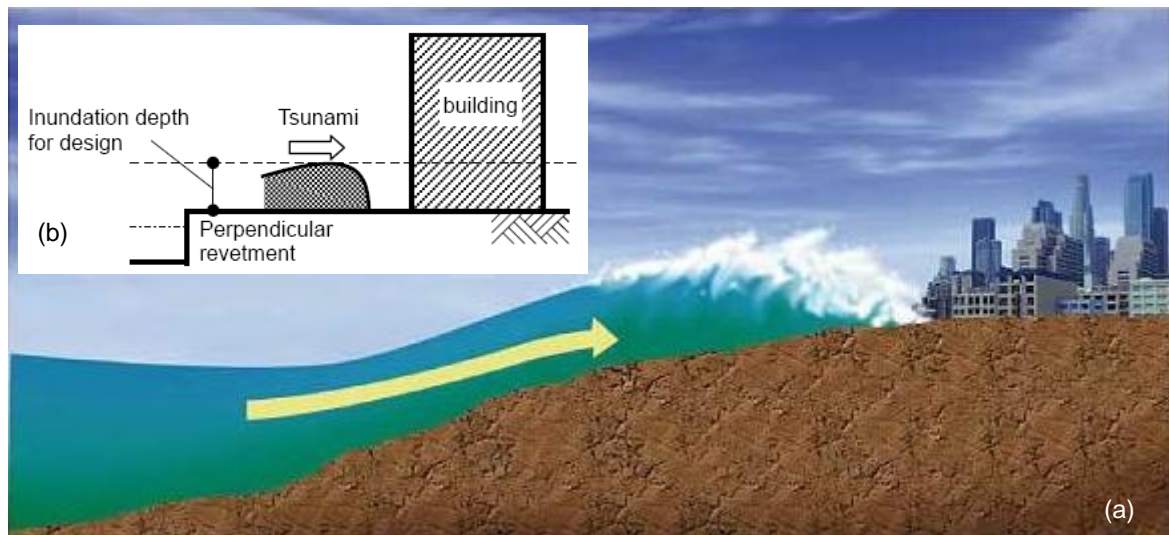
Figure 2.8   Configuration of Tsunami wave approaching inland

2.4.1   Tsunami wave inland-induced forces on structures

A broken tsunami wave running inland generates forces which would impact structures in his path. *Nistor and Palermo (2009)* listed three essential parameters for defining the magnitude and application of Tsunami-induced forces: (1) inundation depth, (2) flow velocity, and (3) flow direction. These three parameters mainly depend on: (a) tsunami wave height and wave period; (b) coast topography; and (c) roughness of the costal inland. Figure 2.8 (b) shows a configuration of the tsunami load on building.

The tsunami wave load on the building is assumed 9 times the hydrostatic force for non-breaking wave where the hydrostatic force is determined by the inundate water depth, see Equation 2.9, where h is the inundate water depth *(USACE, 1990)*.

$$F = 9 \cdot \frac{1}{2} \rho g h^2 = 4.5 \rho g h^2$$

2.9

2.4.2   Overtopping wave loadings

Andreas (2010) and *Den Heijer (1998)* did similar studies under irregular wave conditions to explore the relationship between the overtopping wave force and incident wave parameters but with different test configurations, conditions and criteria. For example, Den Heijer's configuration was similar to the inland case in the present study but with negative freeboard in front of the wall (Figure 2.9), while Andreas did his experimental test using the same facility in Flanders Hydraulic Laboratory (see Section 3.2) and the similar configuration like the dike side case with 0 m crest width, but with a foreshore part

in front of the dike. Figure 2.10 shows the results compared between *Andreas (2010)* and *Den Heijer (1998)*. From their test results, it can be concluded that the overtopping wave force on the building depends on the incident wave height and water depth in front of the dike and that higher incident wave height will give higher wave loads, while for the same wave height, deeper water depth will decrease the overtopping wave impact on the wall.
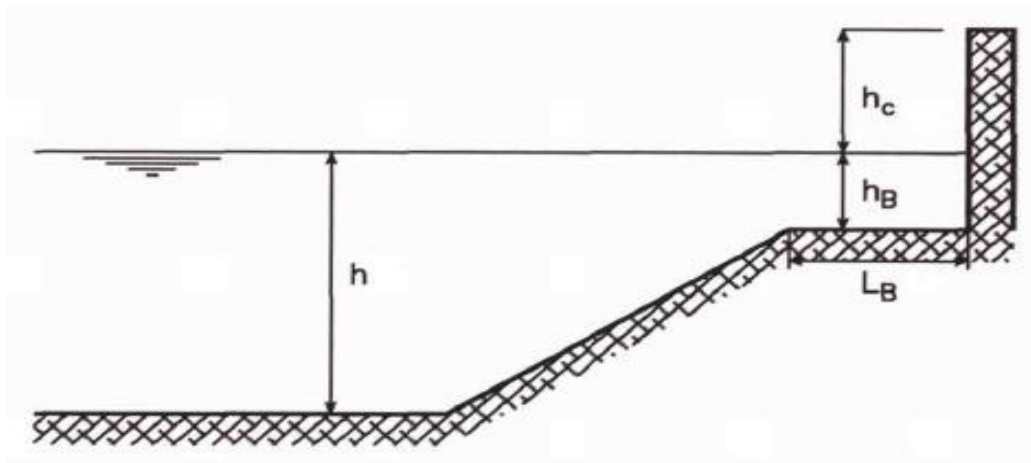
Figure 2.9   Configuration of test Den Heijer (1998).
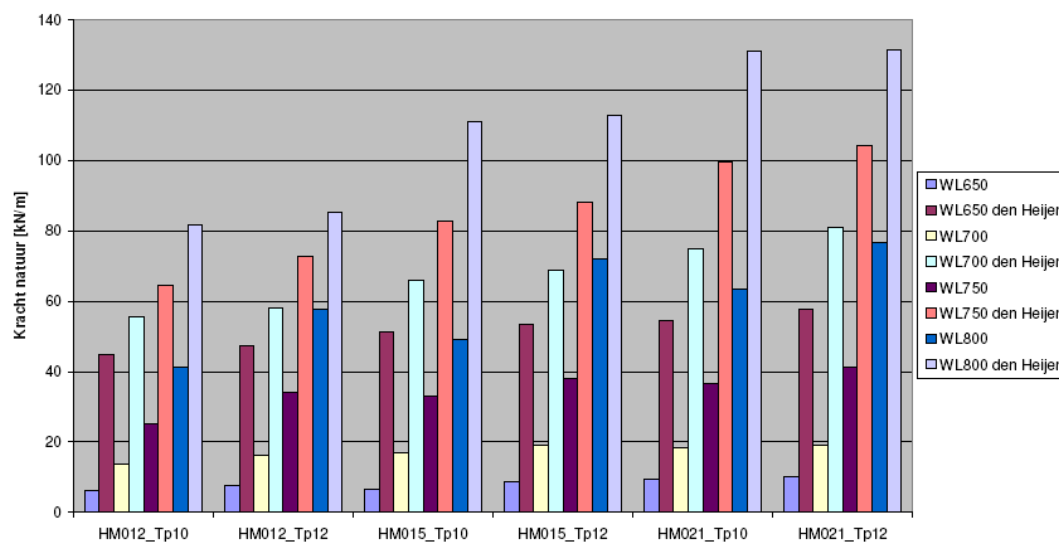
Figure 2.10   Compared the results with *Den Heijer (1998) and Andreas (2010)* (*Andreas, 2010*).

3 Physical model set up

3.1 Introduction

In this chapter, the physical hydraulic model set up is described. Firstly, the test facility is introduced in Section 3.2. Section 3.3 discusses the physical model, and in Section 3.4, the test program is elaborated. Finally, Section 3.5 introduces the laboratory equipment and test instruments.

3.2 Test facility

The tests were performed in the 2-D small wave flume in the Flanders Hydraulics Research laboratory. Figure 3.1 shows the wave flume. The wave flume has dimensions of 26.8 m long, 0.7 m wide and 0.86 m deep. The facility is equipped with a piston type wave generator with a stroke length of 0.3 m, which can generate regular monochromatic and irregular random waves such as JONSWAP and Pierson-Moskowitz spectrum. Figure 3.2 shows the wave generator and a water pump equipped with the flume. An on-line computer is used for wave generation, data acquisition and data processing.

It is noted that the wave paddle in the flume (refer to Figure 3.2) is not equipped with an Active Reflection Compensation (ARC) system. This might influence the results, so the selected data window is used for data analysis. The detail of the data window is discussed further in Chapter 4.
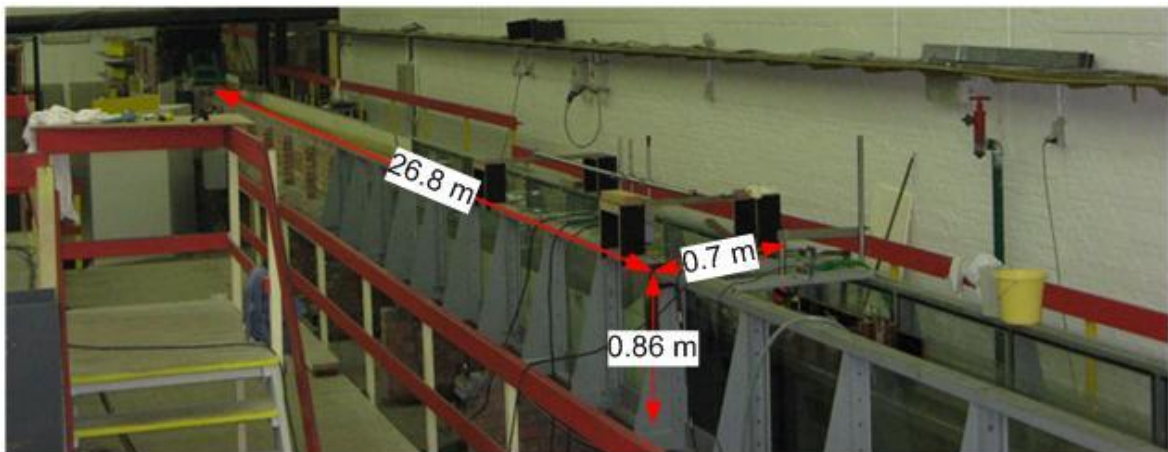
Figure 3.1   2D wave flume in Flanders Hydraulics Research.

Figure 3.2   (a) Wave generator and (b) pump.

3.3 Physical model

The first requirement for the design of the scaled model is to represent a typical coastal defense in Belgium coastal towns.

In this study, the scaled model is simplified to clarify the basic hydraulic characteristics. The simplified model consists of two parts. One is a simplified wide crested coastal sea dike, and the other is a simplified apartment building. Several aspects have been excluded in the model, such as the beach profile, sea walls, and the slope of the crest and the bed roughness of the crest. Regarding the hydraulic conditions, the influence of the wind and the existence of oblique waves are excluded in the physical model.

The scale is decided based on various similarity requirements. The most important scaling criterions are the Froude criterion, the Reynolds criterion and the Strouhal criterion. In the scaled model, geometry, kinematics and dynamics of prototype model have to be scaled down properly. The physical model of this study uses Froude's similarity law. The similarity criterions result in the final dimensions of the scale model (refer Table 3.1). In this study, the scale is decided as 1/30. The final scale factor applied to the model was selected by considering the limitations of equipment and topography.

The test parameters have been decided based on *Andreas (2010)* as shown in Table 3.1. The apartment building height is set as 6 m (only the first two floors of the whole building are considered) in which there is no wave overtopping.

Verwaest (2010) gives the hydraulic boundary conditions for the Belgian coastal towns during extreme storms (with a return period in the range 100 to 10000 years) as shown in Table 3.1.

Table 3.1 Final dimensions in scale model

Configuration dimensions and Hydraulic parameters	Range for Belgain Coastal Town	Adopted Value for this study	Range in 1:30 Scale
Elevation of dike crest (+TAW)		8.75 m	0.625 m
Still water level (+TAW)	6.5~8 m	6.5~8 m	0.55~0.6 m
Freeboard (R_c)	0.5 to 3.0 m	0.75~2.25 m	0.025~0.075 m
Crest Width	10~30 m	15m	0.5 m
Dike slope		1:2.35	1:2.35
Wave height near toe (H_{m0})	0.5~3 m	0.9~3 (m)	0.03~0.1 (m)
Wave Period ($T_{m-1,0}$)	7~10 s	7.6~8.8s (Irregular) 8.3~9.6s (Regular)	1.4~1.6 s (Irregular) 1.54~1.8s (Regular)

3.4 Test Program

3.4.1 Test parameters

Two dike configurations (refer to Table 3.2 and Figure 3.5) were tested with regular and irregular waves. In the each case, water level, free board, wave height and wave period were varied as shown in Table 3.3. The details of the experimental matrix are provided in Appendix 1.
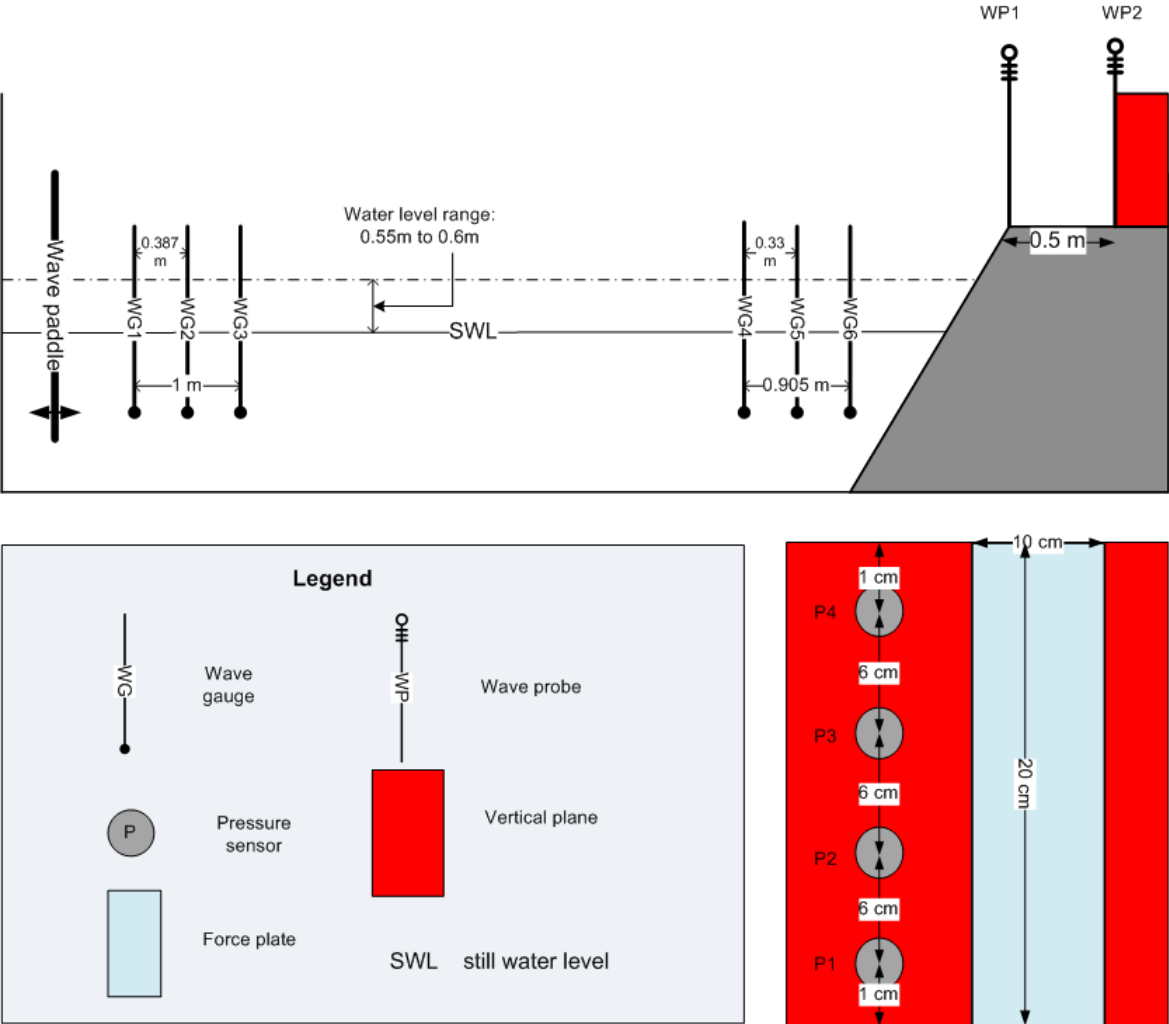
Figure 3.3   Physical model set-up.
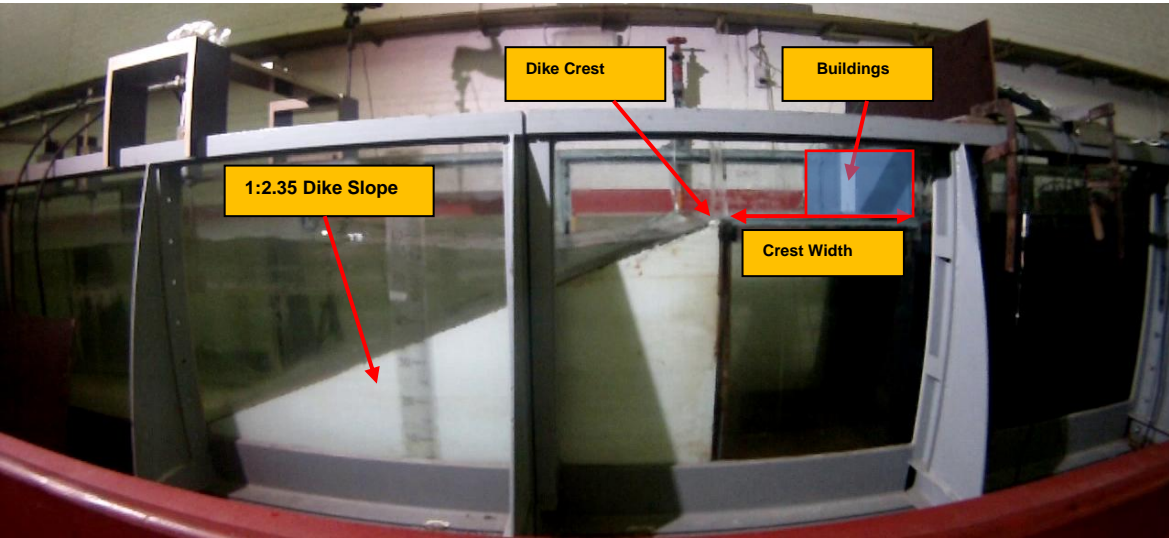
Figure 3.4   Overview of model.

Table 3.2 Two dike configuration

Dike configuration	Seaward slope	Crest level (m)	Crest width (m)
Inland case	1:2.35	0.625	0.5
Dike Side case	1:2.35	0.625	0

Table 3.3 Range of parameters

Wave conditions	Configuration Type	Water level WL (m)	Freeboard Rc (m)	Wave height* H (m)	Wave period T* (s)
Regular wave	Inland	0.567~0.6	0.025~0.058	0.04~0.1	1.2,1.54s,1.8s
	Dike Side	0.55~0.6	0.025~0.075	0.035~0.8	1.54s,1.8s
Irregular wave	Inland	0.567~0.6	0.025~0.058	0.035~0.045	1.4s,1.6s
	Dike Side	0.55~0.6	0.025~0.075	0.035~0.045	1.4s,1.6s

Note*: wave height for irregular test is using H_{m0}, wave periods is using $T_{m-1,0,}$ while for regular test, input value of H equals H_{m0}, and wave periods T equals T_p. All the parameters in Table 3.3 are the values input to the computer.
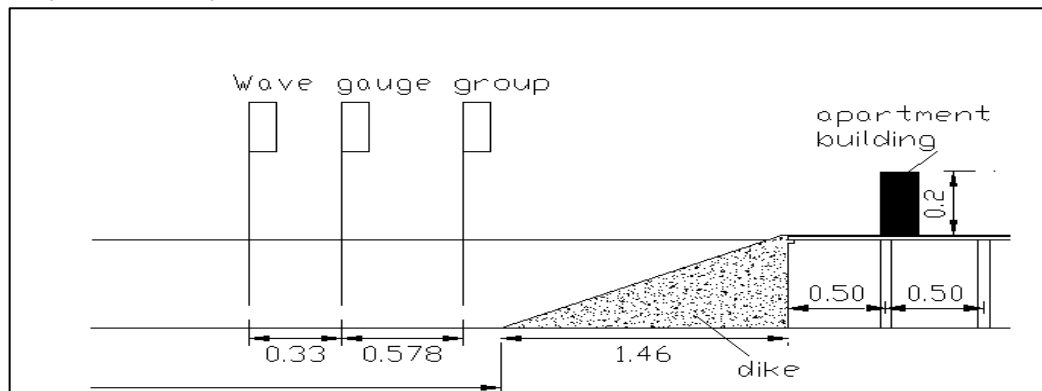
(a)　　Inland case with crest width B=0.5 m
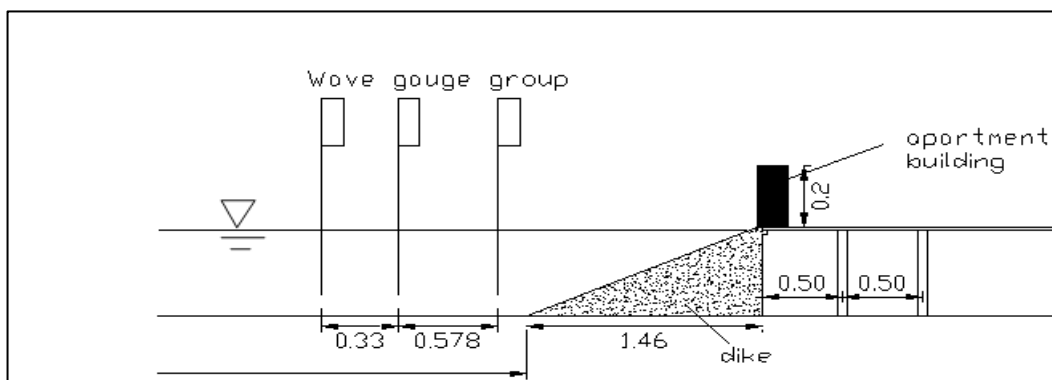
(b)　　Dike side case with crest width B=0 m

Figure 3.5　Tested two dike configurations

3.4.2 Test code

In order to identify the test cases, test codes were used as shown in.Table 3.4.

Table 3.4 Smaple of test code

Case name	Wave type	Water level WL (m)	crest width B (m)	H (m)	T(s)	Test number
RB50_WL06_H08_T180_1	Regular	0.6	0.5	0.08	1.8	1
RB50_WL06_H08_T180_2	Regular	0.6	0.5	0.08	1.8	2
IRB00_WL055_H035_T140	Irregular	0.55	0	0.035 (H_{mo})	1.4 $(T_{m-1,0})$	

3.4.3 Measurement

For each run, water surface elevation, overtopping wave surface elevations in front of the dike crest and building, wave force and pressures on the wall have been measured, Table 3.5. The measurement instruments will be introduced in Section 3.6.

Table 3.5 Measurement paramters

Measurement Parameters	Measurement Instruments
Water surface elevation	Wave gauges 1-6
Overtopping wave surface elevation at crest edge (for Inland case)	Wave probe 1
Overtopping wave surface elevation in front of the building (or wall)	Wave probe 2
Wave force	1 Load cell
Wave pressure	4 Pressure transducers

3.4.3.1 Test duration

In this study, regular wave conditions were preliminarily tested and irregular waves were also investigated. The test durations are different for regular wave and irregular wave conditions. For regular wave conditions, only 10 to 20 waves (depending on the wave period) are chosen for the analysis. In order to avoid standing wave in the wave flume, the test duration is limit to 2-3 minutes. For irregular conditions, more than 1100 waves were used for the analysis in order to obtain statistically significant results.

3.4.3.2 Test procedure

The process of a test consists of three main phases: a preparation phase before the generation of the waves, the phases of the actual test where waves are generated (duration is different between regular and irregular conditions), and the last phase in which generation of the measurement data raw files, data processing and analysis.

- **Preparation**

Before starting the test, all equipment is calibrated. Secondly, the appropriate input files with the correct wave characteristics. In this phase, a steering file which controls the wave generator is created.

- **Experimentation**

When the steering file has been sent to the system, the wave generator starts to generate waves and the measurement system starts to work. The wave data (from the gauges) and force data (from strain gauge and pressure sensors) are stored to the on-line computer. After the wave generation, the wave

generator and the pumps are turned off successively.

- **Data Analysis**

The obtained data are analyzed by WaveLab® and Matlab®. Incident wave height, wave period, wave run-up height and overtopping flow surface elevation on front of wall and wave load impact are obtained in this process. The details of the data processing are presented in Chapter 4.

3.5 Instrumentation

This section describes the instruments used in the experiment to measure incident wave height, the water run-up, the overtopping flow surface elevation in front of the wall and the horizontal wave load on the vertical plane. All details of the calibration process and working principles of these instruments are not included in the present report.

3.5.1   Wave gauges

Wave gauges were used in order to obtain time series of water surface elevation. Due to the displacement of water surface, the voltage will change. This voltage is converted into the water level and thus the actual wave record is obtained. Two sets of three gauges (with specific distance between them) were installed in front of the toe of the structure and in front of the wave paddle respectively (refer to Figure 3.5).

The first three wave gauges are grouped in the deep water, with the distance of 3.2 m, 3.587 m and 4.200 m respectively from the wave paddle. The other three are placed respectively at 1.56 m, 2.138 m and 2.468 m from the crest.
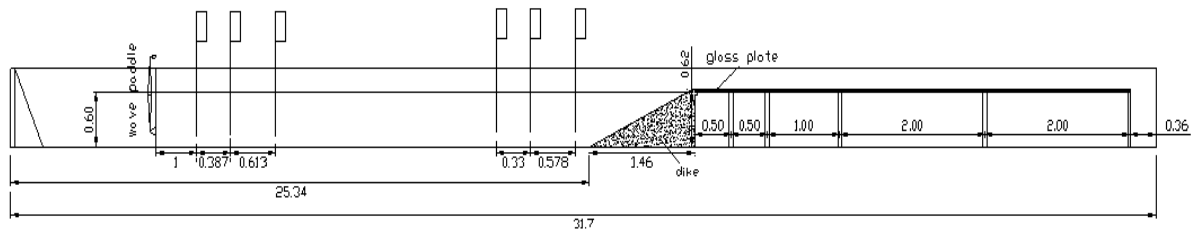
Figure 3.5   Two sets of wave gauges

In addition to the six wave gauges, two wave probes (smaller size of wave gauge) were used for measuring the water surface elevation at the edge of the crest and in front of the wall. Wave probe 1 was fixed at the crest line of the dike in the inland case; while the wave probe 2 was fixed on the surface of the rigid plastic board represented an apartment building in both dike side and inland case models. Figure 3.6 shows the position of these two wave probes in the inland case. As for dike side case, wave probe 1 was removed.

The sample rates of all the wave gauges and probes are 20 Hz.

3.5.2   Load cell

The load cell contains a strain gauge and is connected with a rigid plate with 0.2 m high and 0.1 m wide, used for measuring the horizontal overtopping wave loads on the wall (refer to Figure 3.7). The test range of this load cell is 3 kg, the sample rate is 200 Hz. Details about the working principle and some physical characters can be found in Appendix 4.

Figure 3.6   Wave probes for inland case.

Figure 3.7   Load cell used in all the model tests.

3.5.3   Pressure transducers

Four pressure sensors were also fixed on the surface of the rigid plastic board, the position of these sensors are shown in Figure 3.8, and were placed respectively 1cm, 7cm, 13cm and 19 cm from the surface of the dike crest, the sample rate is 200 Hz. Details about the working principle and some physical characters can be found in Appendix 4.

Load cell in Figure 3.8 is fixed behind this plate.

Druck Pressure sensors with 6 mm diameter

Wave probe2

Pressure sensor type:
PDCR 42
Range: 200 mBar
Sensitivity: 30 mV
nominal
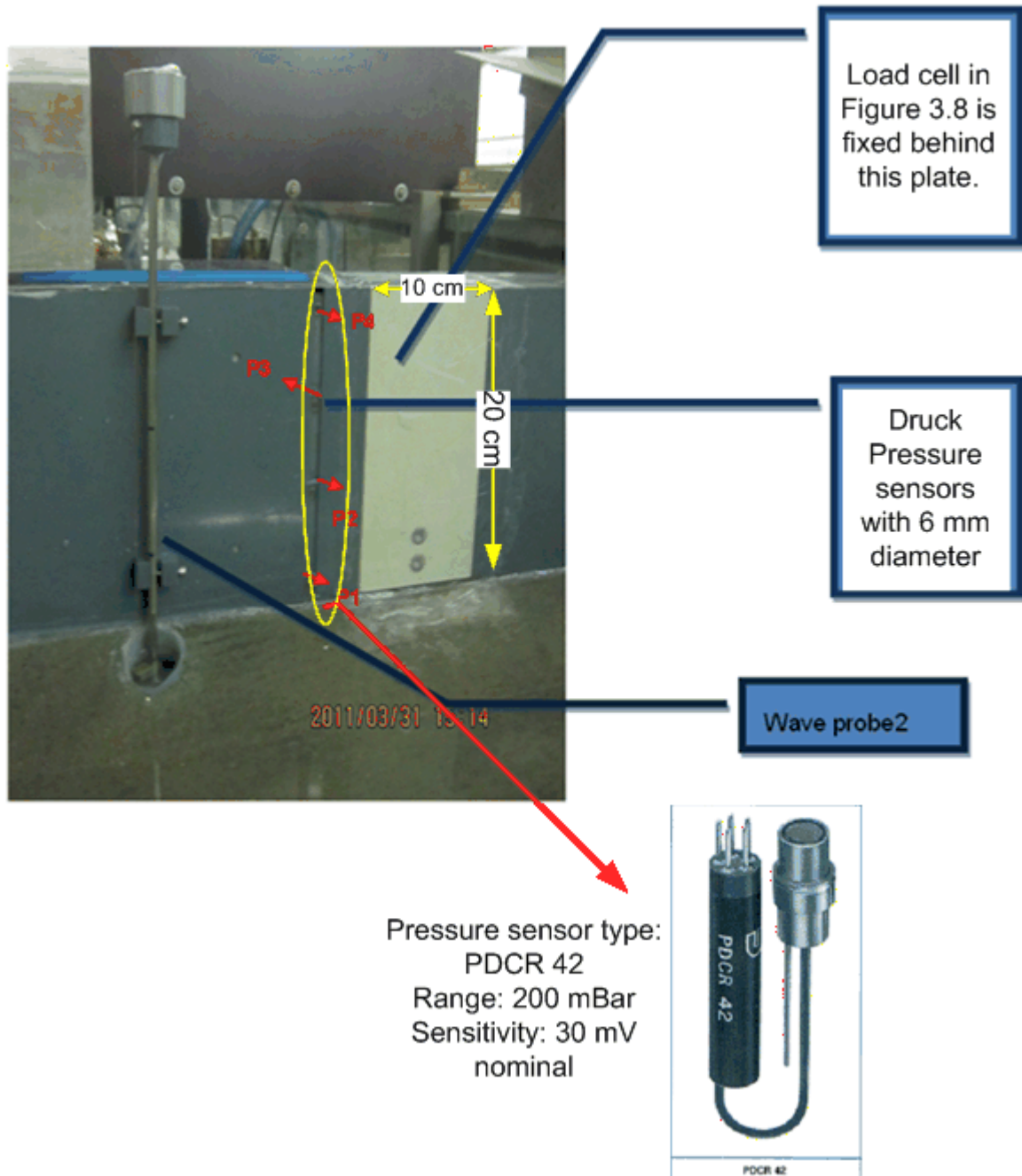
Figure 3.8   Photo of load cell, pressure sensors and wave probe as used in the model.

4 Data Processing

4.1 Introduction

In this chapter, data processing methods are introduced for the regular wave tests.

As mentioned in the previous chapter, there were four kinds of measurement data. These are water surface elevation, overtopping wave surface elevation, wave force and wave pressure.

4.2 Data processing methods

4.2.1 Incident Wave Height and Wave Periods

It was already mentioned in Section 3.2 that there was no Active Reflection Compensation (ARC) System in the wave flume. In order to avoid the influence of the reflected wave from the wave paddle, the surface elevation data measured by wave gauges should be analyzed between a time at which a stable incident wave arrived to a wave guage until a time at which a reflected wave from the wave paddle reached the wave gauge for regular wave *(Suzuki, 2011).*

Figure 4.1(a) and Figure 4.1(b) show examples of the time series of the water surface elevation for the six wave gauges in one test for the case with H=0.065 m and T=1.54 s. It can be observed in Figure 4.1a that at the beginning part of the test, from around 27 s to 47 s, water surface elevation shows a regular pattern. After approximately 47 s, the regular pattern is interrupted by the reflected waves. Figure 4.1b shows that the patterns of the waves are stable from 45 s to 65 s, and after which the wave patterns become unstable. Therefore, 45 s to 65 s was chosen as the data analysis time window. For T=1.8 s, 11 waves were analyzed between 45 s and 65 s. For T=1.54 s and 1.2 s, 13 and 17 waves were analyzed respectively.

The method of *Mansard and Funke (1980)* is used for the separation of incident and reflected waves by using the data of three wave gauges. The method presented by *Mansard and Funke (1980)* assumes that the wave elevation is a summation of regular waves travelling with different frequency and phase. Hence, using the Fourier analysis, the amplitude of the incident and reflected waves for a given frequency can be estimated and moreover, it gives the variation of the measured noise from wave gauge to wave gauge. In this study, the cut-off frequencies $1/3f_p$ and $3f_p$ (default values) were used for the reflection analysis, where f_p is sampling frequency of the wave gauge. Figure 4.2 shows the sample of incident wave time series after reflection analysis.

For each test, the average incident wave height and period was calculated based on the uniform part in the time series (i.e., 11 waves for T=1.8s, 13 waves for T=1.54s and 17 waves for T=1.2s). The average incident wave height (H_m) and period (T_m) were then used to derive further relationships between wave characteristics and wave loads on vertical plane, as discussed further in Chapter 5.
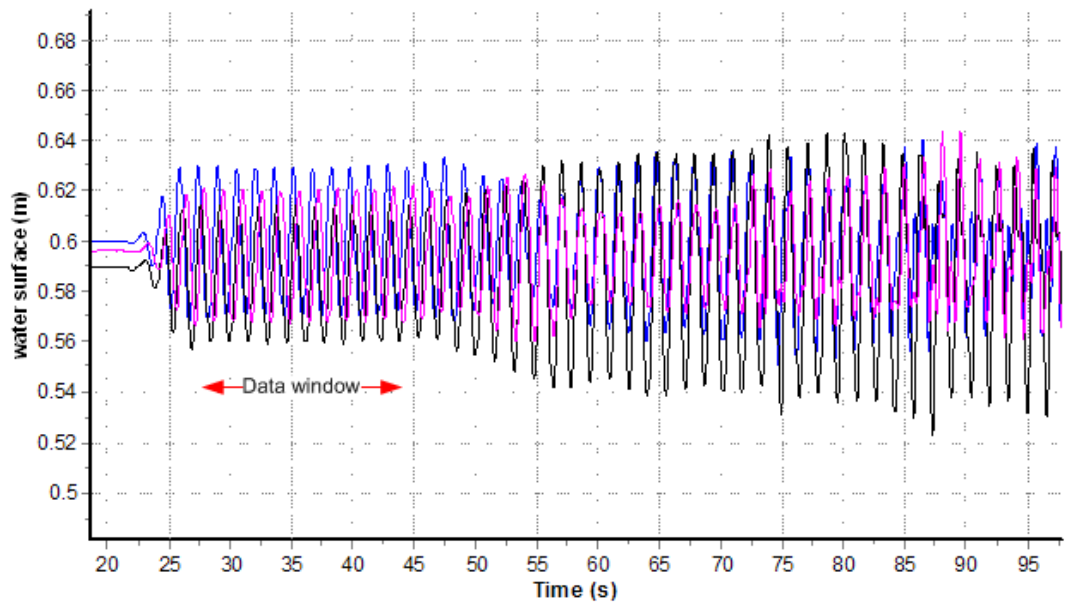
(a) Signals of wave gauge 1, 2, 3 near wave paddle
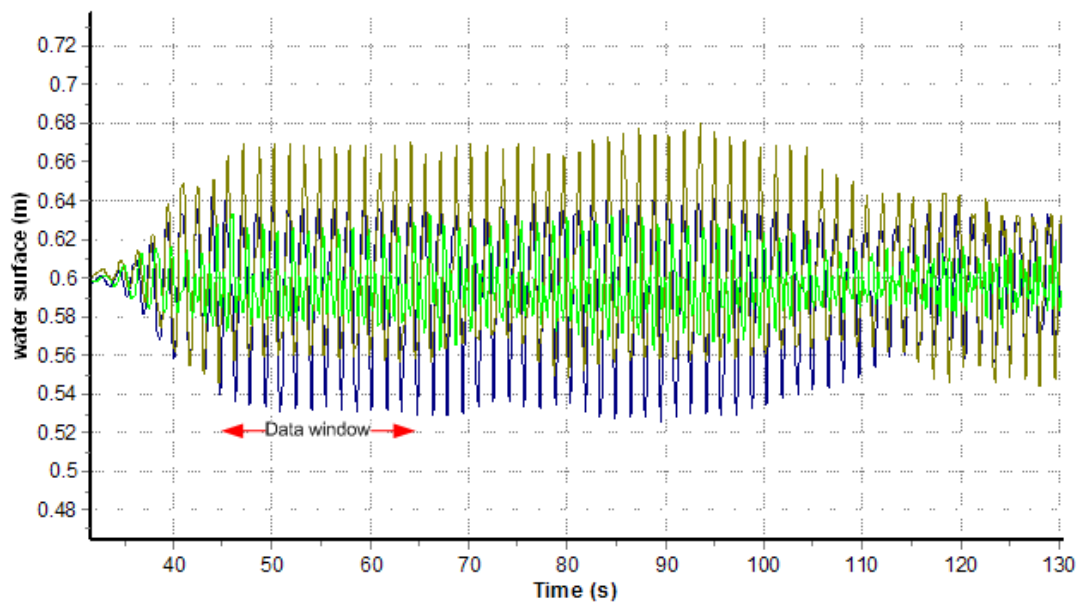
(b) Signals of wave gauge 4, 5, 6 near dike toe

Figure 4.1   Time series of water surface elevation measured by wave gauges
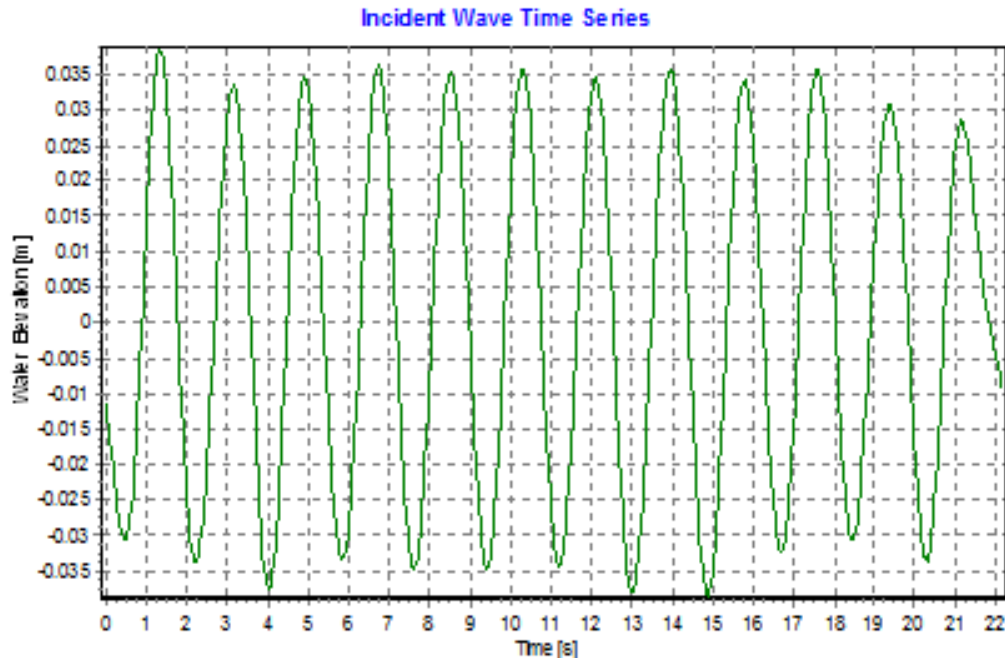
Figure 4.2   Incident wave time series (the time series start at 42s)

4.2.2   Overtopping wave flow layer thickness

In the test, two wave probes were used to measure overtopping wave flow depth in front of the vertical plane and the edge of the dike crest as described in Section 3.3 and outlined in Figure 4.3. The definitions of test parameters are shown in Figure 4.4. The instantaneous water surface elevation in front of the vertical plane or crest is shown as $d(t)$. The highest surface elevation to the top of crest is defined as h and the trough of the time series defines as D. For convenience, the wave elevation parameters $d(t)$, h and D are given a subscript which corresponds to wave probe. $d_1(t)$, h_1 and D_1 correspond to wave elevation surface measured from wave probe1, and $d_2(t)$, h_2 and D_2 are from wave probe 2. Figure 4.5 is an example of time series for h_2 (the dike side case with crest width B=0), while

Figure 4.6 is recorded h_1, h_2 and D_2 for the inland case with B=0.5 m. H_2 is calculated as follows.

$$H_2 = h_2 - D_2 \qquad\qquad \textbf{4.1}$$
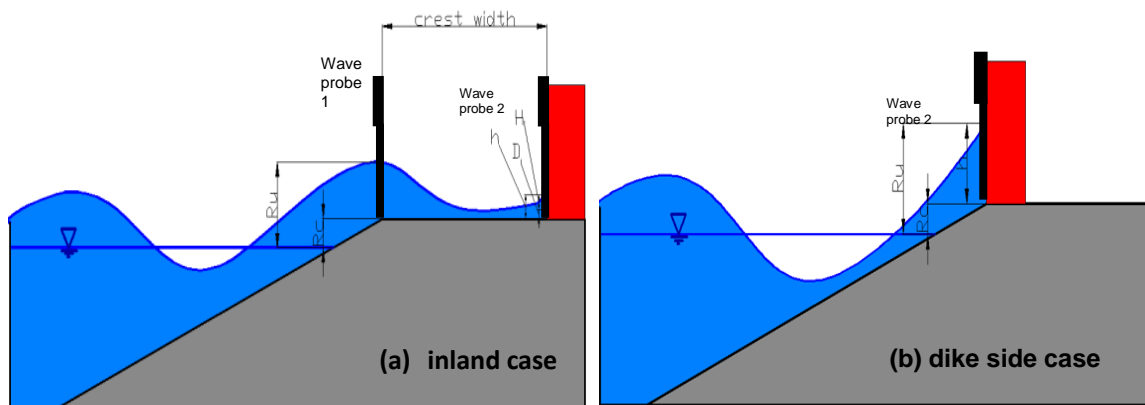
Figure 4.3   Sketch of two wave probes
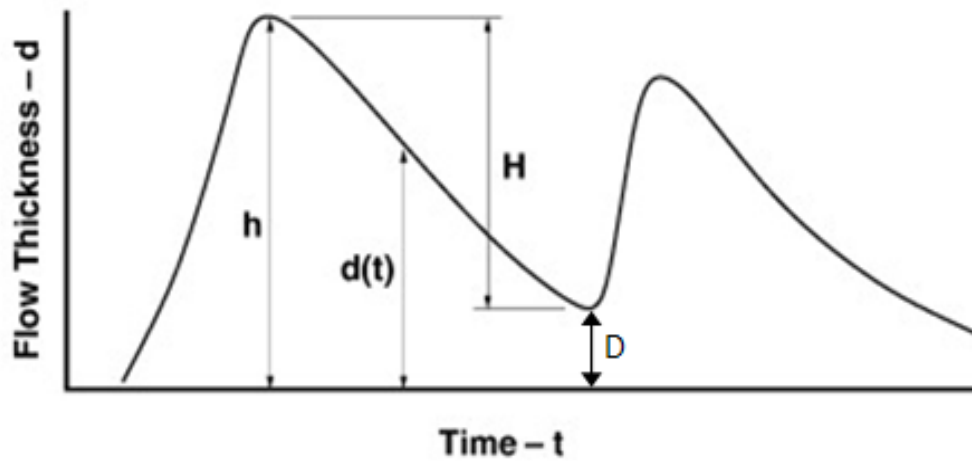
Figure 4.4   Definition of test parameters (Hughes & Nadal, 2009).
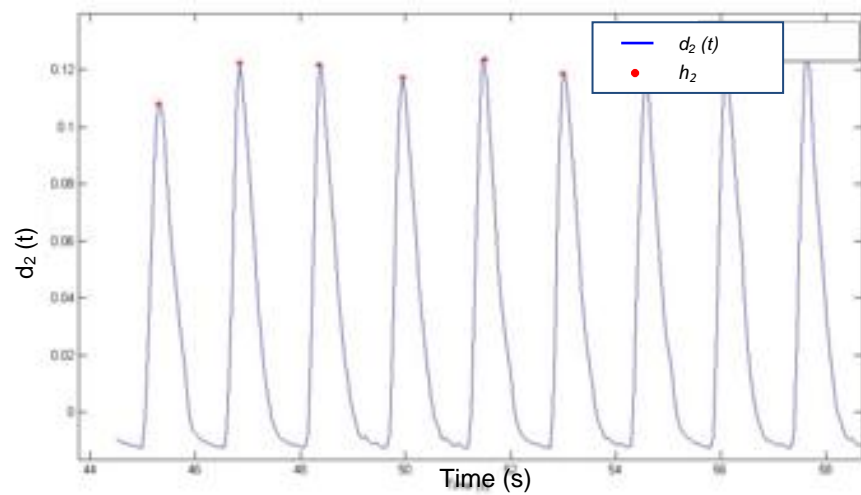
Figure 4.5 Time series sample of $d_2 (t)$ by wave probe2 for Dike side case with crest width=0m.
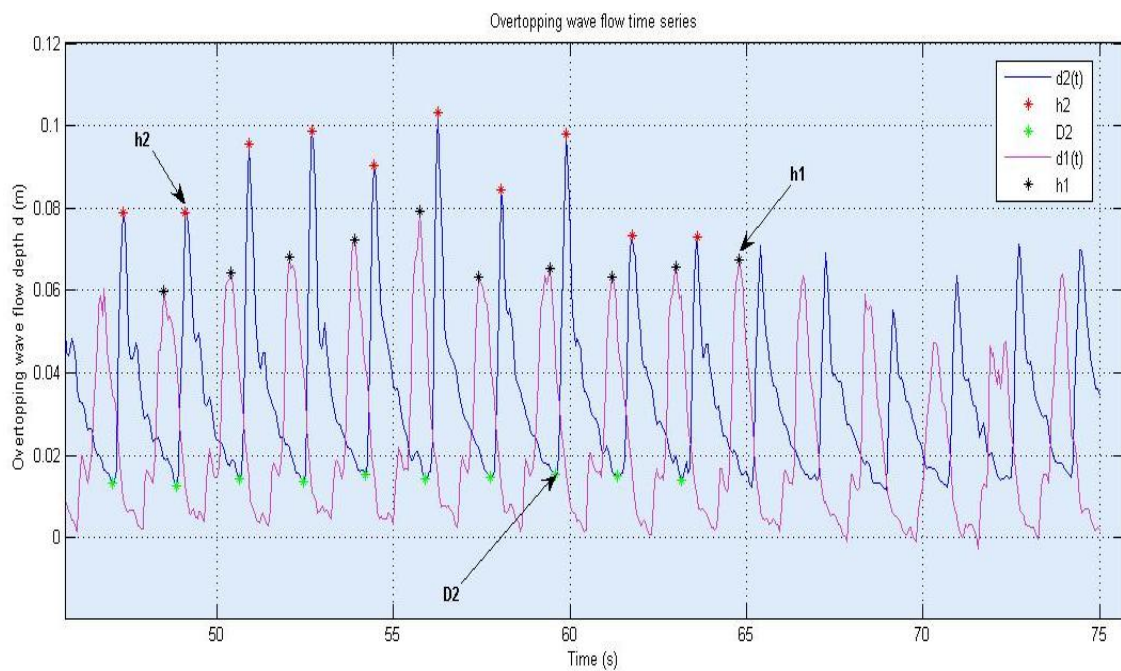
Figure 4.6 Time series sample of overtopping flow, inland case with crest width=0.5m

4.2.3   Overtopping Wave Impact on vertical plane

Two kinds of instruments were used to test the overtopping wave impact on the vertical plane (building model). One was a load cell and the other was a pressure sensor. Some details about these instruments were introduced in Section 3.5 and more details about these instruments themselves such as brand, type, working principle can be found in Appendix 4.

4.2.3.1 Force data measured by strain gauge

The following steps describe the force data processing methods

1.   Event Definition

According to the PROVERBS project report *(McConnell, 1997),* the force time series is used for event definition. The start time t_0 and end time t_t of each event is derived from inspection of the record above and the record below the threshold (refer to Figure 4.7).

2.   Definition of Threshold

During each test, the first 20 seconds is used for warming up the equipment. In order to avoid the influence of the variation in the signal of the stain gauge, these 20 seconds were used to determine the threshold value of the strain gauges. For this study, the real "zero" value of the experimental data is calculated as the maximum value of the first 20 seconds.

3.   Maximum Force of One Event

The maximum force is the peak value of one defined event (refer to Figure 4.7). Therefore, for the entire peak value was used, (e.g. for T=1.8s, there will be 11 maximum force for one test, T=1.54s, there will be 13 maximum force and for T=1.2s, there will be 17 maximum force).

The processed data then are divided by the width of force platform (10 cm) to get the overtopping maximum force per unit width. These maximum per unit width force is used as experimental results for analysis in Chapter 5.

4.2.3.2 Pressure measured by pressure sensors

The data processing method for pressure is slightly different from that for force and is described as the following steps.

1.   Event definition
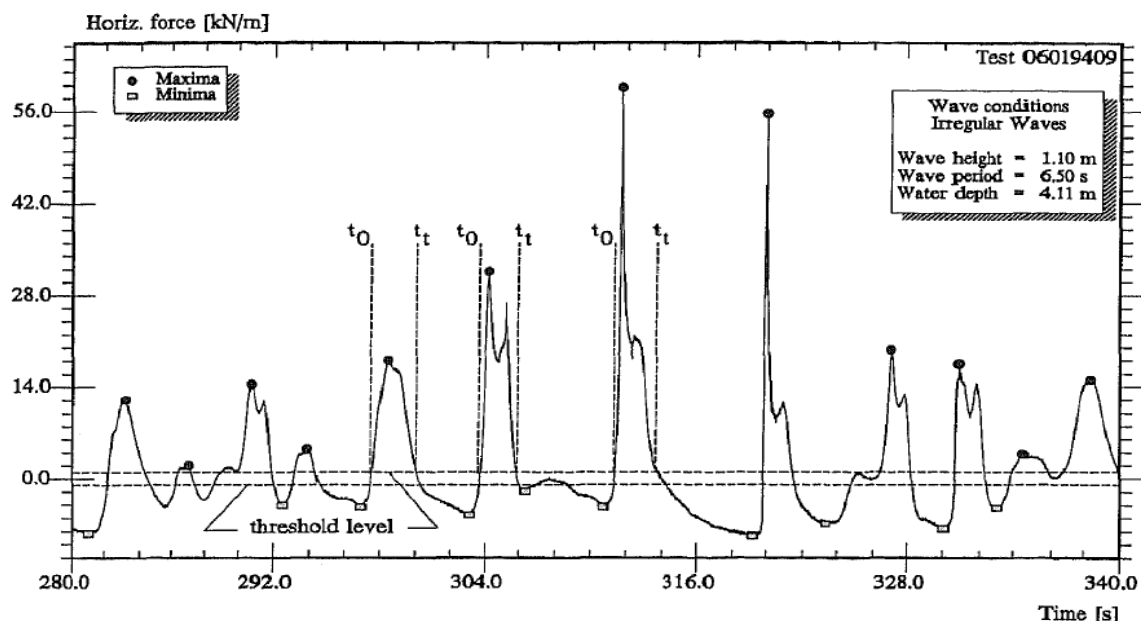
Figure 4.7   Definition of event and threshold (*McConnell, K.L, 1997*).

The step is as same as that of force data (refer to Section 4.2.3.1).

2.   Definition of Threshold

The step is the same with that of force data (refer to Section 4.2.3.1).

3.   Rectangular Integral method for the processed pressure data

There are four pressure sensors to measure the pressure at different position along the vertical plane and the position of these sensors is described in Section 3.6. Figure 4.8 shows the time series of force and pressure data.

As there were not enough pressure sensors distributed along the vertical plane, the integrated pressure results depend on different rectangular integral methods, and noises associated with the signals of the pressure sensors. Therefore, the data from strain gauges is only used for further analysis. More details about the discussions on the pressure integrated method and their results compared with load cell results are shown in Appendix 3.
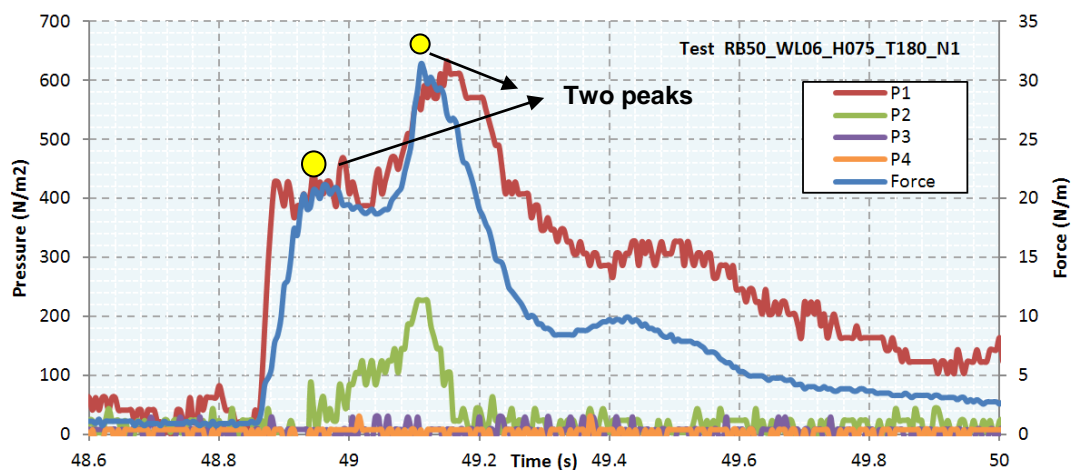
Figure 4.8   Time series signal of force and pressure

4.3 Summary

Here the summary of data processing method used in the present study is listed:

- **Incident wave characters**: raw time series data were analyzed by reflection analysis method, then calculate the average value of one test (11~17 waves according to different wave periods) to represent single event characters.

- **Overtopping wave flow layer thickness**: peak value of one event was used to present experimental result and analysis.

- **Overtopping wave loading:** peak value of one event was used to present experimental result and analysis. Only the time series data obtained from force gauge was applied into the results present and analysis.

5 Experimental Results and Analysis

5.1 Introduction

Different parameters were measured during the experimental study for two cases, i.e. the inland case and the dike side case as referred to in Chapter 3 and the raw data has been processed as described in Chapter 4. In this study, the main objective is to explore the relationship between the overtopping wave force on the vertical plane and incident wave parameters under regular wave conditions (referred to Chapter 1). Therefore, in this chapter, the main efforts are focused on analyzing the relationships for the two cases between:

- The overtopping wave force on the structure and overtopping flow surface elevation;

- The overtopping wave surface elevation and incident wave parameters;

- The overtopping wave force impact on the wall and incident wave parameters.

Chapter 5 is divided into six sections. Section 5.2 gives a brief description of experimental observations for regular waves. The experimental results of inland case and dike side case are introduced in Section 5.3. The analyses of these two cases can be found in Section 5.4. Finally, in Section 5.5, a short summary was given. In Appendix 2, the analysis results in Section 5.4 were applied into the test results under irregular wave conditions.

5.2 General observations

5.2.1 Inland case

For the inland case (refer to Figure 5.1a), the train of regular waves runs over the dike crest before impacting the wall. The wave then collapses and returns seaward. As the wave returns seaward, it is met at the crest of the dike by another incoming regular wave. Because the returning (or reflected) wave meets the incoming wave at the dike crest, it causes a complicated space of the overtopping flow before it reaches the vertical plane.

5.2.2 Dike side case

For the dike side case (see Figure 5.1b), there is no influence of return flow on the dike crest, and the highest surface elevations occur in front of the structure. The highest water surface elevation recorded in front of the structure is approximately the same for each wave in a regular wave train.
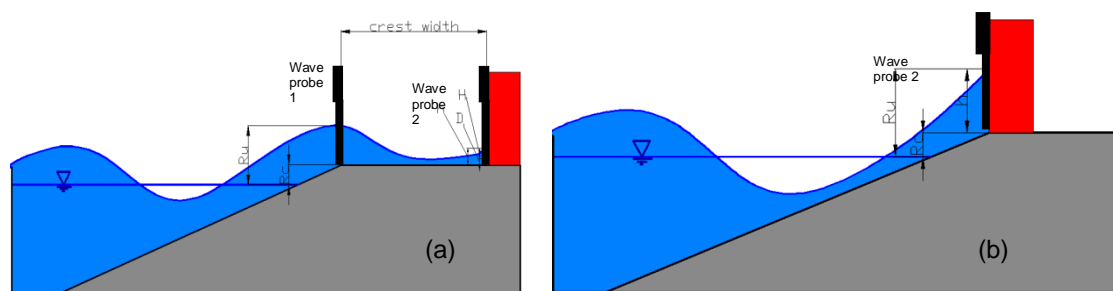
Figure 5.1 inland case (a) and dike side case (b) profile view

5.3 Experimental Results

In this section, experimental data regarded overtopping flow height and wave forces are presented.

Figure 5.2 gives the plots of average overtopping flow highest surface elevation of different overtopping events within one test and the average incident wave height for different wave periods. Figure 5.2a is for the inland case,and Figure 5.2b is for the dike side case. It appears that there is a similar trend between these two parameters for different wave periods with the same R_c.

In order to explore the behavior of overtopping wave force on the wall, it is useful to associate an individual overtopping event with a corresponding overtopping flow surface elevation. Figure 5.3 shows a plot of overtopping wave force (F_{max}) versus the highest surface elevation (h_2) for all 786 overtopping waves for the inland case (Figure 5.3a) and 510 overtopping waves for the dike side case (Figure 5.3b) for different freeboard and different wave periods which were identified from all experiments regarded on regular waves. Larger freeboard appeared to have a slight influence with decreased scatter and a steeper polynomial trend at larger values of R_c, but overall an ascendance trend is clearly that higher h_2 has a larger F_{max}. Data points with smaller wave periods concentrated at the head of the trend while data with larger periods mainly distributed at tail part of the trend. But they are all following the same trend. Some of the observed scatters against the main trend are possibly explained by spray of overtopping flow when it hits the vertical plane.

To reduce the scatter, average value of the identified events for each test were chosen to show the results in the following paragraphs. From Figure 5.4, it can be seen that the relative lowest (or remainder) surface elevation (D_2/h_2) may influence the overtopping wave force (F_{max}). Force will decrease with the increasing level of D_2/h_2.

Figure 5.5 and Figure 5.6 show the plots of dimensionless average overtopping force versus dimensionless freeboard for different wave periods. For the inland case, there is a better correlation of these two parameters than for the dike side case.

Here the finding summaries of data plots are listed:

- The lowest overtopping wave surface elevation has little relation with the incident wave characters.

- For overtopping wave surface elevation, it is proportional to incident wave height.

- Force has a relation with highest overtopping wave surface elevation in front of the building, which does not depend on wave period

- The water layers in front of the wall have a certain influence on the final force on the building.

- Dimensionless overtopping wave force is a function of dimensionless freeboard, incident wave height and breaker parameters for both dike side and inland cases.
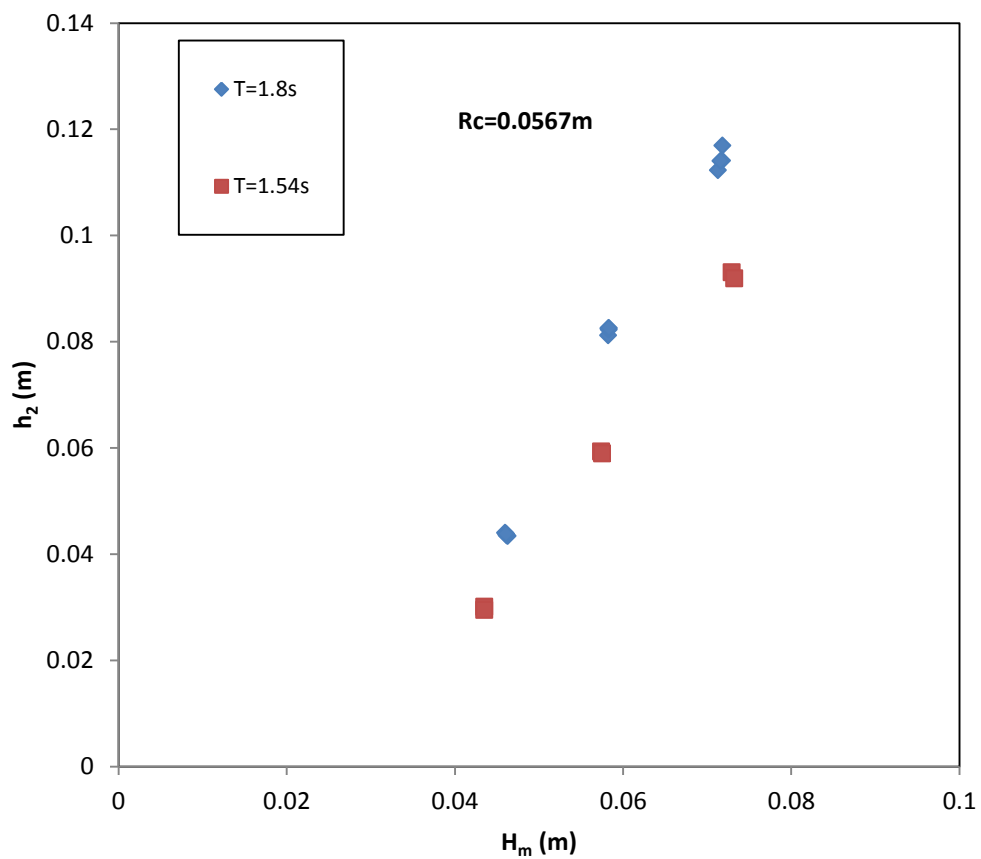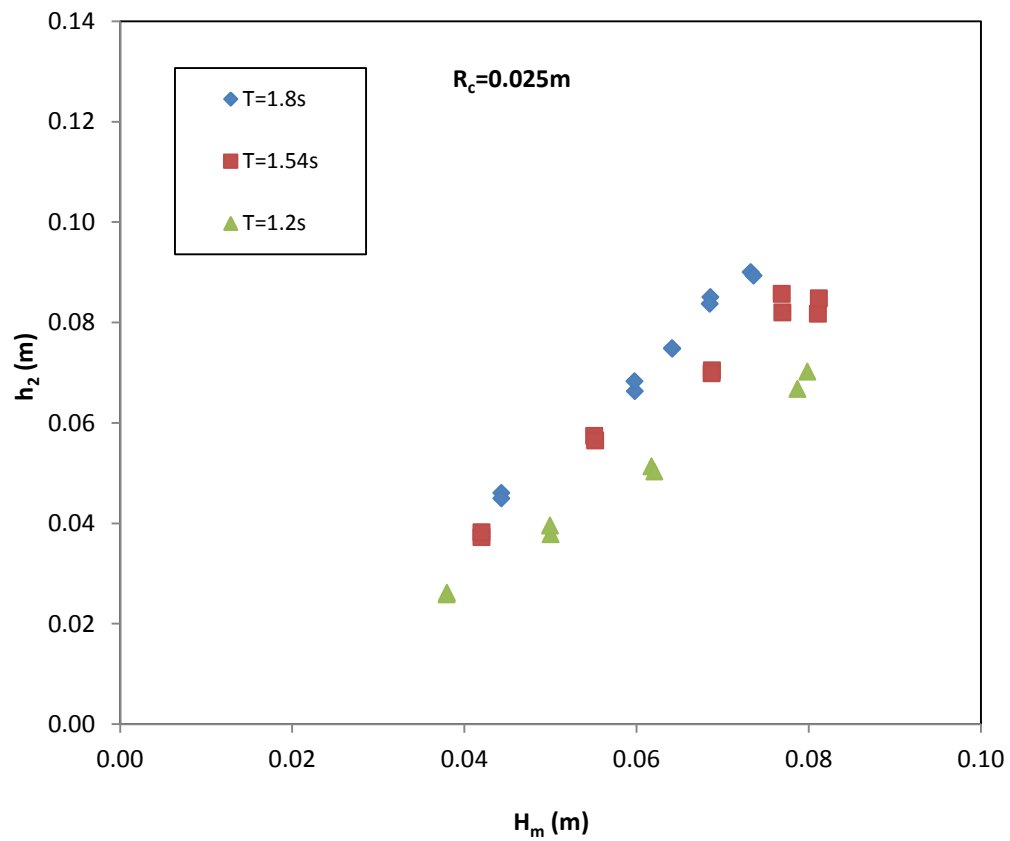
Figure 5.2   Average h_2 versus average H_m with different wave periods, (a) is for inland case and (b) is for dike side case
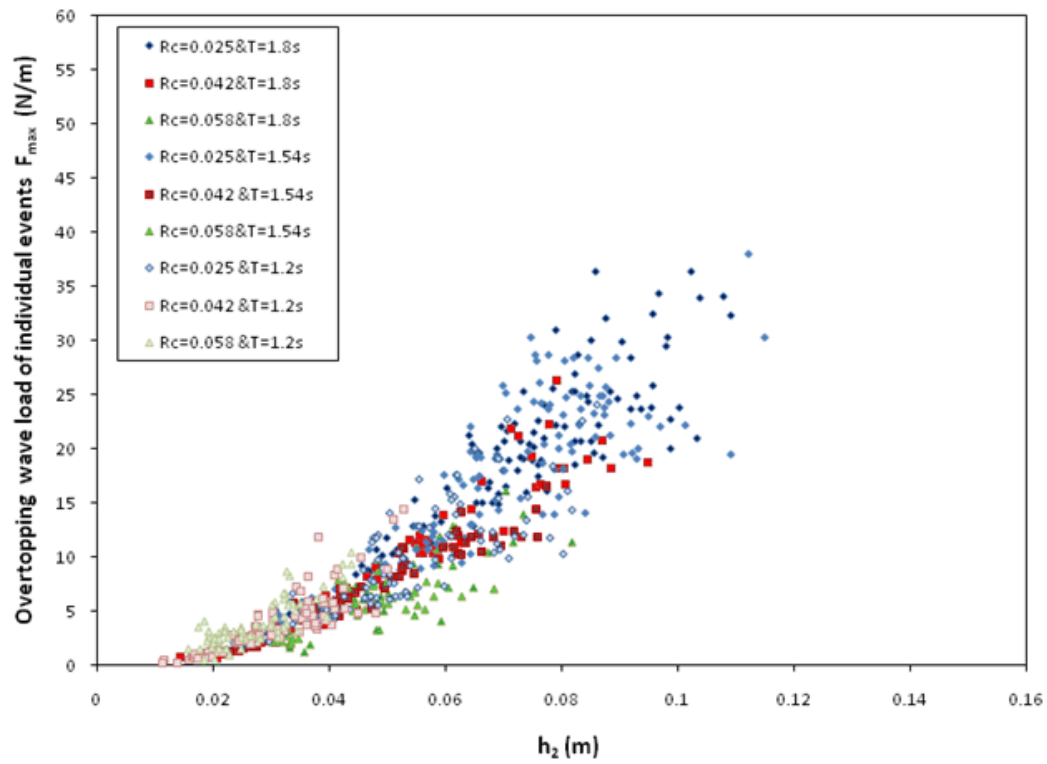
(a) B=0.5m for inland case
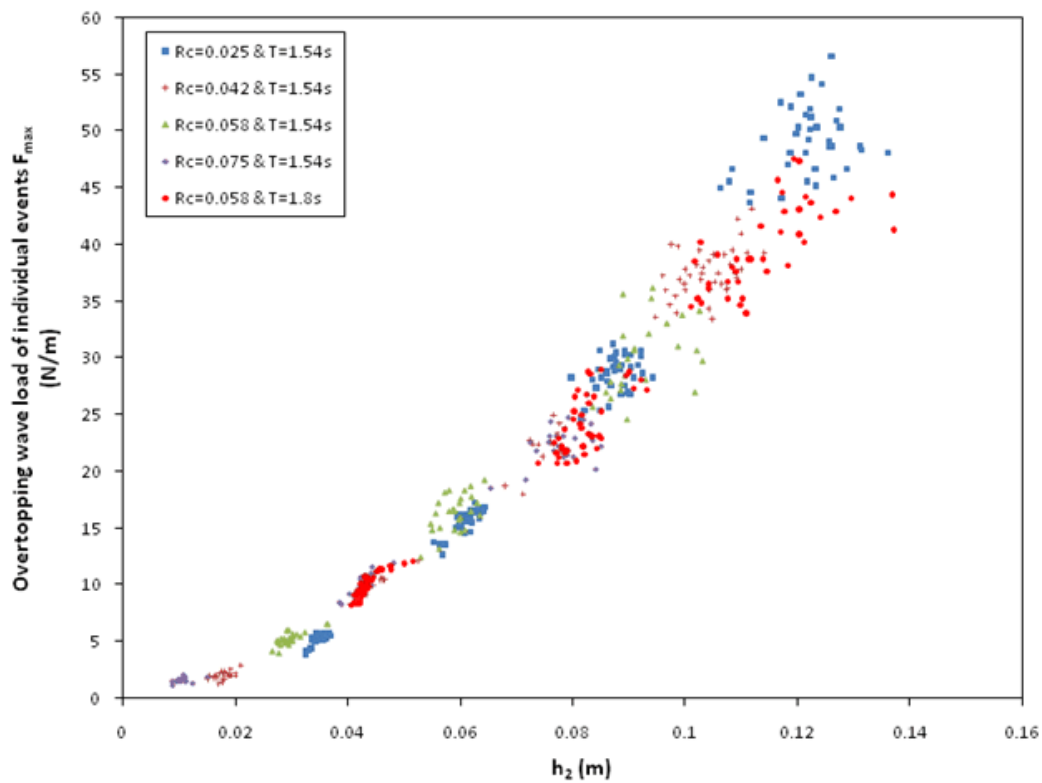
(b) B=0 m for dike side case

Figure 5.3 Individual overtopping wave force versus h_2 with different R_c & T for inland case and dike side case.
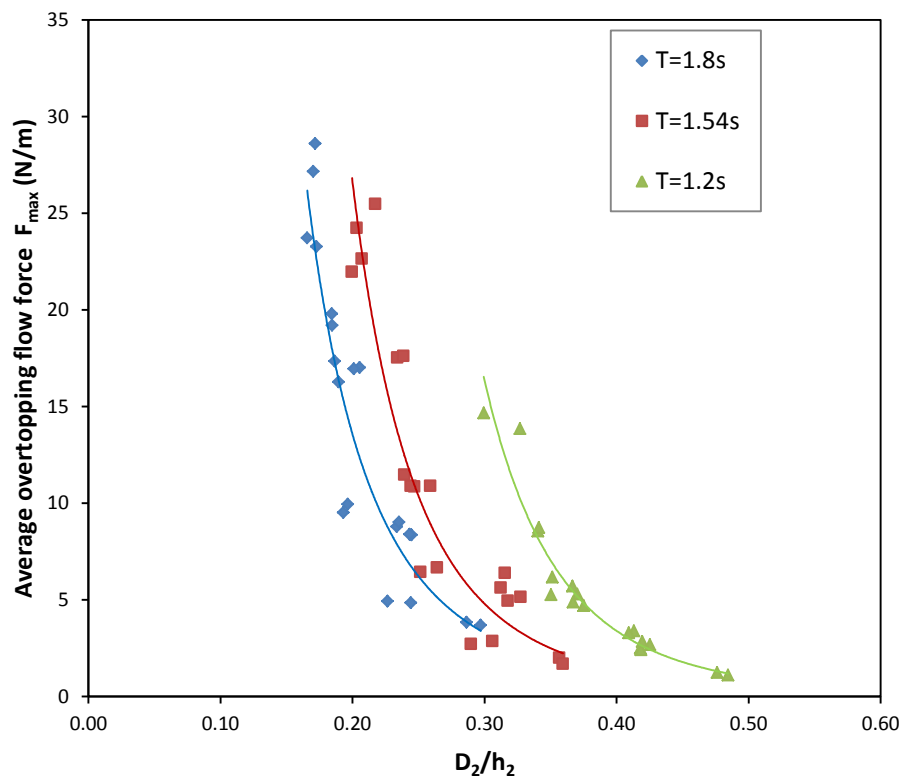
Figure 5.4   Relation between water layer thickness influences on force
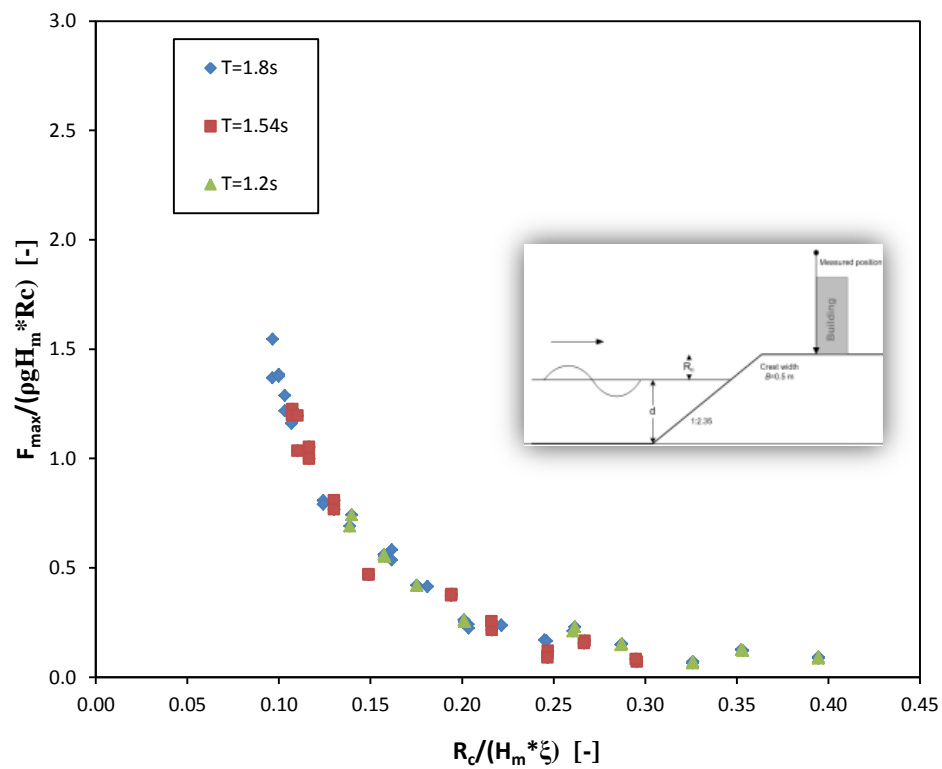
Figure 5.5   Dimensionless overtopping wave force versus dimensionless freeboard for inland case
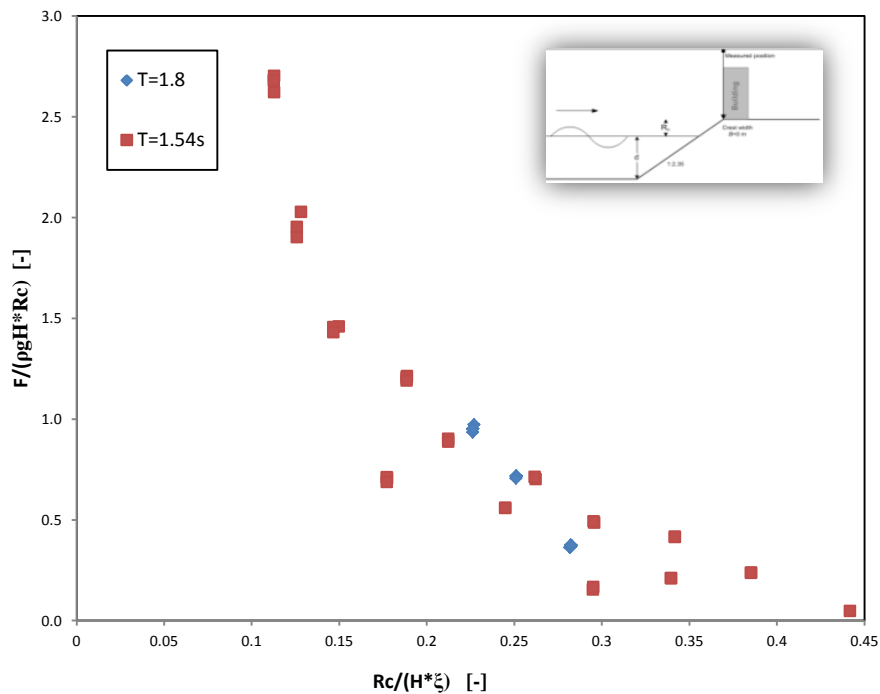
Figure 5.6   Dimensionless overtopping wave force versus dimensionless freeboard for dike side case.

5.4   Experiment data analysis

In this section 5.4, the overtopping wave forces were analyzed by different spatial levels based on regular test data. In Section 5.4.1, the analysis concerns zone 5: overtopping wave in front of the vertical plane. In Section 5.4.2, the analysis concerns zone 3 & 4, overtopping wave on the crest. Finally, in Section 5.4.3, the analysis concerns zone 1 & 2, the incident wave near the toe of the dike.

5.4.1   Overtopping wave force on the building

In the following subsections, the overtopping wave force on the building has been analyzed referring to the concept of wave momentum flux parameter defined by *Hughes (2004)*. Then, the measured force was compared with the derived Equation. Figure 5.7 shows the analyses flow chart, the black arrow in zone 5 means the incident overtopping wave, while the dash arrow means the reflected overtopping wave by the vertical face of the building. In the present study, the reflected overtopping waves are not considered in the force estimation but will be discussed in Chapter 6.
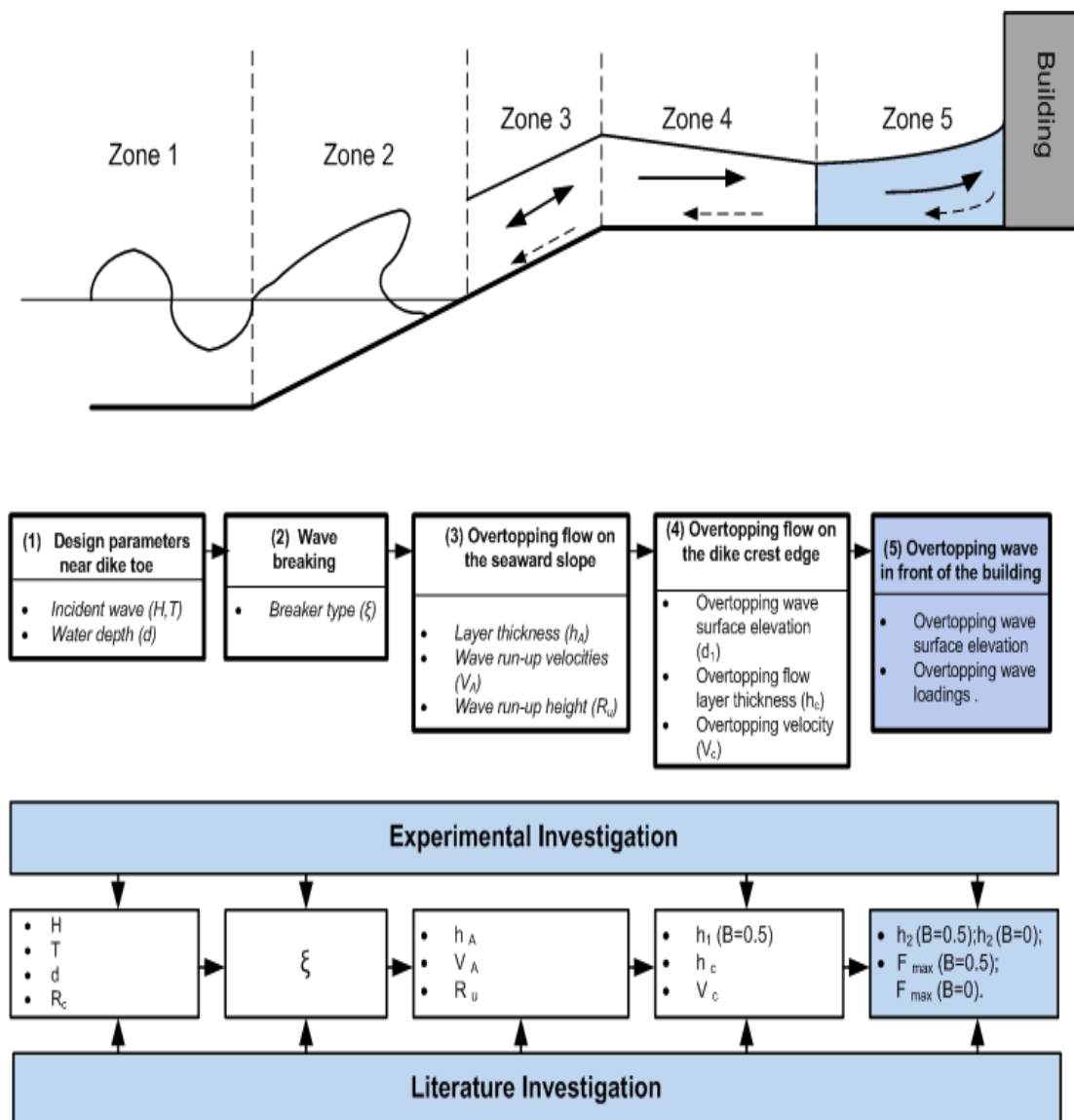
Figure 5.7   Analysis of overtopping wave on the dike crest within zone 5 (adapted from Schüttrumpf and Oumeraci, 2005).

5.4.1.1 Conservation of momentum for overtopping wave

The definition of maximum wave momentum flux in *Hughes (2004)* is the maximum depth-integrated wave momentum flux and has units of force per unit of wave crest and can be used for near shore waves. According to *Hughes (2004)*, the wave force that has "pushed" the water up the slope at the instant of maximum run-up, the fluid within the hatched area on Figure 5.8a has almost no motion and the weight of the fluid contained in the hatched wedge area A'B'C' is proportional to the maximum depth-integrated wave momentum flux of the wave before it reached the toe of the structure slope.

Following the argument by *Hughes (2004)*, a similar derivation is performed for the overtopping wave force for the inland case (refer to Figure 5.8b) and the dike side case (refer to Figure 5.8c). It can be argued that the maximum overtopping wave momentum flux is integrated by water depth in front of the building and is proportional to the weight of water contained in the hatched area *abcd* ($W_{(abcd)}$) on Figure 5.8b for the inland case and *ABC* ($W_{(ABC)}$) on Figure 5.8c for the dike side case, i.e. where β is an unknown constant of proportionality, W is the weight of water

$$F_{max} = \beta W \qquad \qquad \textbf{5.1}$$

The weight of water per unit width contained in quadrangle *abcd* for the inland case and triangle *ABC* for the dike side case shown on Figure 5.8b and Figure 5.8c are given by

$$W_{(abcd)} = \frac{\rho g}{2} \frac{1}{\tan\theta} (H^2 + 2HD) \qquad \qquad \textbf{5.2}$$

$$W_{(ABC)} = \frac{\rho g}{2} \frac{1}{\tan\theta} h^2 \qquad \qquad \textbf{5.3}$$

Where h is the simplification format for h_2 which is the maximum vertical surface elevation from the base of the wall, D is the minimum vertical surface elevation from the base of the wall, H is the elevation difference between h and D. For the dike side case or the inland case, if there is no residual water flow on the crest, D is 0 and H equals h. The θ is an unknown angle between still water level and overtopping wave surface (which is assumed to be a straight line). Substituting Equation 5.2 and Equation 5.3 into Equation 5.1 yield two new equations, i.e., Equation 5.4, where β_2 is an unknown constant relating the angle between overtopping wave surface and still water level. For convenience, the "max" subscript has been dropped from the overtopping wave force.

$$F = \beta_2 \frac{\rho g}{2} (H^2 + 2HD) \qquad \qquad \textbf{5.4}$$

$$F = \beta \frac{\rho g}{2} h^2 \qquad \qquad \textbf{5.5}$$

For the inland case, compared with *H*, *D* is relative small; therefore, $(H^2 + 2HD)$ in Equation 5.4 can be replaced by h^2, then Equation 5.4 and 5.5 can use the same format, namely Equation 5.6, where C_1 is a constant unknown coefficient.

$$F = C_1 \rho g h^2 \qquad \qquad \textbf{5.6}$$
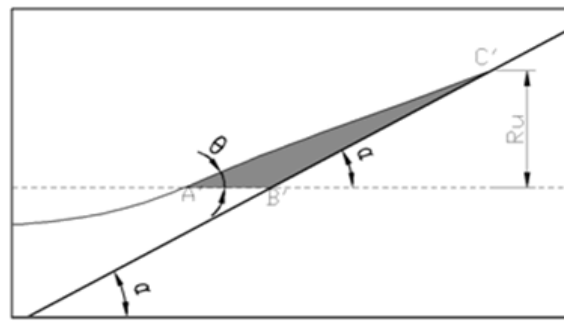
(a) Sketch of wave run-up (Hughes,2004)
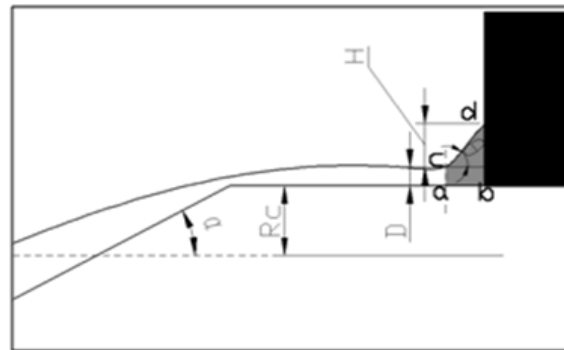
(b) Sketch of overtopping wave for inland case
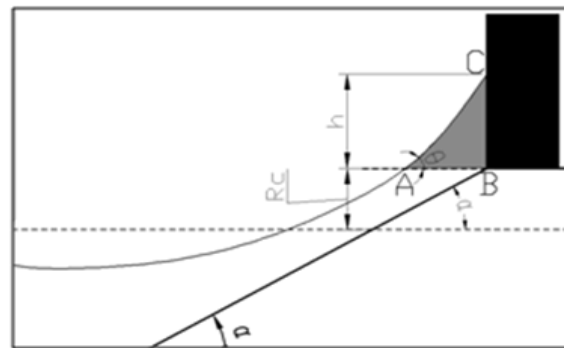
(c) Sketch of overtopping wave for dike side case

Figure 5.8   Sketches of wave run-up and overtopping waves in front of the building

5.4.1.2 Zone 5 data analysis

Figure 5.9 shows the plots of measured individual overtopping wave load obtained from load cell versus $\rho g h^2$ for the inland case and the dike side case.

Figure 5.10a and Figure 5.10b give the relationship of average overtopping wave force versus $\rho g h^2$ for the inland case and the dike side case. Note that from Figure 5.10b, decreased scatters can be seen for longer waves. It can be explained that the estimated area *ABC* in Figure 5.8c is not triangular anymore due to the relatively high surface level and weight of water which caused the line *AC* to be curved instead of a line, so Equation 5.7 gives an overestimation for the force. This part will be discussed in-depth in Chapter 6.

In summary, using the concept of wave momentum flux gives a good estimation of overtopping wave for both the inland case and the dike side case.

$$F = 0.33\rho g h^2 \qquad\qquad 5.7$$
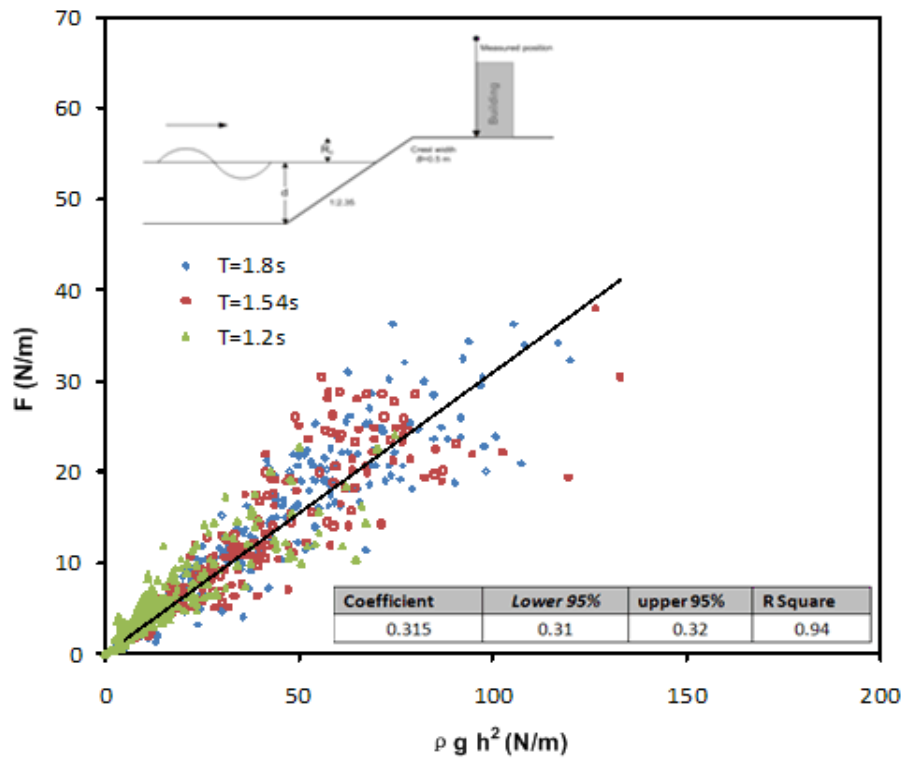
(a) B=0.5 m for inland case
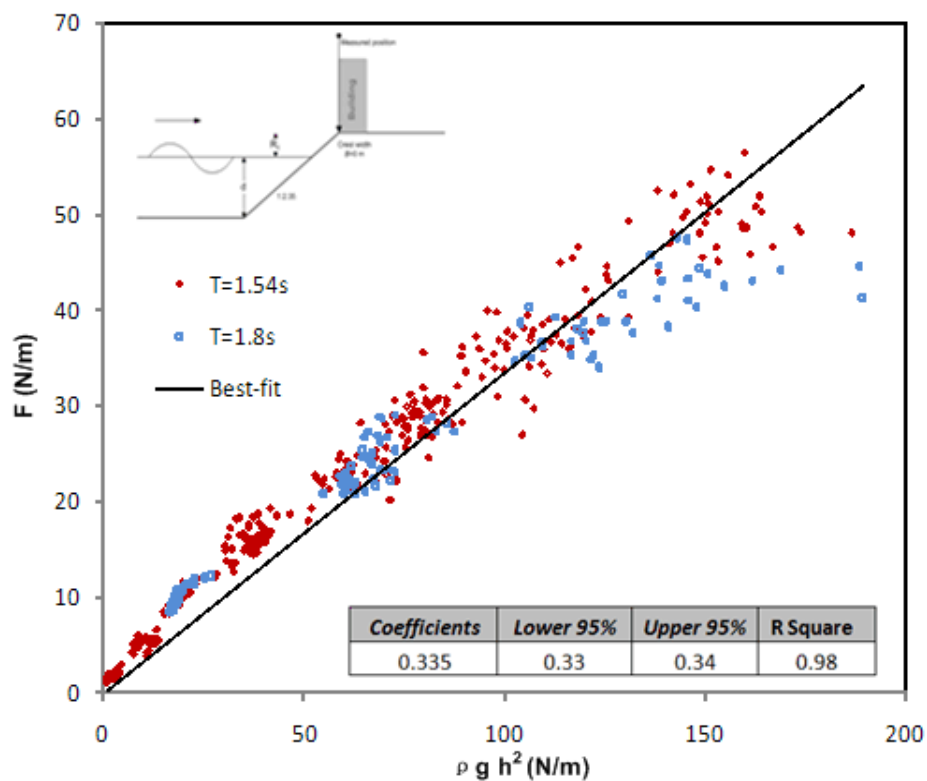
(b) B=0 m for dike side case

Figure 5.9   Individual measured overtopping wave load versus ρgh^2
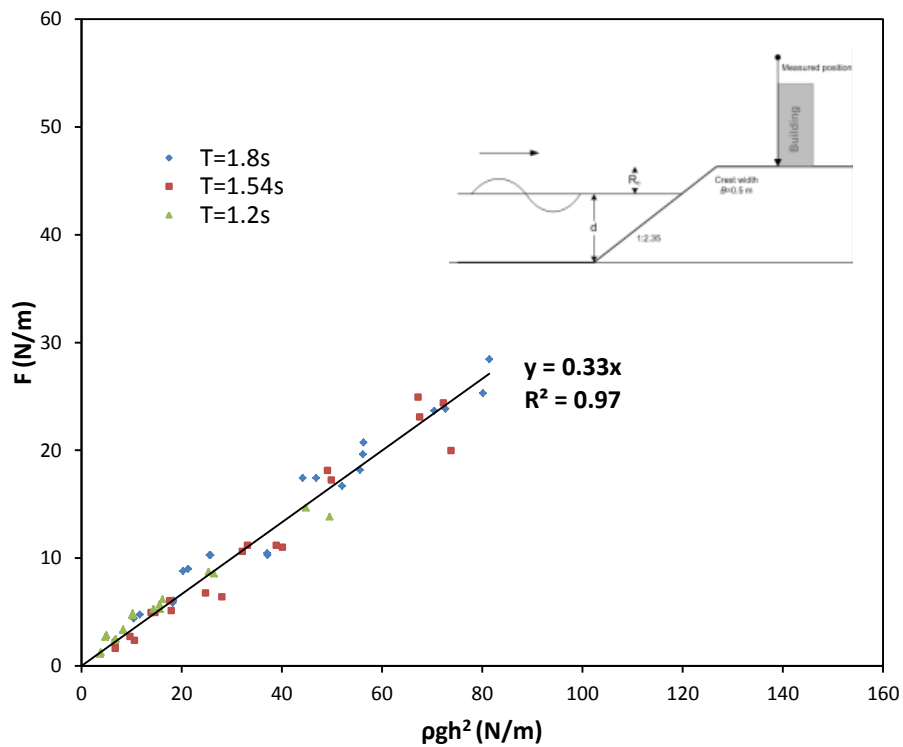
(a) B=0.5 m for inland case
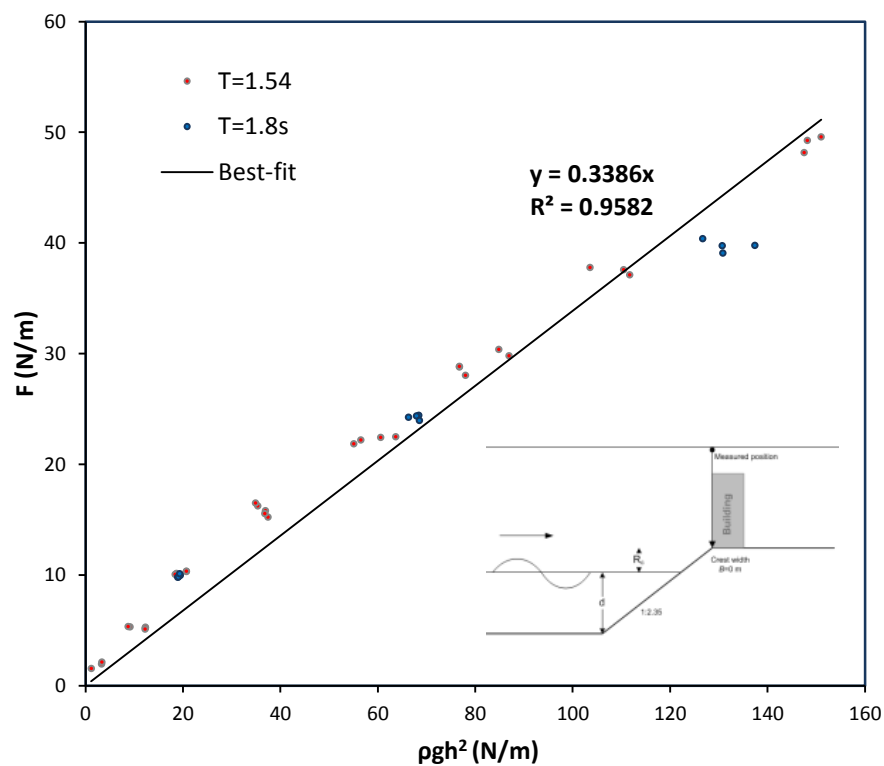
(b) B=0 m for dike side case

Figure 5.10   Averaged measured overtopping wave load versus ρgh^2

5.4.2   Overtopping wave analysis within zone 3 & 4

The transition of the seaward slope of the dike (i.e. zone 3 & 4, refer to Figure 5.11) separates the run-up overtopping wave flow into two fields. One overtops the dike and will potentially hit the building (into zone 4), while the other flow will go back to the wave flume (into zone 3). In this section, in order to build a bridge from zone 5 to zone 1, a few parameters referred to in other literature were introduced to help with analysis of experimental data.
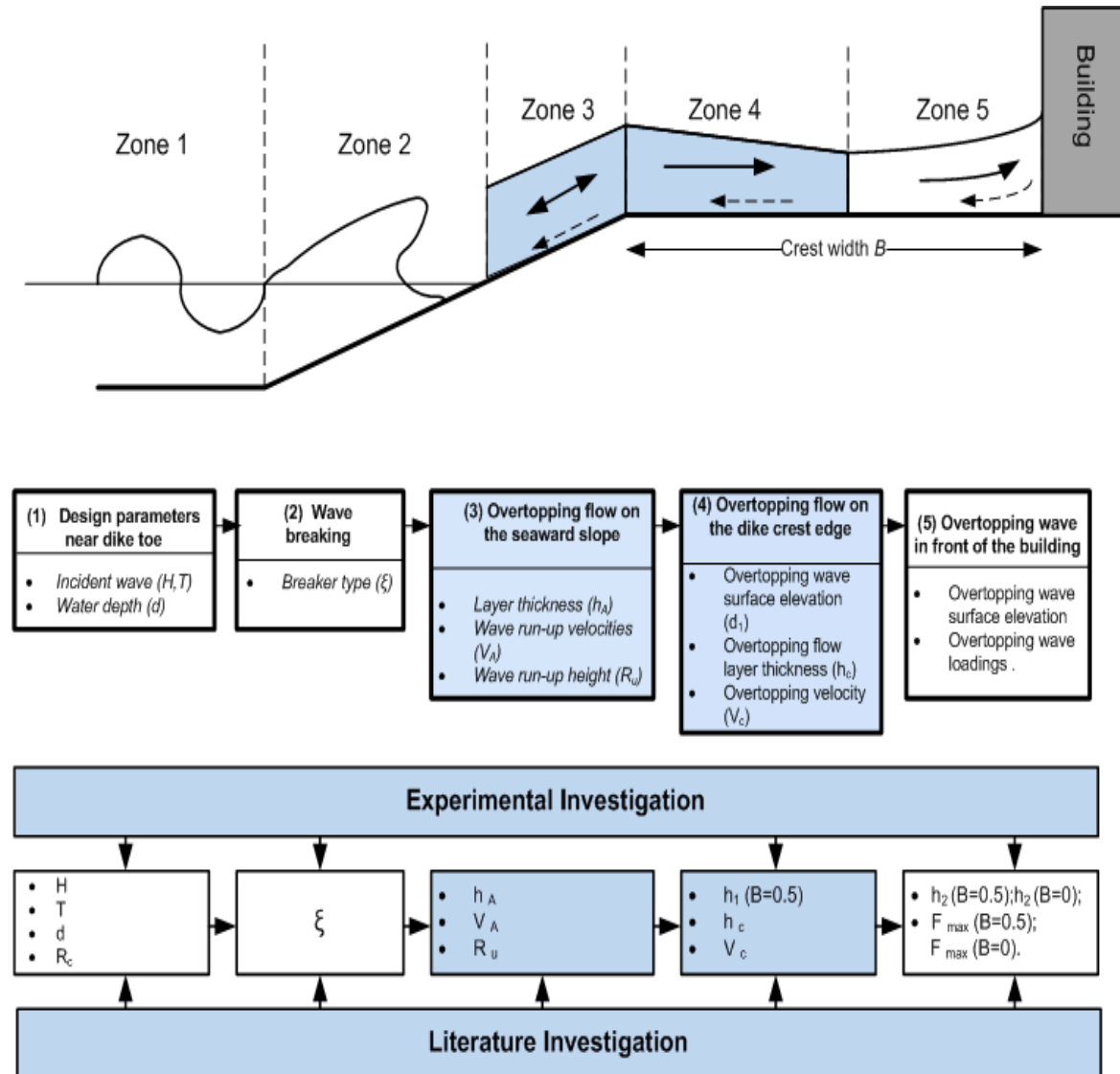
Figure 5.11   Analysis of overtopping wave on the crest within zone 3 & 4 (adapted from Schüttrumpf and Oumeraci, 2005).

5.4.2.1 Overtopping wave tongue thickness analysis

In order to connect zone 5 and zone 1, incident wave parameter near toe should be introduced into the relation of overtopping wave load, i.e., Equation 5.7. A new parameter named water tongue thickness at the crest level is introduced in Equation 5.8, based on work from *Martin and Losada, et al, (1999)*. Where S_0 is the overtopping wave tongue thickness at the beginning of the dike crest, H_m is the average value of incident wave height near the toe of the dike, R_c is the crest freeboard and R_u is the maximum wave-run-up on a smooth impermeable plane slope, Equation 2.2 is recommended by *Schüttrumpf (2001)* (refer to Chapter 2). Note that there are many formulas which can estimate the maximum regular wave run-up on an infinite slope which directly influences the result of S_0 in Equation 5.8. Therefore, in this study, all the formulas related to the regular wave R_u are applied Equation 2.2.

$$S_0 = H_m(1 - \frac{R_c}{R_u}) \qquad \text{5.8}$$

Figure 5.12 plots the relation between the average highest water surface elevations in front of the building (h) and the wave tongue thickness defined by Equation 5.8 for the two cases with the straight best-fit line representing Equation 5.9 in Figure 5.12 (a), and with the straight best-fit line representing Equation 5.10 in Figure 5.12 (b).Therefore, the overtopping wave force can be represented by substituting wave tongue thickness parameter (S_0) directly into the Equation 5.7.and get two new Equation 5.11 and Equation 5.12.

$$h = 1.24 S_0 \qquad \text{5.9}$$

$$h = 2.12 S_0 \qquad \text{5.10}$$

$$F = 0.51 \rho g (H_m)^2 (1 - \frac{R_c}{R_u})^2 \qquad \text{5.11}$$

$$F = 1.48 \rho g (H_m)^2 (1 - \frac{R_c}{R_u})^2 \qquad \text{5.12}$$

Therefore, the measured overtopping wave forces on the vertical plane were compared with those that were estimated for all 784 overtopping events (the inland case) and 510 overtopping events (the dike side case) using the formula given by Equation 5.11 and Equation 5.12. The results are shown in Figure 5.13a is for the inland case, and Figure 5.13b is for the dike side case. From Figure 5.13a most of the data follow the trend and are within the 95% confidence range, but some have much lower values than estimated for T=1.54s caused by higher h recorded by probe 2, and the higher h is probably caused by the spray of water. As for the dike side case (Figure 5.13b), though most of the data are within the 95% confidence range, unlike the data from T=1.54s, the data from T=1.8s are just from the test series under one water level condition and Equation 5.12 gives a lower estimation for small overtopping waves.

Therefore, a uniform equation related average overtopping force can be shown as Equaion 5.13, where C_2 is the coefficient relatted crest width, for the inland case, C_2 is 0.51 while in the dike side, C_2 is 1.48. For regular waves, Equation 5.13 can give a good estimation for overtopping wave force, especially for long wave in the inland case, and large wave for the dike side case.

$$F = C_2 \rho g (H_m)^2 (1 - \frac{R_c}{R_u})^2 \qquad \text{5.13}$$
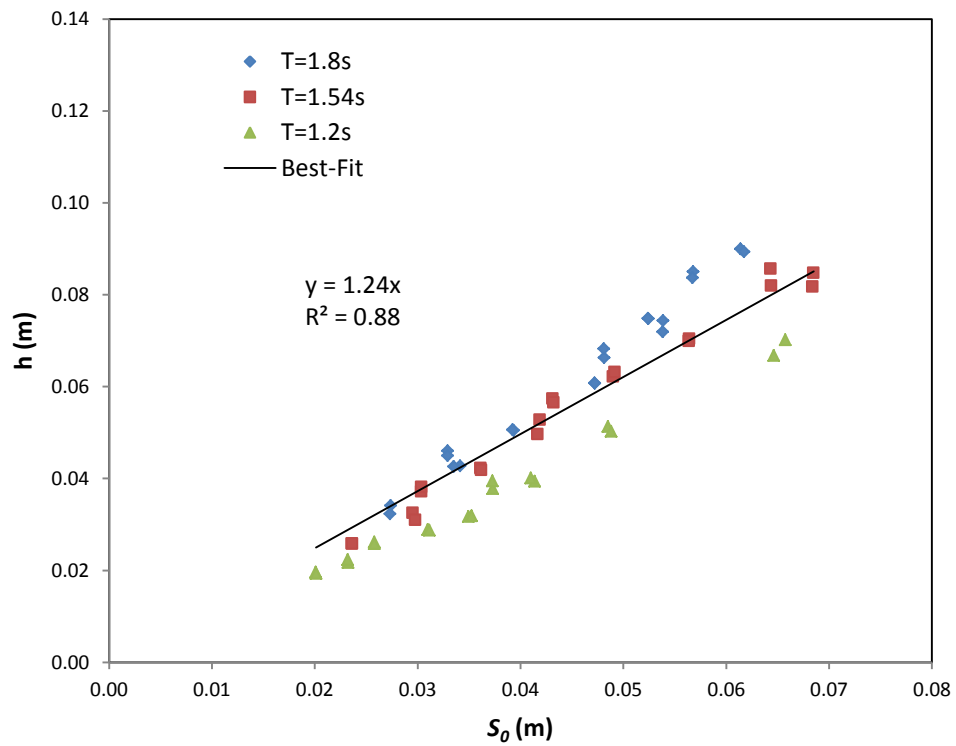
(a) B=0.5 m for inland case
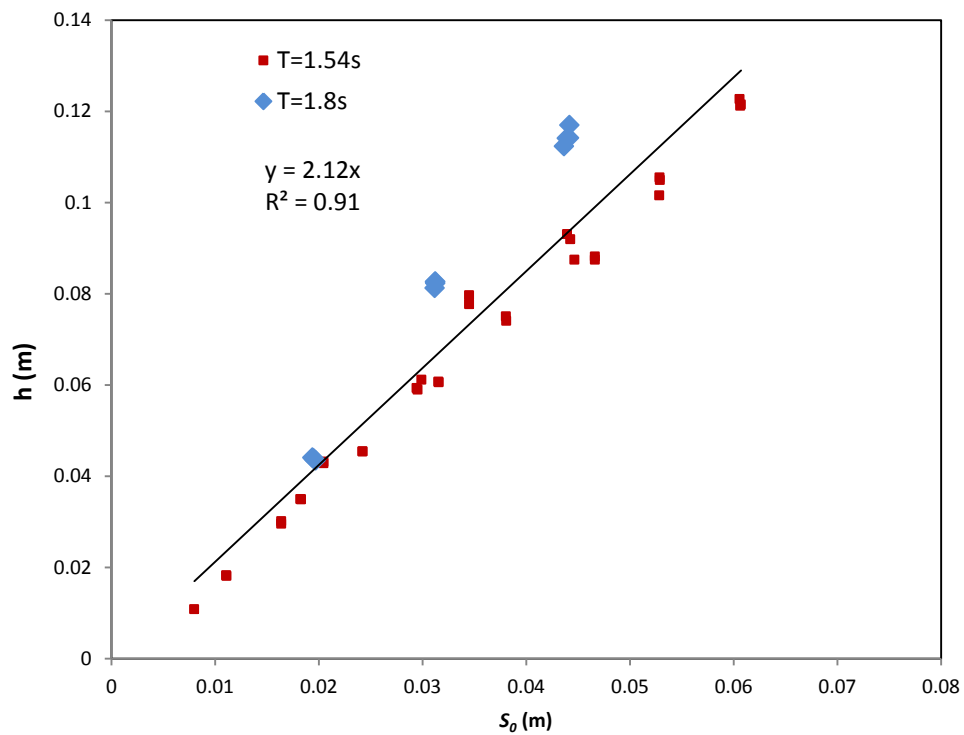
(b) B=0 m for dike side case

Figure 5.12   Highest water surface elevation versus wave tongue thickness, (a) inland case, (b) dike side case.

(a) B=0.5 m for inland case

(b) B=0 m for dike side case
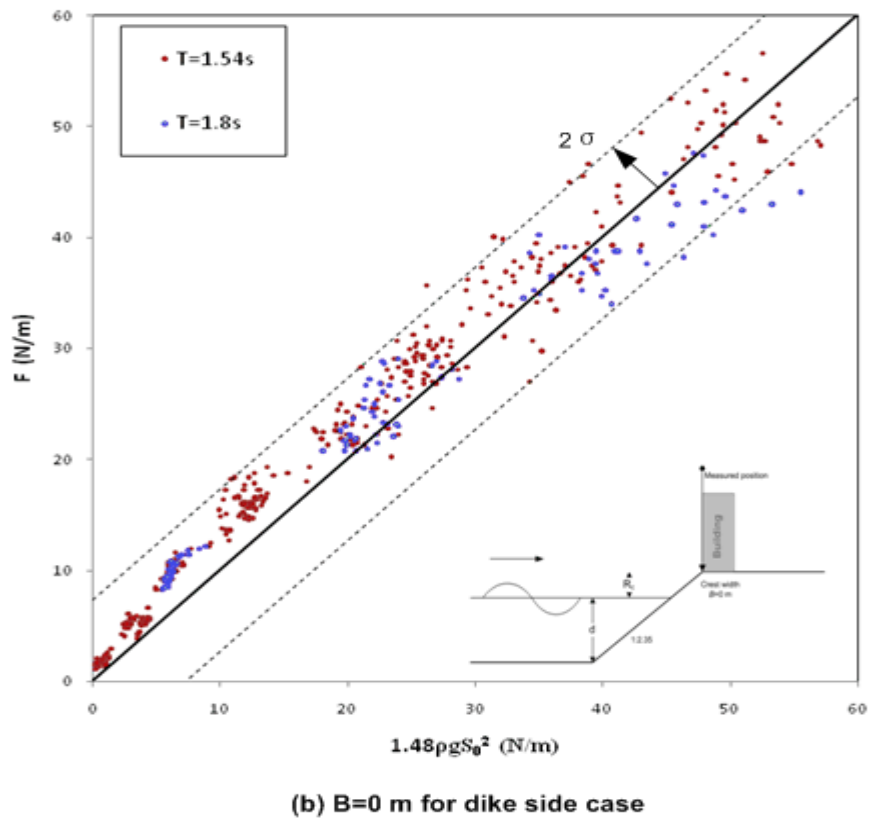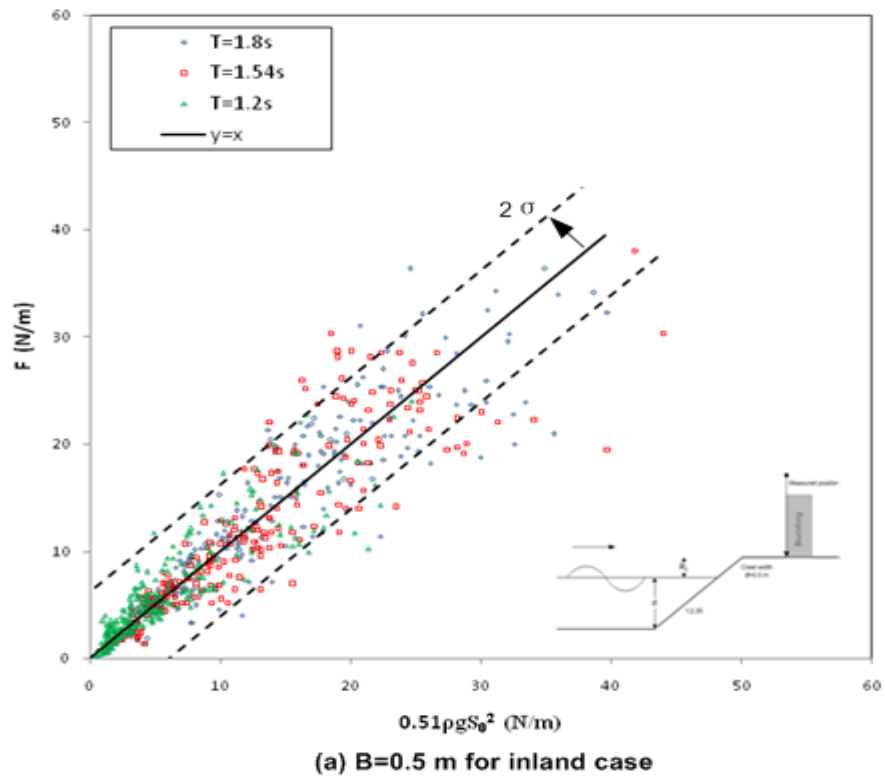
Figure 5.13   Overtopping wave force versus Equation 5.13, (a) inland case, (b) dike side case.

5.4.2.2 Overtopping wave as a function of mean discharge rate and velocity

Propagation waves do not only carry energy across the ocean surface but momentum as well. Unlike the method of integrating water depth in front of the building, the theoretical investigation will be induced in the aspect of overtopping discharge rate first, after which this approach will be compared with the test data.

According the principle of impulsive momentum conversation, we can apply Equation 5.14, where M is the mass, V is the velocity and t is the impact time.

$$F = \frac{M \cdot V}{t}$$

5.14

Assuming that all the impact time of overtopping waves are the same, then overtopping wave force can be easily rewritten as a function which includes overtopping wave flow velocity and the mean overtopping wave discharge, i.e., Equation 5.15, where q_{max} is the maximum overtopping discharge (referring to Equation 5.16 as already shown in Chapter 2) and C_3 is an unknown coefficient related to the crest width which will be discussed in the following chapter.

$$F = C_3 \rho q_{max} V_0 = C_3 \rho h_0 V_0^2$$

5.15

$$q_{max} = h_0 V_0$$

5.16

In the present study, overtopping discharge and overtopping velocity are not the measurement parameters, therefore these two parameters in front of the building are determined using the formulas developed by *Schüttrumpf (2010)* at the beginning of the dike crest. Details related to Schüttrumpf equations can be found in Chapter 2 (referring to Equation 2.6, 2.7 and 2.8). The final equations for both cases can be referred to Equation 5.17 and Equation 5.18.
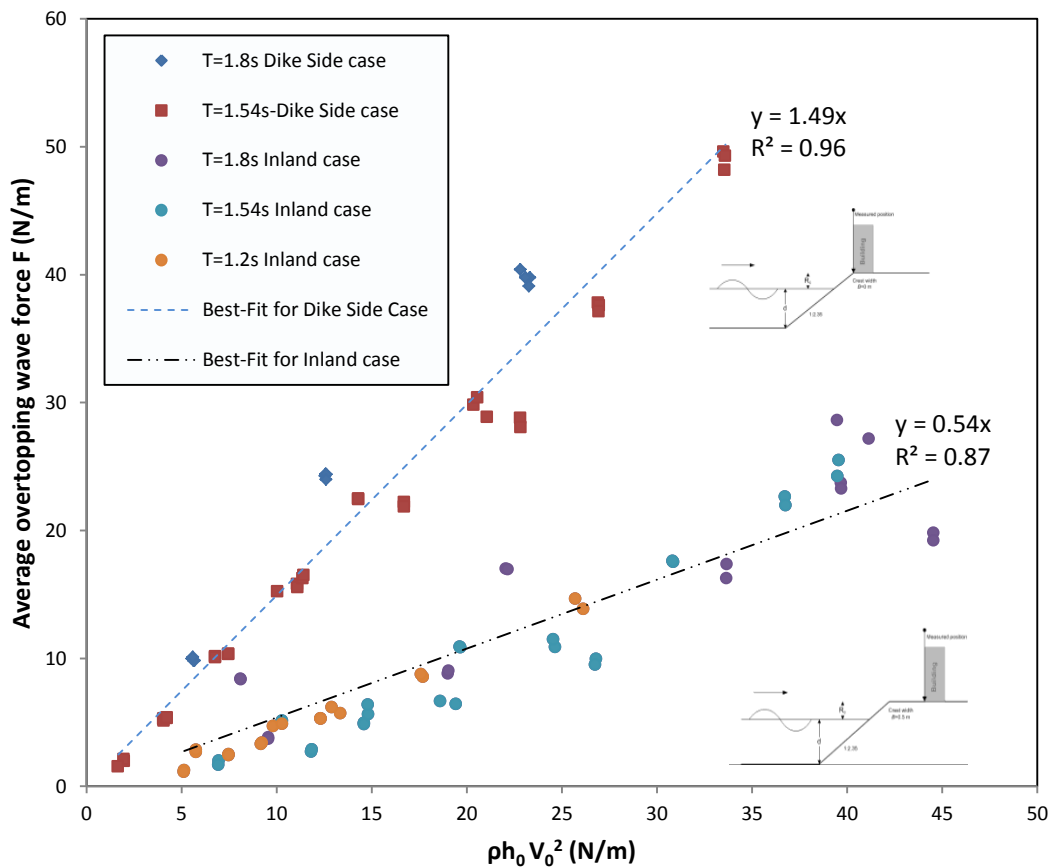
Figure 5.14 Average overtopping wave load versus $\rho h_0 V_0^2$.

$$F = 0.54\rho h_0 V_0^2 \qquad \text{5.17}$$

$$F = 1.49\rho h_0 V_0^2 \qquad \text{5.18}$$

Therefore, the overtopping wave force can be shown as a uniform format as Equation 5.15, where C_3 is the coefficient related to crest width, for the inland case, C_3 is 0.54 while in the dike side, C_3 is 1.49.

5.4.3 Overtopping wave force dimensionless analysis

In the previous two subsections (Section 5.4.1 and Section 5.4.2), the experimental data are analysed directly or indirectly using dimensional method, though a series relationship can be built very well, undeniably, dimensionless parameters can reduce the effect due to different test conditions. Therefore, in this subsection, two new dimensionless parameters are defined based on the findings of the present study; however, its validity should still be researched in the future study.

5.4.3.1 Direct findings from experimental data

In Figure 5.5 and Figure 5.6, two strong relation trends with least scatters were observed, and the analysis in the following is based on these trends. Best-fit curves can be seen in Figure 5.15a for the inland case and Figure 5.15b for the dike side case and the best-fit equations are showed below:

$$\frac{F}{\rho g H_m R_c} = 0.0082 \cdot \left(\frac{R_c}{H_m \xi}\right)^{-2.24} \qquad \text{5.19}$$

$$\frac{F}{\rho g H_m R_c} = 0.025 \cdot \left(\frac{R_c}{H_m \xi}\right)^{-2.15} \qquad \text{5.20}$$

Compared with Equation 5.19 and Equation 5.20, the exponents of the term $\dfrac{R_c}{H_m \xi}$ in the right hand side of the both equations are around -2.2, there is no big difference. For the inland case, the constant is 0.0082, while for the dike side case, the constant is about 0.025. The ratio of the two constants between the two cases is 3 which are in line with previous findings (Equation 5.11/5.12 and Equation 5.17/5.18). A uniform equation to describe the dimensionless parameters is named as Equation 5.22, where C_4 is the undefined constant related to the width of the crest, for the inland case, C_4 is 0.0082; for the dike side case, C_4 is 0.025.

$$\frac{F}{\rho g H_m R_c} = C_4 \cdot \left(\frac{R_c}{H_m \xi}\right)^{-2.2} \qquad \text{5.21}$$

5.4.3.2 Physical meaning of dimensionless overtopping wave force

The left hand part of Equation 5.21 is named as dimensionless overtopping wave force F^*, referring to Equation 5.22, where F is the average overtopping wave force, $\rho g H_m^2$ is the average incident wave energy and $\dfrac{R_c}{H_m}$ is the freeboard divided by the wave used for determining the interaction between the waves and dike crest height.

The use of the wave energy and the ratio of freeboard and wave height provide part of the incident wave energy above the still water level; and this part of energy above the still water level could be transmitted and contribute to the overtopping wave impacting on the structure.

$$F^* = \frac{F}{\rho g H_m^2 \cdot \left(\dfrac{R_c}{H_m}\right)} \qquad \text{5.22}$$

The right hand part of Equation 5.21 is named as dimensionless freeboard R_c^*, referring to Equation 5.23. Equation 5.21 can be rewritten as Equation 5.24.

$$R_c^* = \frac{R_c}{H_m \xi}$$
5.23

$$F^* = C_4 \cdot (R_c^*)^{-2.2}$$
5.24

As mentioned in Section 5.4.3.1, the coefficient C_4 in Equation 5.24 is the undefined constant related to the width of dike crest. In the present study, though only two configurations were explored, the influence of dike crest width is obvious. As for C_4 for example, it is also a dimensionless form and it could also have the format of a crest width divided by wave length $\frac{B}{L}$. However, the coefficient C_4 can not be discovered in the present study due to the limited configurations. So in future study, the relationship between crest width and wave length should be considered under a wide range of changes of the dike crest.
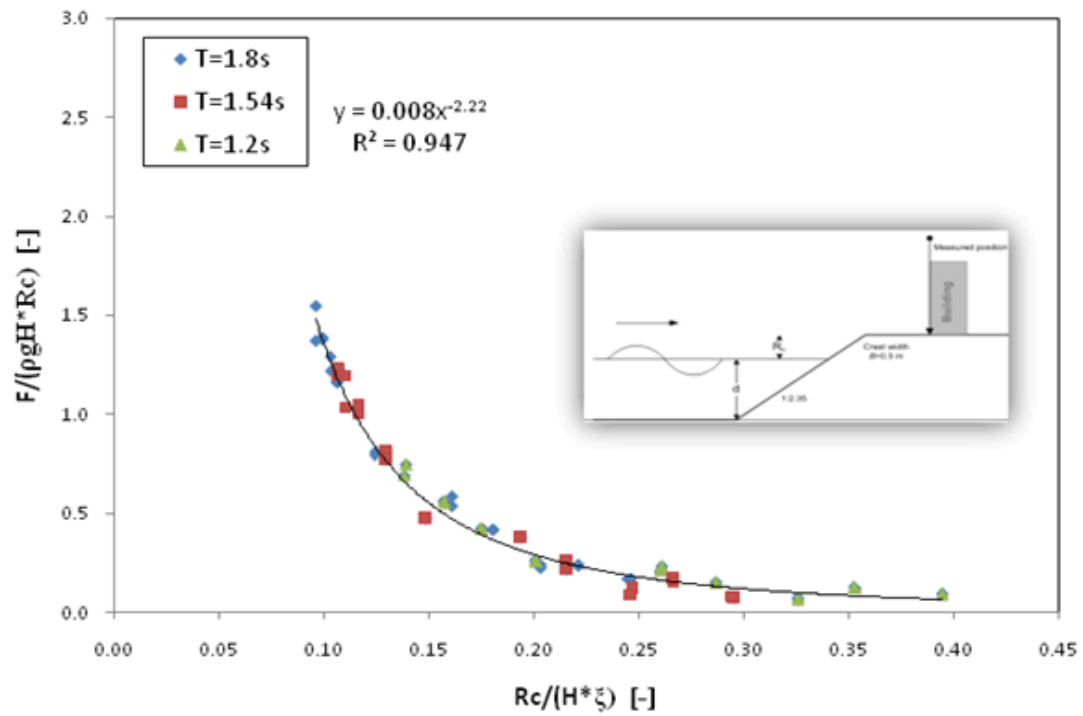
(a) B=0.5 m for inland case
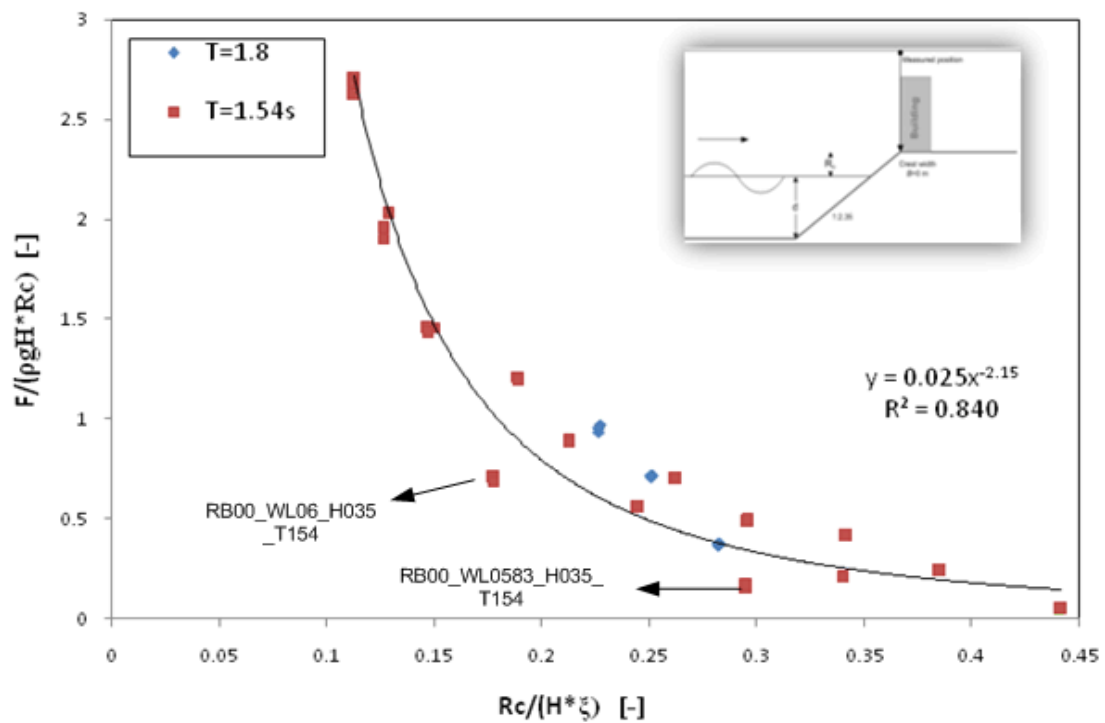
(b) B=0 m for dike side case

Figure 5.15   Dimensionless overtopping wave force versus dimensionless freeboard.

5.5 Summary

Within zone 5, the overtopping wave force is directly proportional to the overtopping wave momentum flux obtained by integrating the maximum water depth in front of the vertical plane for the inland case and the dike side case. The coefficients of these two cases are almost the same around 0.33.

When building the relationship between the overtopping wave force and the incident wave and the dike geometrical characteristics, three different approaches were applied. The reduction effect of crest width on the overtopping wave force is significant. From the ratio of the coefficients (the inland case is divided by the dike side case) of each approach is always around 0.35. That means that with the same incident wave characters, the overtopping wave force could be reduced by 65% due to the influence of the crest width in the present study.

6 Discussion

6.1 Introduction

In this chapter, the discussion is divided into two parts. In Section 6.2, the equations related to the overtopping wave force obtained from Chapter 5 are discussed. Then in Section 6.3, a short summary is given.

6.2 Discussion about the experimental results

Table 6.1 shows the four equations built based on the regular wave test data.

Equation 5.6 is built on the concept of maximum wave momentum flux defined firstly by *Hughes (2004)*, the least scatter for both cases shows that the method of integrating the maximum water depth in front of the vertical plane is useful for the estimation the overtopping wave force. In Equation 5.6, h is the maximum wave surface elevation in front of the plane.

Equation 5.13 is the extension of Equation 5.6 by the substituting the relation between the overtopping wave tongue at the beginning of the crest dike and maximum surface elevation h.

Equation 5.15 is applied the momentum conversation theory by the assumption that the duration of the overtopping wave loading on the plane is a constant for all the overtopping wave events. All the parameters related to incident overtopping wave velocity and layer thickness is using the formulas developed by *Schüttrumpf (2010)*. In Equation 5.15, q_0 is the overtopping discharge rate, and V_0 and h_0 are the velocity and layer thickness at the beginning of the crest.

Equation 5.21 is developed directly on the test data. It describes a relationship between the dimensionless overtopping wave force and dimensionless relative freeboard. In Equation 5.21, H_m is the average incident wave height, R_c is the freeboard and ξ is the Iribarren number.

The discussion related these four equations are shown in the following subsections.

Table 6.1 Equations for overtopping wave force on the building

Equations for overtopping wave force		coefficients	Coefficient Ratios of Inland / dike side
Equation 5.6	$F_{\max} = c_1 \rho g h^2$	C_1=0.33 for both cases	1
Equation 5.13	$F_{\max} = c_2 \rho g \left[H_m \cdot (1 - \frac{R_c}{R_u}) \right]^2$	C_2=1.48 with B=0 m C_2=0.51 with B=0.5 m	0.34
Equation 5.15	$F_{\max} = c_3 \rho q_{0\max} V_0 = c_3 \rho h_0 V_0^2$	C_3=1.49 with B=0 m C_3=0.54 with B=0.5 m	0.36
Equation 5.21	$\dfrac{F}{\rho g H_m R_c} = C_4 \cdot (\dfrac{R_c}{H_m \xi})^{-2.2}$	C_4=0.025 with B=0 m C_4=0.0082 with B=0.5 m	0.328

6.2.1 The maximum wave momentum flux (Equation 5.6)

The argument related to the validity of the maximum wave momentum flux near shore to the

overtopping waves in front of the vertical plane has been discussed in Section 5.4.1. In this section, the finding will be discussed focused on the coefficient 0.33 in Equation 5.6.

In the present study, all the waves are non-breaking waves. Estimation of non-breaking wave forces on vertical walls is largely theory with some empirical adjustments by many researchers.Theoretically, for the wave force exerted on a vertical plane by non-breaking wave can be seen a kind of quasi-static force. Its dynamic pressure is hydrostatic between wave through and wave crest, in the present study, the dynamic pressure of the run-up wave along the vertical plane is ρgh. The dynamic wave force has the same format with hydrostatic force, refer to Figure 6.1a.

However, the test result shows the coefficient is not 0.5, but around 0.33 for average overtopping wave force. The reason can be explained that during the process of the water runs up along the vertical force, the highest vertical extent of the wave with much of thin jet-like crest, is almost in free fall and thus contributing little or nothing to the horizontal force *(ASCE,1995).*

According to the knowledge of gravity centre of triangular, it can be assumed that the water weight around the gravity centre would contribute to the horizontal force. In Figure 6.1b, the gravity centre locates at the position 1/3 h from the base of plane, so its dynamic pressure should be 2/3 ρgh. Using rectangular integral method to estimate the force, the coefficient is about 0.44. Other methods in details are shown in Figure 6.1c and 6.1d.

For the fourth method presented in Figure 1d, it has a similar coefficient with the experimental results. The hatch area is within the surface envelop when the surface is a curve which is quite approaching to the actual run-up wave situation.

Therefore, C_1 in Equation 5.6 might be a kind of contribution coefficient related the shape, surface angle et al of incoming overtopping wave. However, the theoretical and experimental investigation still need be done to explore the water run-up behaviour in front of the vertical plane without water depth like the two cases in the present study configuration.

$$F = \frac{1}{2}\rho gh^2$$

(a) Theoretical sketch for run-up wave force

$$F = \frac{4}{9}\rho gh^2 \approx 0.44\rho gh^2$$

(b) Rectangular integral method for gravity center pressure

$$F = \frac{7}{18}\rho gh^2 \approx 0.38\rho gh^2$$

(c) The third method for overtopping run-up wave force

$$F = \frac{1}{3}\rho gh^2 \approx 0.33\rho gh^2$$

(d) The fourth method for overtopping run-up wave force
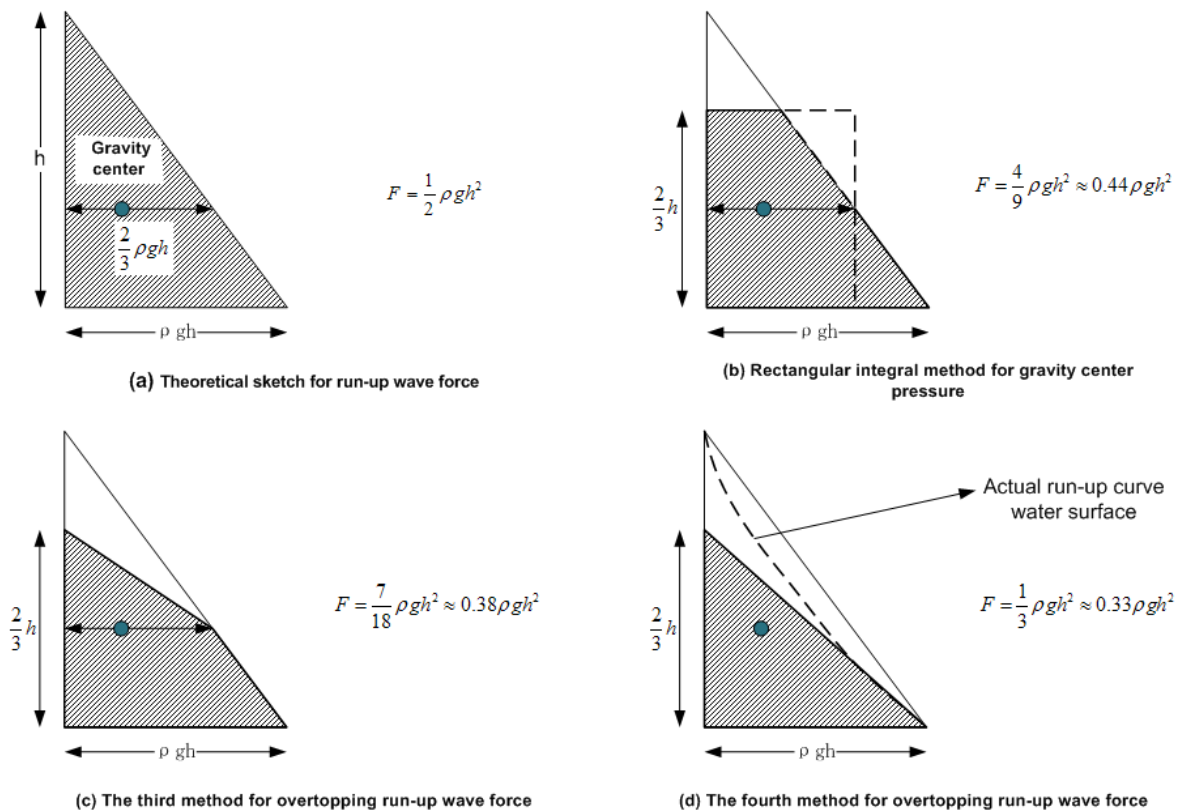
Figure 6.1   Sketches for different overtopping force estimation methods

6.2.2 Force and wave tongue method (Equation 5.13)

Based on Equation 5.6 which does not depend on the incident wave characters, the concept of overtopping wave tongue was introduced to explore the relation between incident wave and overtopping loadings. The R_u in Equation 5.13 is a non-realistic parameter in the present study for the dike slope is not infinite. Therefore the formula of R_u is applied with the findings by *Schüttrumpf (2001).* Note that different regular wave run up formula will cause different coefficient C_2.

For dike side case with 0 m crest width, the C_2 is 1.48, while for inland case, C_2 is 0.51. The ratio between them is about 3 which means due to the influence of wide crest, the overtopping wave force on the building will reduce nearly 65%.

In Section 5.4.2.1, a relative lower level of correlation between the predictions and observations of the individual overtopping wave loadings was found in inland case compared with dike side case, even for average events. Though average value can decrease the scatters to obtain the least scatter tend, it can be observed the difference among tends line with different periods (i.e., refer to Figure 5.13). And the repeatability of inland case is also lower than that of dike side case; this can be seen from the test matrix in Appendix 1.

In the inland case, for the shortest wave with T=1.2s, the overtopping wave will meet the returned flow caused by the reflection of previous one on the vertical plain (refer to Section 4.2) on the crest, as for T=1.8s, the longest wave would give enough time for the return flow on the crest flowing back to the slope or wave flume, which caused the incoming wave and return flow meet below the crest (or on the slope), whereas for the case T=1.54s, the convergent of the overtopping wave just between the previous two wave condition.

The meeting of the two directional wave and return flow will cause the loss of overtopping wave energy and reduce the velocity for the incoming wave landwards. This influence is more obvious for the short wave which is in line with the test results. Therefore, for short waves, the overtopping wave loading is smaller than longer wave. When the meeting occurs near the crest edge or on the slope, due the influence of this return flow, the incoming wave will collapse on this flow layer, which cause lots of air leakage or air content in water. This phenomenon might decrease the energy included in the original overtopping waves.

Therefore, the reduction ratio 65% found by Equation 5.13 is not the entire influence caused by the width of the crest, but also the reflected flows. As for this influence of reflected flow in detail, the present study is not considered.

Equation 5.13 is based on the regular wave condition, but also has a good validity for irregular wave condition tested in present study. The irregular wave test analysis can be found in Appendix 2.

In the future study, the water layer on the crest should be considered as an influence factor, not only for its positive effect on the overtopping loadings for reducing the roughness of the dike, but also its negative effect for interruption of the incoming waves. The response of overtopping waves to three kinds of water layer behaviors should be discovered, one is the static water layer on the crest, one is the relative small overtopping wave flowing to the wall (can be seen a moving landwards water layer) which will be caught up by the next incoming overtopping wave, and the last situation can be modeled as the meeting of the returning flows and the overtopping waves at the different positions on the crest.

In summary, Equation 5.13 could be seen as the rewritten format of Equation 5.6 and has certain validity for irregular test. And more proof should be given in the future study.

6.2.3 Force and momentum change rate (Equation 5.15)

Unlike Equation 5.13, the relation between the overtopping wave loading and wave characters is only based on momentum conservation theory by using overtopping discharge mass flux and its velocity. The overtopping wave thickness at the crest edge and its velocity are determined by the empirical formulas given by *Schüttrumpf (2001)*. The reduction ratio for these two cases is quite similar with Equation 5.13 (refer to Table 6.1). In this equation, it is assumed that the velocity and water layer

thickness is not changed on the dike crest when overtopping wave event occurs.

About the discussion of this finding, mainly effort is focus on the validity of formula applied from *Schüttrumpf (2001)*. There are obvious scatters observed for long wave, that's due to the different waver layer thickness determination method according to the incoming breaker parameters and dike slope. In this case, the calculation is based on the slope 1:3 in the findings of *Schüttrumpf (2001)*. In details can be seen the calculation method for overtopping wave thickness at the edge of crest in *Schüttrumpf (2001)*. So the coefficient in this Equation should be recalculated when the dike slope is smaller than 1:3.

6.2.4   Dimensionless overtopping wave force (Equation 5.21)

Correlations between dimensionless overtopping wave force and dimensionless freeboard in experiments are obtained. In the present study, for the inland case, the test range of wave length is larger than the dike side case, while for the dike side case, the test freeboard and wave height range is larger than inland case. In Figure 5.15, for the inland case, most of the data give a least scatter, the R_c range is from 0.025 m to 0.058 m, wave periods is from 1.2 s to 1.8 s and the incident wave height is changing from 0.1 m to 0.05 m. For the dike side case, the R_c is from 0.025 m to 0.075 m wave period is mainly on 1.54 s, incident wave height is changing from 0.08 m to 0.035 m. The low wave height leads to scatters for the dike side case. It appears that Equation 5.21 is suitable for larger wave height.

For the dike side case, the sample capacity is small compared with the inland case, more tests should be done with large range of wave period and wave height. As for the coefficient C_4 which is also a dimensionless form coefficient, but should be determined in future study under more configurations.

6.3 Summary

Equation 5.6 and Equation 5.13 can estimate the overtopping wave force very well in the present study. By supporting from the theoretical concept of maximum wave momentum flux, these two equations are more suitable than Equation 5.15 and Equation 5.21.

For Equation 5.15, it also gives a method to estimate the overtopping wave force, but the coefficient should be calibrated in the experiment for specific dike configuration, the calibration work didn't done in the present study, therefore the suitability should still be verified.

Equation 5.21 gives a dimensionless function to describe the relation between overtopping wave force and freeboard. The coefficient could be dimensionless in the form of B/L; however this is still to be determined further. In future study, more configurations with variation of the changes of the dike crest width need to be tested.

7 Conclusion and Recommendation

In this study, physical model tests were executed on a schematized model scaled 1/30. The aim was to come up with a relationship describing the force on a vertical plane exerted by the overtopping water as a function of wave parameters and geometrical characteristics. Due to time constraints, only two configurations: the inland case and the dike case were explored and the number of tests had to be restricted. So only a limited number of parameters could be varied. Despite these restrictions, the experiments revealed the most important mechanism of the impact process.

The overtopping wave force could directly be related to the overtopping wave momentum flux, resulting in a simple formulation for the prediction of it. A new dimensionless overtopping wave force parameter is also developed; the least scatter for this parameter gives a rather good potential suitability for force prediction especially with the conditions of large incident wave height impact on relative low freeboard; From a theoretical point of view, it is important to increase the test range to investigate the parameters and further research the physical meaning of the dimensionless parameters.,

The reduction effect for crest width with 0.5 m is about 65%. Due to the fact that only two widths crest were tested in the present study, the relationship between the width and overtopping wave force could not be presented. Therefore, in the future study, for the same scale model, variation of the width of crest should be increased and the effect of the crest width could be found out.

Recommendation could include testing instruments for more than 8 pressure sensors to be distributed on the surface of the vertical plane with small spaces between two sensors. The load cell and pressure sensors should be sampled with a high sample frequency (~1 kHz), to be able to catch the peak values during a very short time.

In order to investigate the overtopping wave crest elevation propagation on the crest, at least two more wave probes should be equipped, or other, more accurate instruments such as laser could be used. This is crucial to expand the findings of the present study in the future. The record for the water surface on the wall should be measured more accurately and its time series should be measured with the same sample frequency of pressure and force.

For other recommendations, the findings in the present study can be compared with other datasets, and using the results to analyses forces on buildings and actual damage to buildings.

Reference

Andreas, D. B. (2010). *Wave forces on vertical (Golfkrachten op verticale structuren op de zeedijk).* Msc thesis of VUB-Vrije Universiteit Brussel.

ASCE. (1995). *Wave forces on inclined and vertical wall structures.*

National Hurricane Centre. (2010, 12 6). *Storm Surge Overview.* Opgehaald van National Hurricane Center: http://www.nhc.noaa.gov/surge/

EurOTop. (2007). *EurOTop: Wave Overtopping of Sea Defences and Related Structures: Assessment Manual.*

FEMA. (2005). *Guidelines and Specification for Flood Hazard Mapping Partners Section D.4.5 Wave Setup, Runup, and Overtopping.*

FEMA. (2006). *Hurricane Katrina in the Gulf Coast (FEMA 549).* Washington DC: Federal Emergency Management Agency.

Hughes, S. A. (2004). Estimation of wave run-up on smooth, impermeable slopes using the wave momentum flux parameter. *Coastal Engineering* , pp. 1085-1104.

Hughes, S. A. (2004). Wave momentum flux parameter: a descriptor for near shore waves. *Coastal Engineering, pp. 1067-1084*

Hughes, S.A., and Nadal, N. (2009). Laboratory study of combined wave overtopping and storm surge overflow if a levee. *Coastal Engineering* , 244-259.

Jeremy Lowe, W. A., John Alderson, Tim Pullen, Jo Wright, Nick Dodd. (2006). Coastal Inundation-Modelling of wave Overtopping Bore Heights and Velocities.

J. Wilson, R. Gupta, J. van de Lindt, M. Clauson, and R. Garcia,(2009)"Behavior of a One-Sixth Scale

Wood-Framed Residential Structure under Wave Loading," J. of Performance of Constructed Facilities, Vol.23, No.5, pp. 336-345.

Kester, D. v. (2009). *spatial distribution of wave overtopping.* Master thesis of TU Delft.

GKVP. (2011).*Geïntegreerd Kustveiligheidsplan: Masterplan Kustveiligheid.* Coastal Division of the Agency for Maritime and Coastal Services (MDK). Document Ref: 5195-505-088-07, Dated: 27/01/11, Version 9.

Linham, M. a. (2010). *Technologies for Climate Change Adaptation: Coastal erosion and flooding.* TNA Guidebook Series. UNEP/GEF.

Linham, M. M., & Nicholls, R. J. (2010). *Sea dikes.* Opgehaald van Climate Tech Wiki: http://climatetechwiki.org/content/sea-dikes

Lioutas, A. C. (2010). *Experimental research on spatial overtopping of overtopping.* Master thesis of TU Delft.

Longuet-Higgins, M. (1964). Radiation stresses in water waves:a physical discussion, with applications. *Deep-Sea Research* , 529-562.

Cox, J.C and Machemehl, J (1986). Overload Bore Propagation Due to An Overtopping Wave. Waterway, Port, Coastal and Ocean Engineering, 112(1), 3.

Mansard, E., & Funke, E. (1980). The measurement of incident and reflected spectra using a leastsquare method. *ICCE'80* (pp. 154-172). Sydney: ASCE.

Martin, F. L., Losada, M. A., & Medina, R. (1999). Wave loads on rubble mound breakwater crown walls. *coastal engineering* , 149-174.

McConnell, K.J., Kortenhaus, A. (1997). Analysis of pressure measurements from hydraulic model tests and prototype measurements. Proceedings 1st Overall Project Workshop, MAST III, PROVERBS-Project, Annex C3.

Nistor, I., Palermo, D., Nouri, Y., Murty, T., & Saatcioglu, M. (2009). Tsunami-Induced Forces on

Structures. In *Handbook of Coastal and Ocean Engineering* (pp. 261-286).

Noguchi, K., & Sato, S. (sd). Large-Scale Physical Model Test on Tsunami Overtopping and Bed Scour Around Coastal Revetment. 597-604.

Schüttrumpf, H. F. (2001). *Wellenüberlaufströmung bei Seedeichen-Experimentelle und Theoretische Untersuchungen. PhD thesis.* http://www.biblio.tu-bs.de/ediss/data/20010703a/20010703a.html.

Schüttrumpf, H., & Oumeraci, H. (2005). Layer thicknesses and velocities of wave overtopping flow at seadikes. *Coastal Engineering* , pp. 473-495.

Suzuki, T. (2011). *Wave Dissipation Over Vegetation Fields.* PhD thesis of TU Delft.

USACE. (1990). *Wave Force on a Wall Shoreward of the Still Water Level.* Vicksburg: Costal Engineering Research Centre.

Van Broekhoven, P. (2011). *The influence of armour layer and core permeability on the wave run-up.* Delft: Master of science thesis.

Verwaest, T. (2006). Coastal flooding risk calculations for the Belgian coast.

Verwaest, T., Vanpoucke, P., Willems, M., & Mulder, T. D. (2010). Waves overtopping a wide-crested dike. *Coastal Engineering 2010*, (pp. 1-9).

Appendix 1 Test Matrix

Table A.1 Average event of a wave train for the inland case

Test code	R_c	H_m	T_o	T	L	Ir	h_1	h_2	F_{max}
RB50_WL_06_H08_T180_1	0.025	0.073	1.823	1.8	5.054	3.322	0.075	0.09	28.611
RB50_WL_06_H08_T180_2	0.025	0.074	1.824	1.8	5.054	3.314	0.077	0.089	27.16
RB50_WL_06_H075_T180_1	0.025	0.069	1.823	1.8	5.054	3.433	0.067	0.085	23.723
RB50_WL_06_H075_T180_2	0.025	0.069	1.826	1.8	5.054	3.435	0.067	0.084	23.272
RB50_WL_06_H07_T180_1	0.025	0.064	1.825	1.8	5.054	3.55	0.065	0.075	19.802
RB50_WL_06_H07_T180_2	0.025	0.064	1.823	1.8	5.054	3.551	0.063	0.075	19.202
RB50_WL_06_H065_T180_1	0.025	0.06	1.796	1.8	5.054	3.677	0.057	0.066	17.016
RB50_WL_06_H065_T180_2	0.025	0.06	1.796	1.8	5.054	3.677	0.059	0.068	16.95
RB50_WL_06_H05_T180_1	0.025	0.044	1.834	1.8	5.054	4.271	0.051	0.046	8.358
RB50_WL_06_H05_T180_2	0.025	0.044	1.834	1.8	5.054	4.271	0.05	0.045	8.391
RB50_WL_0583_H08_T180_1	0.042	0.074	1.84	1.8	5.054	3.31	0.057	0.072	16.266
RB50_WL_0583_H08_T180_2	0.042	0.074	1.841	1.8	5.054	3.309	0.061	0.074	17.35
RB50_WL_0583_H065_T180_1	0.042	0.059	1.844	1.8	5.054	3.707	0.046	0.05	8.792
RB50_WL_0583_H065_T180_2	0.042	0.059	1.844	1.8	5.054	3.71	0.046	0.051	9.025
RB50_WL_0583_H05_T180_1	0.042	0.047	1.798	1.8	5.054	4.164	0.036	0.034	3.837
RB50_WL_0583_H05_T180_2	0.042	0.047	1.797	1.8	5.054	4.167	0.034	0.032	3.687
RB50_WL_0567_H08_T180_1	0.058	0.075	1.816	1.8	5.054	3.285	0.048	0.061	9.943
RB50_WL_0567_H08_T180_2	0.058	0.075	1.815	1.8	5.054	3.284	0.051	0.061	9.509
RB50_WL_0567_H065_T180_1	0.058	0.061	1.81	1.8	5.054	3.633	0.044	0.043	4.938
RB50_WL_0567_H065_T180_2	0.058	0.061	1.801	1.8	5.054	3.651	0.045	0.043	4.855
RB50_WL_06_H08_T154_1	0.025	0.069	1.544	1.54	3.7	2.934	0.074	0.07	17.532
RB50_WL_06_H08_T154_2	0.025	0.069	1.543	1.54	3.7	2.935	0.07	0.07	17.603
RB50_WL_06_H065_T154_1	0.025	0.055	1.542	1.54	3.7	3.277	0.057	0.057	10.855
RB50_WL_06_H065_T154_2	0.025	0.055	1.542	1.54	3.7	3.275	0.06	0.057	10.898
RB50_WL_06_H05_T154_1	0.025	0.042	1.539	1.54	3.7	3.754	0.031	0.037	5.138
RB50_WL_06_H05_T154_2	0.025	0.042	1.536	1.54	3.7	3.753	0.031	0.038	4.941
RB50_WL_06_H95_T154_1	0.025	0.081	1.544	1.54	3.7	2.702	0.065	0.082	25.48
RB50_WL_06_H95_T154_2	0.025	0.081	1.544	1.54	3.7	2.7	0.066	0.085	24.237
RB50_WL_06_H09_T154_1	0.025	0.077	1.546	1.54	3.7	2.774	0.067	0.082	22.642
RB50_WL_06_H09_T154_2	0.025	0.077	1.546	1.54	3.7	2.774	0.07	0.086	21.965
RB50_WL_0583_H08_T154_1	0.042	0.07	1.544	1.54	3.7	2.912	0.059	0.062	10.884
RB50_WL_0583_H08_T154_2	0.042	0.07	1.543	1.54	3.7	2.908	0.059	0.063	11.476
RB50_WL_0583_H065_T154_1	0.042	0.056	1.538	1.54	3.7	3.242	0.036	0.042	5.632
RB50_WL_0583_H065_T154_2	0.042	0.056	1.538	1.54	3.7	3.24	0.035	0.042	6.381
RB50_WL_0583_H05_T154_1	0.042	0.043	1.539	1.54	3.7	3.7	0.023	0.026	2.005
RB50_WL_0583_H05_T154_2	0.042	0.043	1.538	1.54	3.7	3.7	0.024	0.026	1.68

Continue from previous page

RB50_WL_0567_H08_T154_1	0.058	0.07	1.542	1.54	3.7	2.899	0.041	0.05	6.663
RB50_WL_0567_H08_T154_2	0.058	0.071	1.542	1.54	3.7	2.894	0.042	0.053	6.437
RB50_WL_0567_H065_T154_1	0.058	0.058	1.538	1.54	3.7	3.209	0.027	0.033	2.71
RB50_WL_0567_H065_T154_2	0.058	0.058	1.543	1.54	3.7	3.202	0.026	0.031	2.866
RB50_WL_06_H08_T120_1	0.025	0.062	1.207	1.2	2.246	2.412	0.038	0.051	8.56
RB50_WL_06_H08_T120_2	0.025	0.062	1.207	1.2	2.246	2.406	0.039	0.05	8.744
RB50_WL_06_H065_T120_1	0.025	0.05	1.207	1.2	2.246	2.68	0.035	0.038	5.289
RB50_WL_06_H065_T120_2	0.025	0.05	1.207	1.2	2.246	2.682	0.033	0.04	5.268
RB50_WL_06_H05_T120_1	0.025	0.038	1.205	1.2	2.246	3.076	0.025	0.026	2.504
RB50_WL_06_H05_T120_2	0.025	0.038	1.205	1.2	2.246	3.077	0.025	0.026	2.418
RB50_WL_06_H10_T120_1	0.025	0.08	1.205	1.2	2.246	2.121	0.052	0.07	13.86
RB50_WL_06_H10_T120_2	0.025	0.079	1.205	1.2	2.246	2.137	0.051	0.067	14.67
RB50_WL_0583_H08_T120_1	0.042	0.064	1.204	1.2	2.246	2.372	0.032	0.039	5.71
RB50_WL_0583_H08_T120_2	0.042	0.063	1.207	1.2	2.246	2.381	0.031	0.04	6.175
RB50_WL_0583_H065_T120_1	0.042	0.053	1.202	1.2	2.246	2.615	0.027	0.029	3.39
RB50_WL_0583_H065_T120_2	0.042	0.053	1.202	1.2	2.246	2.61	0.025	0.029	3.292
RB50_WL_0583_H05_T120_1	0.042	0.041	1.2	1.2	2.246	2.968	0.019	0.02	1.241
RB50_WL_0583_H05_T120_2	0.042	0.041	1.2	1.2	2.246	2.967	0.019	0.019	1.112
RB50_WL_0567_H08_T120_1	0.058	0.066	1.202	1.2	2.246	2.329	0.027	0.032	4.696
RB50_WL_0567_H08_T120_2	0.058	0.067	1.202	1.2	2.246	2.323	0.026	0.032	4.879
RB50_WL_0567_H065_T120_1	0.058	0.053	1.202	1.2	2.246	2.601	0.02	0.022	2.677
RB50_WL_0567_H065_T120_2	0.058	0.053	1.202	1.2	2.246	2.601	0.02	0.022	2.85

Table A.2 Average event of a wave train for the dike side case

Test Code	H_m	T_m	T_0	L_0	Ir	R_c	F_{max}	h_2
RB00_WL0567_H08_T180_1	0.072	1.792	1.800	5.054	3.569	0.058	39.489	0.117
RB00_WL0567_H08_T180_2	0.072	1.793	1.800	5.054	3.571	0.058	41.142	0.114
RB00_WL0567_H08_T180_3	0.071	1.791	1.800	5.054	3.583	0.058	39.680	0.112
RB00_WL0567_H08_T180_4	0.072	1.793	1.800	5.054	3.576	0.058	39.701	0.114
RB00_WL0567_H065_T180_1	0.058	1.791	1.800	5.054	3.963	0.058	44.557	0.083
RB00_WL0567_H065_T180_2	0.058	1.791	1.800	5.054	3.965	0.058	44.557	0.081
RB00_WL0567_H065_T180_3	0.058	1.791	1.800	5.054	3.962	0.058	22.057	0.082
RB00_WL0567_H065_T180_4	0.058	1.791	1.800	5.054	3.962	0.058	22.167	0.083
RB00_WL0567_H05_T180_1	0.046	1.790	1.800	5.054	4.462	0.058	8.122	0.044
RB00_WL0567_H05_T180_2	0.046	1.800	1.800	5.054	4.448	0.058	8.109	0.043
RB00_WL0567_H05_T180_3	0.046	1.790	1.800	5.054	4.452	0.058	33.658	0.044
RB00_WL0567_H05_T180_4	0.046	1.790	1.800	5.054	4.456	0.058	33.679	0.044
RB00_WL06_H08_T154_1	0.073	1.539	1.540	3.700	3.027	0.025	19.021	0.123
RB00_WL06_H08_T154_2	0.073	1.540	1.540	3.700	3.026	0.025	19.053	0.121
RB00_WL06_H08_T154_3	0.073	1.540	1.540	3.700	3.025	0.025	9.569	0.121
RB00_WL06_H065_T154_1	0.059	1.538	1.540	3.700	3.377	0.025	9.570	0.087
RB00_WL06_H065_T154_2	0.057	1.522	1.540	3.700	3.438	0.025	26.816	0.087
RB00_WL06_H065_T154_3	0.059	1.538	1.540	3.700	3.377	0.025	26.761	0.088
RB00_WL06_H05_T154_1	0.042	1.516	1.540	3.700	4.015	0.025	14.610	0.061
RB00_WL06_H05_T154_2	0.043	1.538	1.540	3.700	3.936	0.025	14.613	0.061
RB00_WL06_H05_T154_3	0.043	1.538	1.540	3.700	3.935	0.025	30.860	0.061
RB00_WL06_H035_T154_1	0.030	1.538	1.540	3.700	4.757	0.025	30.834	0.035
RB00_WL06_H035_T154_2	0.030	1.538	1.540	3.700	4.753	0.025	19.666	0.035
RB00_WL06_H035_T154_3	0.030	1.538	1.540	3.700	4.752	0.025	19.633	0.035
RB00_WL0583_H08_T154_1	0.074	1.541	1.540	3.700	3.012	0.042	10.298	0.102
RB00_WL0583_H08_T154_2	0.074	1.541	1.540	3.700	3.010	0.042	10.246	0.105
RB00_WL0583_H08_T154_3	0.074	1.541	1.540	3.700	3.011	0.042	39.561	0.105
RB00_WL0583_H065_T154_1	0.058	1.541	1.540	3.700	3.388	0.042	39.497	0.075
RB00_WL0583_H065_T154_2	0.058	1.541	1.540	3.700	3.388	0.042	36.745	0.074
RB00_WL0583_H05_T154_1	0.044	1.541	1.540	3.700	3.907	0.042	36.768	0.045
RB00_WL0583_H05_T154_2	0.044	1.541	1.540	3.700	3.907	0.042	24.659	0.045
RB00_WL0583_H035_T154_1	0.030	1.540	1.540	3.700	4.706	0.042	24.545	0.018
RB00_WL0583_H035_T154_2	0.030	1.542	1.540	3.700	4.710	0.042	14.826	0.018
RB00_WL0567_H08_T154_1	0.073	1.542	1.540	3.700	3.031	0.058	14.805	0.093
RB00_WL0567_H08_T154_2	0.073	1.542	1.540	3.700	3.024	0.058	6.956	0.092
RB00_WL0567_H065_T154_1	0.057	1.542	1.540	3.700	3.416	0.058	6.944	0.059
RB00_WL0567_H065_T154_2	0.058	1.541	1.540	3.700	3.413	0.058	18.614	0.059
RB00_WL0567_H05_T154_1	0.043	1.541	1.540	3.700	3.925	0.058	19.438	0.030
RB00_WL0567_H05_T154_2	0.044	1.541	1.540	3.700	3.924	0.058	11.827	0.029
RB00_WL055_H08_T154_1	0.072	1.540	1.540	3.700	3.053	0.075	11.863	0.078
RB00_WL055_H08_T154_2	0.072	1.540	1.540	3.700	3.054	0.075	17.707	0.080

Continue from previous page

RB00_WL055_H065_T154_1	0.057	1.539	1.540	3.700	3.443	0.075	17.593	0.043
RB00_WL055_H065_T154_2	0.057	1.538	1.540	3.700	3.443	0.075	12.318	0.043
RB00_WL055_H05_T154_1	0.043	1.538	1.540	3.700	3.947	0.075	12.333	0.011
RB00_WL055_H05_T154_2	0.041	1.539	1.540	3.700	4.056	0.075	7.480	X

Table A.3 Individual event of a wave train for the inland case, T=1.8s

Test code	D	h2	h1	H2	Fmax	Fmin
RB50_WL_06_H08_T180_1	0.01529	0.08754	0.06788	0.07225	32.1143	0.3671
	0.0161	0.09826	0.07175	0.08216	30.2792	0.3671
	0.01692	0.09561	0.07547	0.07869	25.875	0.5506
	0.01529	0.10918	0.08654	0.09389	32.2979	0.5506
	0.01705	0.08591	0.06811	0.06886	36.3351	0.3671
	0.01631	0.09181	0.07632	0.0755	28.4441	0.3671
	0.01651	0.10382	0.09296	0.08731	33.9494	0.1836
	0.01563	0.07852	0.0661	0.06289	25.508	0.1836
	0.0138	0.08218	0.06765	0.06838	26.9761	0.3671
	0.01407	0.08062	0.0733	0.06655	22.0213	0.3671
	0.01312	0.07696	0.0767	0.06384	20.9202	0.1836
RB50_WL_06_H08_T180_2	0.01692	0.08517	0.06354	0.06825	30.0957	0.3671
	0.01658	0.0929	0.07601	0.07632	24.9574	0.3671
	0.01651	0.10016	0.09165	0.08365	23.8564	0.3671
	0.01502	0.09568	0.07608	0.08066	32.4814	0.5506
	0.01481	0.1024	0.08584	0.08759	36.3351	0.5506
	0.01427	0.08272	0.07175	0.06845	28.6276	0.3671
	0.01488	0.10776	0.0791	0.09288	34.133	0.3671
	0.0157	0.08707	0.06416	0.07137	19.2686	0.3671
	0.01508	0.08177	0.08081	0.06669	25.3245	0.3671
	0.01434	0.08306	0.07725	0.06872	22.3883	0.3671
	0.01325	0.06413	0.07903	0.05088	21.2872	0.3671
RB50_WL_06_H065_T180_1	0.01413	0.06488	0.06385	0.05075	12.8457	0
	0.01359	0.06583	0.0517	0.05224	19.6356	0
	0.01359	0.06902	0.05928	0.05543	14.8643	0
	0.01332	0.06461	0.05851	0.05129	20.3696	0
	0.01461	0.08225	0.05456	0.06764	18.5345	0
	0.01441	0.06583	0.05773	0.05142	17.4334	0
	0.0142	0.06759	0.05533	0.05339	16.8829	0
	0.01393	0.07017	0.05526	0.05624	20.7366	0
	0.01325	0.06522	0.06974	0.05197	19.2685	0
	0.01264	0.05816	0.05704	0.04552	13.7632	0
	0.01224	0.05627	0.04767	0.04403	12.8457	0
RB50_WL_06_H065_T180_2	0.01319	0.06631	0.06339	0.05312	15.0479	0.1836
	0.01393	0.07499	0.05425	0.06106	18.9016	0.1836
	0.01366	0.07404	0.06617	0.06038	15.9654	0.1836
	0.01386	0.06542	0.05472	0.05156	19.4521	0.1836
	0.01447	0.07641	0.06834	0.06194	18.9016	0.1836
	0.014	0.06983	0.06254	0.05583	17.984	0.1836
	0.01502	0.06732	0.06207	0.0523	16.3325	0
	0.01339	0.06875	0.05479	0.05536	20.0027	0.1836
	0.01312	0.07587	0.06594	0.06275	17.4335	0

Continue from previous page

	0.01285	0.05464	0.05518	0.04179	15.2314	0
	0.01359	0.05783	0.04674	0.04424	11.1942	0.1836
RB50_WL_06_H05_T180_1	0.01129	0.05009	0.05696	0.0388	8.992	0
	0.01162	0.04867	0.05185	0.03705	9.3591	0
	0.01176	0.0467	0.05634	0.03494	8.8085	0
	0.01156	0.04799	0.05866	0.03643	10.6436	0
	0.01162	0.04792	0.05278	0.0363	9.3591	0
	0.01149	0.04765	0.0541	0.03616	8.992	0
	0.0121	0.05172	0.05572	0.03962	10.6436	0
	0.01162	0.05253	0.04031	0.04091	9.1756	0
	0.01068	0.0446	0.04	0.03392	6.6064	0
	0.01068	0.03578	0.05038	0.0251	4.5878	0
	0.00966	0.03327	0.03969	0.02361	4.7713	0
RB50_WL_06_H05_T180_2	0.01129	0.04846	0.05386	0.03717	8.8085	0
	0.01129	0.04446	0.05712	0.03317	8.4415	0
	0.01061	0.04568	0.05293	0.03507	9.1756	0
	0.01149	0.04853	0.0551	0.03704	9.5426	0
	0.01101	0.04907	0.0558	0.03806	10.0931	0
	0.01156	0.04697	0.0462	0.03541	8.625	0
	0.01149	0.04996	0.05402	0.03847	11.7447	0
	0.01142	0.05084	0.04132	0.03942	10.2766	0
	0.01	0.04195	0.04031	0.03195	6.2394	0
	0.00986	0.0353	0.04775	0.02544	4.9548	0
	0.01034	0.03361	0.0407	0.02327	4.4043	0
RB50_WL_06_H075_T180_1	0.01251	0.07892	0.05967	0.06641	31.0133	0.3671
	0.01434	0.09548	0.06424	0.08114	23.8564	0.3671
	0.01373	0.09887	0.06811	0.08514	20.0027	0.5506
	0.01549	0.09046	0.07221	0.07497	29.9122	0.5506
	0.01413	0.10335	0.07926	0.08922	20.9202	0.3671
	0.01468	0.08428	0.06331	0.0696	24.9574	0.3671
	0.01522	0.09812	0.0654	0.0829	29.5452	0.3671
	0.01481	0.07336	0.06323	0.05855	25.3245	0.1836
	0.0138	0.07302	0.06563	0.05922	20.7367	0.3671
	0.01224	0.07092	0.06741	0.05868	18.9016	0.3671
	0.01407	0.06902	0.06377	0.05495	15.7819	0.1836
RB50_WL_06_H075_T180_2	0.01447	0.09378	0.06896	0.07931	23.6729	0.3671
	0.0157	0.08333	0.06757	0.06763	20.7367	0.1836
	0.01441	0.09188	0.06927	0.07747	23.6729	0.3671
	0.01502	0.09873	0.07128	0.08371	22.7553	0.3671
	0.01468	0.08958	0.07066	0.0749	24.5904	0.5506
	0.01522	0.08456	0.06943	0.06934	24.4069	0.5506
	0.01441	0.09663	0.07167	0.08222	34.3165	0.1836
	0.01468	0.07709	0.07012	0.06241	24.0399	0.1836
	0.01359	0.07194	0.0613	0.05835	22.3883	0.3671

Continue from previous page

	0.01366	0.07343	0.05797	0.05977	19.0851	0.1836
	0.01312	0.06027	0.06021	0.04715	16.3325	0.1836
RB50_WL_06_H07_T180_1	0.01427	0.07594	0.0575	0.06167	22.5717	0.367
	0.01468	0.07601	0.07291	0.06133	18.5345	0.367
	0.01346	0.08225	0.06416	0.06879	25.3244	0.367
	0.01407	0.08551	0.06672	0.07144	19.6356	0.367
	0.01461	0.07451	0.06741	0.0599	20.3696	0.367
	0.01373	0.07289	0.06161	0.05916	19.2685	0.1835
	0.01468	0.08849	0.07454	0.07381	25.3244	0.1835
	0.01373	0.06956	0.06277	0.05583	22.0212	0.1835
	0.01359	0.07038	0.05983	0.05679	16.5159	0.1835
	0.01291	0.06814	0.06029	0.05523	15.0478	0.367
	0.01196	0.05925	0.06331	0.04729	13.2127	0.1835
RB50_WL_06_H07_T180_2	0.01427	0.08232	0.05262	0.06805	20.7366	0.1835
	0.0142	0.0775	0.06633	0.0633	16.1489	0.367
	0.01291	0.07892	0.05758	0.06601	22.2047	0.1835
	0.01502	0.08625	0.07066	0.07123	22.2047	0.1835
	0.01319	0.08517	0.07516	0.07198	20.7366	0.367
	0.01468	0.07072	0.06284	0.05604	21.6542	0.1835
	0.01386	0.07519	0.06323	0.06133	21.4707	0.367
	0.01393	0.07533	0.07392	0.0614	20.1861	0.1835
	0.014	0.07248	0.05487	0.05848	17.984	0.1835
	0.01325	0.06529	0.05549	0.05204	15.0478	0.1835
	0.01271	0.05443	0.06068	0.04172	12.8457	0
RB50_WL_0583_H08_T180_1	0.01529	0.08048	0.05549	0.06519	18.167	0
	0.01325	0.0756	0.06641	0.06235	16.332	0
	0.01454	0.07153	0.05735	0.05699	21.838	0
	0.01481	0.08462	0.06424	0.06981	18.901	0
	0.01427	0.0872	0.05866	0.07293	20.737	0
	0.01312	0.08076	0.06826	0.06764	16.699	0
	0.01278	0.07268	0.06315	0.0599	21.104	0
	0.01373	0.06447	0.05588	0.05074	14.314	0
	0.01271	0.07017	0.03846	0.05746	12.295	0
	0.01359	0.05504	0.04666	0.04145	11.194	0
	0.0119	0.04928	0.04906	0.03738	7.3404	0
RB50_WL_0583_H08_T180_2	0.01393	0.07506	0.0551	0.06113	19.269	0
	0.01346	0.07655	0.08166	0.06309	16.7	0
	0.01319	0.07797	0.05696	0.06478	22.205	0
	0.01488	0.07933	0.06857	0.06445	18.168	0.1836
	0.0157	0.07926	0.06803	0.06356	26.242	0.1836
	0.01637	0.09487	0.07229	0.0785	18.718	0
	0.01386	0.08863	0.06826	0.07477	18.168	0
	0.01224	0.06631	0.06137	0.05407	16.883	0
	0.01407	0.07309	0.04186	0.05902	11.745	0.1836

Continue from previous page

	0.01257	0.05966	0.04388	0.04709	13.763	0
	0.01237	0.04799	0.05394	0.03562	8.992	0
RB50_WL_0583_H065_T180_1	0.01169	0.0581	0.0469	0.04641	10.2766	0
	0.01217	0.05606	0.04117	0.04389	10.6436	0
	0.0123	0.05878	0.04426	0.04648	10.0931	0
	0.0123	0.0566	0.04295	0.0443	10.8271	0
	0.01339	0.05565	0.04318	0.04226	10.2766	0
	0.01285	0.05301	0.04837	0.04016	10.6436	0
	0.01183	0.05844	0.05084	0.04661	10.6436	0
	0.01122	0.0484	0.04953	0.03718	7.891	0
	0.01115	0.03727	0.04457	0.02612	5.6889	0
	0.01047	0.03951	0.04225	0.02904	6.4229	0
	0.01034	0.03354	0.04945	0.0232	3.3032	0
RB50_WL_0583_H065_T180_2	0.01203	0.05694	0.05193	0.04491	11.5612	0
	0.01217	0.05613	0.04194	0.04396	10.2766	0
	0.01183	0.05911	0.04318	0.04728	9.7261	0
	0.01264	0.05396	0.04209	0.04132	11.5612	0
	0.01339	0.05633	0.04767	0.04294	11.1942	0
	0.01298	0.05572	0.04806	0.04274	11.9282	0
	0.01257	0.06278	0.05363	0.05021	11.1942	0
	0.0119	0.04656	0.0541	0.03466	8.0745	0
	0.01135	0.04059	0.04264	0.02924	4.7713	0
	0.01088	0.0389	0.04047	0.02802	5.6889	0
	0.00932	0.03042	0.04179	0.0211	3.3032	0
RB50_WL_0583_H05_T180_1	0.00979	0.0351	0.03729	0.02531	4.7713	0
	0.01013	0.03659	0.03311	0.02646	4.7713	0
	0.00986	0.03551	0.03861	0.02565	4.7713	0
	0.01013	0.03869	0.03582	0.02856	5.1383	0
	0.01027	0.037	0.03722	0.02673	4.7713	0
	0.01013	0.03856	0.04039	0.02843	4.9548	0
	0.01006	0.03815	0.03606	0.02809	5.5053	0
	0.01013	0.03958	0.04256	0.02945	3.6702	0
	0.00952	0.03082	0.04604	0.0213	2.0187	0
	0.00891	0.02445	0.02793	0.01554	1.2846	0
	0.00857	0.02085	0.01871	0.01228	0.5506	0
RB50_WL_0583_H05_T180_2	0.01	0.03754	0.03807	0.02754	4.5878	0
	0.01013	0.03551	0.03853	0.02538	4.0373	0
	0.00993	0.03612	0.03768	0.02619	4.4043	0
	0.01027	0.03802	0.03582	0.02775	5.1383	0
	0.01034	0.03673	0.03799	0.02639	4.5878	0
	0.01006	0.03985	0.0359	0.02979	4.4043	0
	0.01013	0.03951	0.04225	0.02938	5.5053	0
	0.00993	0.0313	0.04705	0.02137	4.0373	0
	0.00871	0.02472	0.02793	0.01601	1.8351	0

Continue from previous page

	0.00844	0.02173	0.02111	0.01329	1.2846	0
	0.00769	0.01447	0.01716	0.00678	0.7341	0
RB50_WL_0567_H08_T180_1	0.01115	0.06169	0.03962	0.05054	10.2766	0
	0.01298	0.08177	0.04248	0.06879	11.3777	0
	0.01162	0.05504	0.0455	0.04342	11.0107	0
	0.01169	0.07336	0.05007	0.06167	13.9468	0
	0.01251	0.06006	0.0445	0.04755	11.1942	0.1836
	0.0123	0.07031	0.04132	0.05801	16.1489	0
	0.01407	0.05884	0.05363	0.04477	9.3591	0
	0.0119	0.06047	0.05921	0.04857	7.1569	0
	0.01068	0.04487	0.04821	0.03419	4.5878	0
	0.01006	0.0484	0.05139	0.03834	9.7261	0
	0.01257	0.05457	0.04697	0.042	4.5878	0
RB50_WL_0567_H08_T180_2	0.01196	0.06115	0.05626	0.04919	9.1755	0
	0.0119	0.0716	0.05247	0.0597	11.3776	0
	0.01224	0.05857	0.04813	0.04633	10.6435	0
	0.01183	0.0619	0.05007	0.05007	12.6622	0
	0.01285	0.06115	0.05131	0.0483	12.8457	0
	0.01257	0.05898	0.04782	0.04641	11.9281	0
	0.01264	0.06726	0.04659	0.05462	10.46	0
	0.01169	0.06481	0.05789	0.05312	7.1569	0
	0.01006	0.04935	0.05464	0.03929	4.9547	0
	0.01061	0.05443	0.05115	0.04382	9.359	0
	0.01068	0.05925	0.04868	0.04857	4.0372	0
RB50_WL_0567_H065_T180_1	0.00925	0.04399	0.05108	0.03474	6.7899	0
	0.00945	0.04439	0.04953	0.03494	6.0559	0
	0.01	0.04426	0.04984	0.03426	5.6889	0
	0.00993	0.04731	0.04713	0.03738	6.4229	0
	0.01027	0.0467	0.04906	0.03643	6.6064	0
	0.01068	0.04636	0.05363	0.03568	6.6064	0
	0.00993	0.05009	0.05077	0.04016	6.6064	0
	0.01054	0.04812	0.03908	0.03758	3.3032	0
	0.00891	0.0332	0.03606	0.02429	1.6516	0
	0.0083	0.0296	0.02514	0.0213	2.7527	0
	0.00932	0.03659	0.02831	0.02727	1.8351	0
RB50_WL_0567_H065_T180_2	0.01095	0.04412	0.05317	0.03317	6.2394	0
	0.00993	0.04833	0.05038	0.0384	5.8724	0
	0.01006	0.04778	0.05046	0.03772	5.6889	0
	0.01115	0.0488	0.04945	0.03765	6.4229	0
	0.01088	0.04365	0.05595	0.03277	6.6064	0
	0.01088	0.04446	0.05061	0.03358	7.3405	0
	0.01108	0.04575	0.05595	0.03467	6.0559	0
	0.01122	0.0486	0.03962	0.03738	3.3032	0
	0.01013	0.03313	0.0366	0.023	2.0187	0

Continue from previous page

0.00837	0.02879	0.02769	0.02042	2.5692	0
0.00986	0.03564	0.02777	0.02578	1.2846	0

Table A.4 Individual event of a wave train for the inland case, T=1.54s

Test code	D	h2	h1	H2	Fmax	Fmin
RB50_WL_06_H08_T154_1	0.01692	0.06542	0.06865	0.0485	19.2686	0
	0.01658	0.07879	0.07864	0.06221	13.9468	0.3671
	0.01753	0.06481	0.05773	0.04728	17.25	0.5506
	0.01732	0.06542	0.07678	0.0481	19.6356	0
	0.01644	0.0623	0.0798	0.04586	17.25	0.3671
	0.01529	0.06868	0.07678	0.05339	15.2314	0.3671
	0.01773	0.08842	0.08615	0.07069	21.2872	0.1836
	0.01617	0.07953	0.08863	0.06336	15.5984	0.1836
	0.01698	0.07302	0.06958	0.05604	15.4149	0.3671
	0.01495	0.07017	0.07725	0.05522	17.984	0
	0.01386	0.06447	0.06137	0.05061	13.0293	0.1836
	0.01698	0.05966	0.06703	0.04268	17.617	0.1836
	0.01753	0.07533	0.07012	0.0578	24.4069	0.5506
RB50_WL_06_H08_T154_2	0.0157	0.08015	0.06602	0.06445	18.1676	0.3671
	0.01651	0.06563	0.07291	0.04912	16.3325	0.3671
	0.01671	0.06916	0.05758	0.05245	14.3138	0.3671
	0.01746	0.0642	0.07856	0.04674	19.8192	0
	0.01603	0.07431	0.05913	0.05828	19.8192	0.1836
	0.01719	0.06264	0.08228	0.04545	14.4974	0.3671
	0.01807	0.06875	0.06292	0.05068	19.4521	0.1836
	0.01651	0.06854	0.06873	0.05203	19.0851	0.1836
	0.01807	0.07682	0.08189	0.05875	13.9468	0.5506
	0.01753	0.06169	0.07779	0.04416	17.617	0
	0.0159	0.06312	0.05239	0.04722	16.6995	0.3671
	0.01502	0.07682	0.0743	0.0618	18.7181	0.3671
	0.01624	0.07709	0.08127	0.06085	20.3697	0.3671
RB50_WL_06_H065_T154_1	0.01475	0.04962	0.05727	0.03487	9.3591	0.3671
	0.01339	0.05789	0.05239	0.0445	12.2952	0.1836
	0.01495	0.05247	0.06323	0.03752	9.5426	0.1836
	0.01475	0.05674	0.05619	0.04199	11.3777	0.1836
	0.01468	0.05504	0.06408	0.04036	12.8458	0.1836
	0.014	0.05973	0.05936	0.04573	11.1942	0.1836
	0.01475	0.06135	0.05603	0.0466	10.0931	0.1836
	0.01447	0.06285	0.05952	0.04838	9.5426	0.1836
	0.01447	0.05776	0.05626	0.04329	11.9282	0
	0.01346	0.0642	0.05704	0.05074	13.0293	0.1836
	0.01271	0.05342	0.06331	0.04071	9.3591	0.1836
	0.01373	0.05219	0.04775	0.03846	8.8085	0
	0.0142	0.06339	0.04883	0.04919	11.7447	0.1836
RB50_WL_06_H065_T154_2	0.01468	0.04677	0.06137	0.03209	10.6436	0.1836
	0.01488	0.05857	0.05053	0.04369	11.1942	0.1836

Continue from previous page

	0.01427	0.05559	0.06192	0.04132	8.992	0.1836
	0.01488	0.05145	0.05371	0.03657	12.6623	0
	0.01366	0.05606	0.06896	0.0424	12.4787	0.1836
	0.01441	0.06162	0.0582	0.04721	10.8271	0.1836
	0.01576	0.05694	0.06517	0.04118	10.6436	0.1836
	0.01556	0.05491	0.06308	0.03935	10.6436	0.1836
	0.01393	0.06434	0.05936	0.05041	10.2766	0.1836
	0.01393	0.05789	0.06037	0.04396	13.0293	0.1836
	0.01393	0.05335	0.07066	0.03942	9.5426	0
	0.01454	0.05803	0.05348	0.04349	9.1756	0
	0.0159	0.05959	0.05216	0.04369	11.5612	0.1836
RB50_WL_06_H05_T154_1	0.01149	0.03408	0.03002	0.02259	4.2207	0
	0.01251	0.03747	0.03373	0.02496	5.5053	0
	0.01224	0.03897	0.03242	0.02673	4.5877	0
	0.01217	0.03673	0.02862	0.02456	4.5877	0
	0.01251	0.03795	0.03064	0.02544	4.9547	0
	0.01244	0.03964	0.03009	0.0272	4.4042	0
	0.01224	0.03856	0.02824	0.02632	4.9547	0
	0.01217	0.03822	0.03048	0.02605	5.3217	0
	0.01264	0.03693	0.03133	0.02429	5.5053	0
	0.01162	0.03693	0.03157	0.02531	6.2393	0
	0.0123	0.03625	0.03435	0.02395	4.9547	0
	0.01203	0.03137	0.02855	0.01934	4.5877	0
	0.0121	0.04107	0.0328	0.02897	6.9733	0
RB50_WL_06_H05_T154_2	0.01176	0.03646	0.03172	0.0247	4.0373	0
	0.01224	0.03937	0.0287	0.02713	5.3218	0
	0.01203	0.03903	0.02816	0.027	4.2208	0
	0.01203	0.03734	0.03381	0.02531	4.4043	0
	0.01237	0.03944	0.03319	0.02707	4.7713	0
	0.01203	0.03876	0.02917	0.02673	4.4043	0
	0.01251	0.04086	0.03381	0.02835	4.9548	0
	0.01217	0.03802	0.03126	0.02585	5.5053	0
	0.01298	0.03802	0.03164	0.02504	5.3218	0
	0.01169	0.0408	0.03149	0.02911	6.0559	0
	0.0119	0.03523	0.02986	0.02333	5.1383	0
	0.01142	0.03157	0.03056	0.02015	4.0373	0
	0.01271	0.04195	0.03149	0.02924	6.0559	0
RB50_WL_06_H095_T154_1	0.01705	0.06441	0.05967	0.04736	22.0213	0.1836
	0.0178	0.06997	0.07229	0.05217	25.875	0.9176
	0.02011	0.08015	0.06099	0.06004	23.1223	0.1836
	0.01726	0.08306	0.05681	0.0658	22.2048	0.7341
	0.01759	0.07051	0.05603	0.05292	25.141	0
	0.01888	0.07567	0.08197	0.05679	28.0771	0.7341
	0.01909	0.07804	0.06315	0.05895	24.0399	0.5506

Continue from previous page

	0.018	0.09697	0.06068	0.07897	22.0213	0.7341
	0.01936	0.08476	0.06672	0.0654	25.875	0.7341
	0.01563	0.08761	0.05332	0.07198	25.6915	0.5506
	0.01719	0.07648	0.07051	0.05929	24.2234	0.5506
	0.01651	0.08333	0.05456	0.06682	24.9574	0.3671
	0.01644	0.1121	0.08429	0.09566	37.9867	0.9176
RB50_WL_06_H095_T154_2	0.01726	0.08584	0.05224	0.06858	21.1036	0
	0.01692	0.07947	0.05928	0.06255	21.2871	0.5505
	0.01963	0.07764	0.07268	0.05801	28.6276	0.5505
	0.01753	0.09324	0.05448	0.07571	20.0026	0.9175
	0.01732	0.08198	0.0599	0.06466	28.444	0.367
	0.01624	0.08815	0.075	0.07191	24.4068	0.9175
	0.01793	0.08449	0.06966	0.06656	28.444	0.5505
	0.01536	0.08727	0.07152	0.07191	23.8563	0.734
	0.01854	0.08625	0.08445	0.06771	27.5265	0.1835
	0.01692	0.0872	0.05557	0.07028	24.9574	0.734
	0.01861	0.08564	0.0637	0.06703	23.3058	0.5505
	0.0157	0.07872	0.05557	0.06302	18.1675	0.5505
	0.0161	0.08659	0.08267	0.07049	24.9574	0.5505
RB50_WL_06_H09_T154_1	0.01916	0.0659	0.05108	0.04674	17.4334	0.367
	0.01875	0.0777	0.08096	0.05895	23.6728	0.5505
	0.01678	0.09073	0.06648	0.07395	19.452	0.367
	0.01739	0.09209	0.06215	0.0747	19.6356	0.367
	0.01631	0.095	0.05386	0.07869	22.9387	0.5505
	0.01726	0.08076	0.08507	0.0635	24.7738	0.5505
	0.01495	0.07248	0.06873	0.05753	23.6728	0.734
	0.01821	0.08727	0.07306	0.06906	23.1222	0.734
	0.01597	0.0832	0.07082	0.06723	23.6728	0.5505
	0.01746	0.08048	0.06633	0.06302	28.077	0.367
	0.01461	0.08157	0.05874	0.06696	20.3696	0.9175
	0.01658	0.06943	0.05657	0.05285	19.085	0.367
	0.01726	0.08944	0.08267	0.07218	28.444	0.5505
RB50_WL_06_H09_T154_2	0.01705	0.0661	0.05201	0.04905	19.2685	0.1835
	0.01827	0.07553	0.0863	0.05726	28.6276	0.5505
	0.01692	0.08408	0.0637	0.06716	14.1303	0.734
	0.01651	0.07628	0.06679	0.05977	26.0584	0.367
	0.01719	0.09283	0.06223	0.07564	19.085	0.734
	0.01658	0.10918	0.06718	0.0926	19.4521	0.5505
	0.01739	0.09202	0.06842	0.07463	22.3882	0.367
	0.01698	0.08191	0.06989	0.06493	19.8191	0.367
	0.01787	0.07465	0.07384	0.05678	30.2792	0.5505
	0.01583	0.10118	0.07508	0.08535	22.2047	0.5505
	0.01658	0.07947	0.06192	0.06289	20.0026	0.367
	0.01759	0.06576	0.07206	0.04817	13.9467	0.1835

Continue from previous page

	0.01759	0.11495	0.0942	0.09736	30.2792	0.1835
RB50_WL_0583_H08_T154_1	0.01468	0.05063	0.05998	0.03595	8.0745	0
	0.01515	0.06644	0.05797	0.05129	10.46	0
	0.01631	0.05219	0.0589	0.03588	10.277	0
	0.01481	0.0623	0.05301	0.04749	11.928	0
	0.0161	0.05314	0.06463	0.03704	9.1756	0
	0.01624	0.06834	0.05727	0.0521	11.745	0
	0.01475	0.06366	0.06052	0.04891	11.194	0
	0.01461	0.06468	0.06524	0.05007	11.745	0
	0.01495	0.06129	0.07005	0.04634	11.928	0
	0.01481	0.07587	0.05998	0.06106	11.745	0
	0.01502	0.05274	0.05363	0.03772	8.625	0
	0.01468	0.06217	0.05022	0.04749	10.277	0
	0.01556	0.07574	0.05712	0.06018	14.314	0
RB50_WL_0583_H08_T154_2	0.01529	0.05213	0.05975	0.03684	8.0745	0
	0.01603	0.06271	0.0551	0.04668	10.093	0
	0.01556	0.0526	0.06176	0.03704	10.827	0
	0.01468	0.06291	0.05518	0.04823	14.13	0
	0.01508	0.06834	0.05851	0.05326	11.745	0
	0.0157	0.06156	0.06021	0.04586	10.827	0
	0.0157	0.05979	0.0709	0.04409	10.827	0
	0.01475	0.0659	0.06207	0.05115	12.112	0
	0.01515	0.06203	0.06068	0.04688	12.295	0
	0.01441	0.07194	0.06184	0.05753	12.295	0
	0.01488	0.05457	0.05549	0.03969	8.4415	0
	0.01427	0.06963	0.04736	0.05536	11.011	0
	0.01515	0.07757	0.05781	0.06242	16.516	0
RB50_WL_0583_H065_T154_1	0.01251	0.03883	0.03211	0.02632	4.7713	0
	0.01346	0.04738	0.03265	0.03392	5.1383	0
	0.01373	0.04168	0.04031	0.02795	4.4043	0
	0.01237	0.04107	0.03412	0.0287	4.4043	0
	0.01346	0.04487	0.0335	0.03141	4.9548	0
	0.01312	0.04134	0.03528	0.02822	5.6889	0
	0.01407	0.04249	0.03923	0.02842	6.7899	0
	0.01366	0.04229	0.03784	0.02863	6.7899	0
	0.01366	0.0431	0.03629	0.02944	6.9734	0
	0.01291	0.04256	0.04024	0.02965	6.6064	0
	0.01291	0.03829	0.04256	0.02538	5.1383	0
	0.0119	0.03625	0.03087	0.02435	4.5878	0
	0.014	0.04962	0.03652	0.03562	6.9734	0
RB50_WL_0583_H065_T154_2	0.0121	0.03734	0.02777	0.02524	5.6889	0
	0.01278	0.04466	0.03505	0.03188	6.6064	0
	0.01203	0.03924	0.03737	0.02721	5.5053	0
	0.01291	0.04215	0.03505	0.02924	5.6889	0

Continue from previous page

	0.01366	0.041	0.03575	0.02734	5.8724	0
	0.01366	0.04215	0.03675	0.02849	6.4229	0
	0.01312	0.04324	0.03536	0.03012	6.7899	0
	0.01373	0.04317	0.0383	0.02944	6.0559	0
	0.01346	0.04555	0.03962	0.03209	7.1569	0
	0.01454	0.04195	0.03691	0.02741	6.9734	0
	0.01386	0.037	0.03791	0.02314	5.5053	0
	0.01264	0.03401	0.03025	0.02137	5.6889	0
	0.01312	0.0526	0.03373	0.03948	8.992	0
RB50_WL_0583_H05_T154_1	0.01	0.02187	0.02189	0.01187	1.1011	0
	0.00952	0.02614	0.0246	0.01662	2.0187	0
	0.00911	0.02438	0.02088	0.01527	2.2022	0
	0.00911	0.02485	0.02367	0.01574	2.2022	0
	0.00945	0.02567	0.0232	0.01622	2.0187	0
	0.00979	0.0273	0.02413	0.01751	2.2022	0
	0.00945	0.02587	0.02367	0.01642	2.2022	0
	0.00878	0.02682	0.02491	0.01804	2.0187	0
	0.00952	0.02675	0.02444	0.01723	2.2022	0
	0.00911	0.02913	0.02491	0.02002	2.2022	0
	0.0085	0.0254	0.02142	0.0169	1.6516	0
	0.00844	0.02228	0.02042	0.01384	1.2846	0
	0.00925	0.03008	0.0256	0.02083	2.7527	0
RB50_WL_0583_H05_T154_2	0.01013	0.0216	0.01856	0.01147	0.9175	0
	0.00945	0.02526	0.02297	0.01581	1.6515	0
	0.00945	0.02533	0.02514	0.01588	1.6515	0
	0.00945	0.0258	0.02065	0.01635	1.6515	0
	0.00911	0.02574	0.02018	0.01663	1.6515	0
	0.00986	0.02757	0.02676	0.01771	1.6515	0
	0.00939	0.02648	0.02467	0.01709	1.6515	0
	0.00945	0.02655	0.02243	0.0171	1.6515	0
	0.00918	0.02608	0.02622	0.0169	2.0186	0
	0.00925	0.02838	0.02754	0.01913	2.0186	0
	0.00884	0.02526	0.02351	0.01642	1.468	0
	0.00823	0.02295	0.02173	0.01472	1.2845	0
	0.00918	0.02954	0.02692	0.02036	2.5691	0
RB50_WL_0567_H08_T154_1	0.01257	0.04338	0.03644	0.03081	7.1569	0
	0.01305	0.04154	0.039	0.02849	7.891	0
	0.01325	0.04616	0.04295	0.03291	5.1383	0
	0.01224	0.04914	0.03977	0.0369	5.6889	0
	0.01312	0.05084	0.03637	0.03772	6.2394	0
	0.01352	0.05884	0.04302	0.04532	7.524	0
	0.01461	0.04996	0.04511	0.03535	7.7075	0
	0.01319	0.04765	0.04093	0.03446	7.3405	0
	0.01325	0.05464	0.04047	0.04139	6.7899	0

Continue from previous page

	0.01346	0.05281	0.04728	0.03935	6.7899	0
	0.01251	0.04405	0.0455	0.03154	4.9548	0
	0.01278	0.05002	0.03629	0.03724	5.6889	0
	0.01298	0.05674	0.04589	0.04376	7.7075	0
RB50_WL_0567_H08_T154_2	0.0121	0.04256	0.03877	0.03046	7.7075	0
	0.01427	0.04833	0.03737	0.03406	8.625	0
	0.01264	0.04453	0.0486	0.03189	5.6889	0
	0.0123	0.05314	0.04031	0.04084	5.1383	0
	0.01332	0.05518	0.04078	0.04186	5.5053	0
	0.01271	0.06285	0.04209	0.05014	6.4229	0
	0.01427	0.05396	0.04349	0.03969	6.4229	0
	0.01352	0.05789	0.0414	0.04437	6.4229	0
	0.01413	0.05477	0.04597	0.04064	6.7899	0
	0.01475	0.04751	0.04643	0.03276	7.524	0
	0.01291	0.0412	0.04628	0.02829	5.3218	0
	0.01271	0.05647	0.03621	0.04376	5.1383	0
	0.01312	0.06834	0.04271	0.05522	6.9734	0
RB50_WL_0567_H065_T154_1	0.01061	0.02662	0.02723	0.01601	2.3857	0
	0.0102	0.03177	0.02359	0.02157	2.5692	0
	0.00925	0.03191	0.02723	0.02266	2.2022	0
	0.00925	0.0332	0.02452	0.02395	1.8351	0
	0.00939	0.03354	0.02684	0.02415	2.0187	0
	0.00952	0.03272	0.02816	0.0232	2.7527	0
	0.00966	0.03456	0.02676	0.0249	2.3857	0
	0.00918	0.03367	0.02653	0.02449	2.3857	0
	0.00952	0.03293	0.02924	0.02341	3.1197	0
	0.00966	0.03293	0.02707	0.02327	3.3032	0
	0.00878	0.02981	0.02824	0.02103	2.3857	0
	0.00857	0.02886	0.02467	0.02029	2.5692	0
	0.00891	0.04019	0.028	0.03128	5.3218	0
RB50_WL_0567_H065_T154_2	0.01034	0.02723	0.02622	0.01689	2.3857	0
	0.00986	0.03048	0.02243	0.02062	2.3857	0
	0.00952	0.03103	0.02707	0.02151	2.2022	0
	0.00966	0.03089	0.02599	0.02123	2.3857	0
	0.00918	0.03035	0.02297	0.02117	2.7527	0
	0.01006	0.03137	0.02591	0.02131	3.3032	0
	0.00966	0.03028	0.02483	0.02062	2.9362	0
	0.00932	0.03137	0.02723	0.02205	3.1197	0
	0.00966	0.03232	0.02692	0.02266	3.3032	0
	0.00911	0.03232	0.028	0.02321	3.3032	0
	0.00898	0.03008	0.02506	0.0211	2.2022	0
	0.00891	0.02906	0.0222	0.02015	2.5692	0
	0.00918	0.03666	0.03242	0.02748	4.4043	0

Table A.5 Individual event of a wave train for the inland case, T=1.2s

Test code	D	h2	h1	H2	F_{max}	F_{min}
RB50_WL_06_H08_T120_1	0.01352	0.04751	0.02986	0.03399	11.7446	0.1835
	0.01651	0.06142	0.03993	0.04491	15.5983	0.5505
	0.02078	0.05538	0.04318	0.0346	17.2499	0.5505
	0.01739	0.04948	0.05324	0.03209	8.4414	0.367
	0.01746	0.04229	0.03729	0.02483	5.3217	0.1835
	0.01909	0.04643	0.03745	0.02734	7.1569	0.5505
	0.01712	0.04724	0.04209	0.03012	7.8909	0.5505
	0.01719	0.04812	0.03962	0.03093	6.2393	0.5505
	0.01827	0.05986	0.03637	0.04159	7.3404	0.5505
	0.01624	0.05816	0.03884	0.04192	9.726	0.5505
	0.01732	0.05029	0.04341	0.03297	7.5239	0.5505
	0.01678	0.05111	0.03513	0.03433	7.5239	0.734
	0.01888	0.05213	0.03729	0.03325	6.4228	0.734
	0.01793	0.05335	0.03381	0.03542	6.6063	0.734
	0.01712	0.04704	0.03621	0.02992	7.8909	0.1835
	0.01814	0.05328	0.03528	0.03514	6.7898	0.1835
	0.01766	0.05043	0.02808	0.03277	6.0558	0
RB50_WL_06_H08_T120_2	0.01278	0.04826	0.02909	0.03548	12.1117	0.1836
	0.01766	0.06088	0.0407	0.04322	15.7819	0.7341
	0.02004	0.06101	0.04279	0.04097	15.2314	0.5506
	0.01956	0.05281	0.03846	0.03325	9.9096	0.5506
	0.01793	0.04243	0.03815	0.0245	6.4229	0.3671
	0.01692	0.04663	0.04767	0.02971	6.2394	0.5506
	0.01787	0.04575	0.03698	0.02788	8.8085	0.7341
	0.01793	0.04704	0.03218	0.02911	6.4229	0.3671
	0.01719	0.04616	0.03691	0.02897	6.2394	0.7341
	0.01495	0.05355	0.04357	0.0386	6.4229	0.7341
	0.01753	0.04833	0.03908	0.0308	5.5053	1.1011
	0.0159	0.05145	0.04078	0.03555	6.4229	0.5506
	0.01631	0.04717	0.0479	0.03086	5.6889	0.5506
	0.01624	0.05532	0.04651	0.03908	7.1569	0.7341
	0.01929	0.0505	0.03931	0.03121	8.4415	0.5506
	0.01515	0.04772	0.03218	0.03257	7.7075	1.1011
	0.01861	0.05043	0.03211	0.03182	14.1303	0.3671
RB50_WL_06_H065_T120_1	0.00973	0.03313	0.02576	0.0234	5.8723	0
	0.01312	0.04724	0.02808	0.03412	11.3776	0
	0.01651	0.05192	0.03497	0.03541	10.46	0.1835
	0.01644	0.03863	0.02847	0.02219	5.3217	0.1835
	0.01481	0.03238	0.03489	0.01757	2.9361	0
	0.01319	0.03184	0.03698	0.01865	3.3031	0.1835
	0.014	0.03917	0.04217	0.02517	4.5877	0.367
	0.01529	0.03849	0.04171	0.0232	5.5053	0.367

Continue from previous page

	0.01461	0.03564	0.03443	0.02103	4.4042	0.1835
	0.01454	0.03422	0.02537	0.01968	4.2207	0.1835
	0.01413	0.03659	0.03776	0.02246	5.3217	0.367
	0.01319	0.03652	0.03311	0.02333	4.4042	0.1835
	0.01407	0.03727	0.03598	0.0232	4.7712	0.367
	0.01346	0.03612	0.0414	0.02266	4.2207	0.367
	0.01339	0.03822	0.03737	0.02483	4.4042	0
	0.01441	0.03774	0.03846	0.02333	4.4042	0
	0.01352	0.03869	0.03002	0.02517	4.4042	0.1835
RB50_WL_06_H065_T120_2	0.01013	0.03361	0.02622	0.02348	6.6064	0
	0.01339	0.04806	0.02878	0.03467	11.7447	0.1836
	0.01644	0.04833	0.02893	0.03189	9.7261	0.3671
	0.01508	0.04351	0.03327	0.02843	5.1383	0.5506
	0.01597	0.03232	0.02793	0.01635	3.3032	0.3671
	0.01373	0.03374	0.02947	0.02001	3.8538	0.5506
	0.014	0.03958	0.0294	0.02558	5.1383	0.5506
	0.01386	0.04032	0.0366	0.02646	4.4043	0.5506
	0.01352	0.04066	0.03799	0.02714	4.2208	0.3671
	0.01298	0.03856	0.03249	0.02558	4.5878	0.3671
	0.01454	0.041	0.04295	0.02646	5.3218	0.3671
	0.0142	0.0353	0.0287	0.0211	4.5878	0.1836
	0.01488	0.03802	0.03435	0.02314	3.4867	0.3671
	0.01332	0.04012	0.0383	0.0268	4.2208	0.5506
	0.01366	0.03856	0.03412	0.0249	4.2208	0.5506
	0.01332	0.041	0.03637	0.02768	4.5878	0.3671
	0.01257	0.03951	0.03195	0.02694	4.4043	0.3671
RB50_WL_06_H05_T120_1	0.00681	0.02092	0.01802	0.01411	2.0186	0
	0.00932	0.03055	0.0232	0.02123	5.1382	0
	0.01162	0.0353	0.02615	0.02368	5.8723	0
	0.01305	0.02886	0.0304	0.01581	3.3031	0
	0.01101	0.02024	0.027	0.00923	1.101	0
	0.01027	0.01902	0.01964	0.00875	1.2845	0
	0.0119	0.02954	0.02444	0.01764	2.5691	0
	0.01095	0.02865	0.02266	0.0177	2.7526	0
	0.01088	0.02472	0.02754	0.01384	1.6515	0
	0.0102	0.02451	0.02367	0.01431	1.8351	0
	0.01162	0.02797	0.02971	0.01635	2.3856	0
	0.01101	0.02655	0.02754	0.01554	2.0186	0
	0.01142	0.0239	0.02429	0.01248	2.2021	0
	0.01196	0.02587	0.02305	0.01391	2.0186	0
	0.01129	0.02655	0.02707	0.01526	2.2021	0
	0.01156	0.02669	0.02824	0.01513	2.2021	0
	0.01122	0.02533	0.02359	0.01411	2.0186	0
RB50_WL_06_H05_T120_2	0.00667	0.02017	0.01871	0.0135	1.8351	0

Continue from previous page

	0.00959	0.03062	0.02398	0.02103	4.9547	0
	0.01169	0.03578	0.02707	0.02409	5.8723	0
	0.01298	0.02859	0.028	0.01561	3.1196	0
	0.01101	0.01997	0.02227	0.00896	1.101	0
	0.01027	0.01949	0.02545	0.00922	1.101	0
	0.01149	0.02892	0.02522	0.01743	2.5691	0
	0.01142	0.0254	0.02351	0.01398	2.7526	0
	0.01047	0.02228	0.02413	0.01181	1.468	0
	0.01006	0.02343	0.02421	0.01337	2.0186	0
	0.01162	0.02967	0.02452	0.01805	2.2021	0
	0.01095	0.02709	0.02785	0.01614	2.0186	0
	0.01081	0.0256	0.02336	0.01479	2.0186	0
	0.01142	0.02458	0.02088	0.01316	2.0186	0
	0.01095	0.02608	0.02367	0.01513	1.8351	0
	0.01135	0.02709	0.02444	0.01574	2.2021	0
	0.01115	0.02465	0.03017	0.0135	2.0186	0
RB50_WL_06_H10_T120_1	0.0197	0.06508	0.0328	0.04538	20.0026	0.1835
	0.02635	0.08605	0.05286	0.0597	24.0398	0.5505
	0.0254	0.07859	0.07895	0.05319	18.351	0.9175
	0.02248	0.0604	0.0695	0.03792	12.1116	0.734
	0.02017	0.07099	0.04388	0.05082	9.9095	0.367
	0.01861	0.08184	0.04248	0.06323	14.3138	0.734
	0.02228	0.06597	0.05115	0.04369	12.4787	1.101
	0.01854	0.06834	0.05208	0.0498	10.46	1.101
	0.02044	0.06095	0.04922	0.04051	11.9281	0.734
	0.01854	0.06875	0.04968	0.05021	11.1941	0.5505
	0.01766	0.06936	0.04628	0.0517	10.6436	0.5505
	0.01848	0.07804	0.04488	0.05956	11.7446	0.367
	0.0218	0.06203	0.05766	0.04023	17.6169	0.5505
	0.02207	0.06922	0.05309	0.04715	15.4148	0.734
	0.02234	0.0739	0.05038	0.05156	13.3962	0
	0.02173	0.07336	0.05309	0.05163	12.1116	1.101
	0.02085	0.06101	0.05239	0.04016	9.9095	1.468
RB50_WL_06_H10_T120_2	0.022	0.07065	0.03195	0.04865	22.7552	0.1835
	0.02438	0.08367	0.04411	0.05929	22.5717	1.101
	0.02492	0.08103	0.06083	0.05611	16.1489	0
	0.02153	0.0526	0.07198	0.03107	9.9095	1.2845
	0.02343	0.05545	0.04566	0.03202	12.8457	0.367
	0.02302	0.06882	0.04117	0.0458	19.2685	0.9175
	0.02275	0.06617	0.05502	0.04342	11.5611	1.2845
	0.02214	0.06176	0.04837	0.03962	13.9467	0.734
	0.02268	0.07418	0.04573	0.0515	15.5983	1.2845
	0.02085	0.05816	0.06269	0.03731	14.4973	1.2845
	0.01861	0.06257	0.05317	0.04396	14.8643	0

Continue from previous page

	0.02126	0.06807	0.05084	0.04681	12.2952	1.2845
	0.01929	0.05715	0.05332	0.03786	12.6622	1.101
	0.0216	0.06909	0.05255	0.04749	19.085	0
	0.02112	0.07187	0.04612	0.05075	11.9281	1.101
	0.02112	0.08015	0.04813	0.05903	10.2765	1.468
	0.02031	0.05403	0.04883	0.03372	9.1755	1.101
RB50_WL_0583_H08_T120_1	0.00966	0.03639	0.02622	0.02673	8.0745	0
	0.01393	0.05118	0.02615	0.03725	13.396	0.3671
	0.01651	0.04555	0.03428	0.02904	9.9096	0.1836
	0.01678	0.03544	0.03118	0.01866	4.2208	0.1836
	0.01549	0.03503	0.03048	0.01954	2.9362	0
	0.01285	0.03422	0.03172	0.02137	4.4043	0.3671
	0.01631	0.04256	0.03304	0.02625	6.9734	0.3671
	0.01502	0.04046	0.03559	0.02544	3.6702	0.3671
	0.01488	0.037	0.03195	0.02212	4.7713	0.3671
	0.01495	0.03564	0.03195	0.02069	5.3218	0.3671
	0.01447	0.03659	0.0376	0.02212	5.5053	0.3671
	0.01393	0.03686	0.02769	0.02293	5.1383	0.3671
	0.01447	0.0372	0.0366	0.02273	4.4043	0.5506
	0.01271	0.04514	0.03342	0.03243	4.7713	0.5506
	0.01536	0.04276	0.03218	0.0274	5.1383	0.3671
	0.01434	0.04093	0.03536	0.02659	5.1383	0.1836
	0.01427	0.03788	0.02638	0.02361	3.3032	0.1836
RB50_WL_0583_H08_T120_2	0.01006	0.03835	0.0256	0.02829	11.745	0
	0.01454	0.05287	0.02638	0.03833	14.314	0.3671
	0.01563	0.05023	0.03807	0.0346	8.8085	0.3671
	0.01624	0.03761	0.02707	0.02137	3.4867	0.3671
	0.01407	0.03598	0.02769	0.02191	5.1383	0
	0.01244	0.04012	0.03226	0.02768	5.8724	0.3671
	0.01475	0.04806	0.03551	0.03331	4.7713	0.1836
	0.01386	0.03924	0.02839	0.02538	5.6889	0
	0.01495	0.03523	0.03249	0.02028	6.7899	0.1836
	0.01576	0.03937	0.02754	0.02361	4.0373	0.5506
	0.01386	0.03652	0.02917	0.02266	5.8724	0.3671
	0.01413	0.03768	0.03273	0.02355	3.8538	0.3671
	0.01325	0.0391	0.03443	0.02585	6.0559	0.3671
	0.01495	0.04086	0.03946	0.02591	5.6889	0.1836
	0.01393	0.0393	0.03118	0.02537	4.4043	0.3671
	0.01488	0.03612	0.03064	0.02124	3.6702	0.1836
	0.01264	0.03618	0.02545	0.02354	4.7713	0.1836
RB50_WL_0583_H065_T120_1	0.00762	0.02777	0.02042	0.02015	4.5878	0
	0.01095	0.03449	0.0246	0.02354	7.1569	0
	0.01359	0.04093	0.02483	0.02734	8.258	0.1836
	0.01264	0.0256	0.02545	0.01296	2.5692	0

Continue from previous page

	0.01251	0.01902	0.02173	0.00651	1.1011	0
	0.01183	0.02682	0.028	0.01499	2.7527	0
	0.01203	0.03028	0.03033	0.01825	4.2208	0.1836
	0.01183	0.03021	0.03079	0.01838	3.3032	0.1836
	0.01156	0.02424	0.02793	0.01268	2.0187	0
	0.01101	0.02519	0.03257	0.01418	2.5692	0
	0.01366	0.03252	0.02715	0.01886	3.1197	0
	0.01257	0.0315	0.03009	0.01893	2.9362	0
	0.01237	0.02458	0.02878	0.01221	2.0187	0
	0.01176	0.02818	0.02622	0.01642	2.5692	0
	0.01237	0.03116	0.03172	0.01879	3.3032	0
	0.0121	0.03116	0.02824	0.01906	3.1197	0
	0.01264	0.02764	0.02537	0.015	2.0187	0
RB50_WL_0583_H065_T120_2	0.00776	0.02797	0.02003	0.02021	4.4043	0
	0.01061	0.03517	0.02436	0.02456	6.7899	0
	0.01332	0.04154	0.02421	0.02822	8.8085	0
	0.01237	0.02757	0.02096	0.0152	2.5692	0
	0.01122	0.01977	0.02328	0.00855	1.2846	0
	0.01176	0.02635	0.01941	0.01459	2.3857	0
	0.01224	0.03028	0.02653	0.01804	4.7713	0.1836
	0.01203	0.03123	0.02599	0.0192	3.3032	0.1836
	0.01149	0.0239	0.02777	0.01241	2.5692	0
	0.0104	0.02641	0.02746	0.01601	2.2022	0
	0.01251	0.03157	0.02375	0.01906	2.3857	0
	0.01278	0.03042	0.03234	0.01764	2.5692	0
	0.01183	0.02601	0.03443	0.01418	2.2022	0
	0.01257	0.02675	0.02429	0.01418	2.3857	0
	0.01278	0.03001	0.02514	0.01723	2.7527	0
	0.01264	0.02811	0.02692	0.01547	2.7527	0
	0.0121	0.02648	0.02475	0.01438	1.8351	0
RB50_WL_0583_H05_T120_1	0.00749	0.02343	0.01709	0.01594	2.7527	0
	0.00939	0.02736	0.02104	0.01797	3.4867	0
	0.01034	0.02492	0.02901	0.01458	2.2022	0
	0.0083	0.01603	0.01608	0.00773	0.3671	0
	0.00735	0.01156	0.01724	0.00421	0.3671	0
	0.00742	0.02105	0.01438	0.01363	1.1011	0
	0.00945	0.022	0.01941	0.01255	1.2846	0
	0.00993	0.01936	0.02444	0.00943	1.1011	0
	0.00959	0.01719	0.02227	0.0076	0.9176	0
	0.00959	0.01698	0.01809	0.00739	0.9176	0
	0.00959	0.01637	0.016	0.00678	0.7341	0
	0.00966	0.01807	0.01593	0.00841	0.9176	0
	0.00952	0.01854	0.01515	0.00902	0.7341	0
	0.00979	0.01759	0.01701	0.0078	0.7341	0

Continue from previous page

	0.00986	0.01909	0.01685	0.00923	0.7341	0
	0.00952	0.01759	0.015	0.00807	0.7341	0
RB50_WL_0583_H05_T120_2	0.00755	0.02316	0.01786	0.01561	2.7526	0
	0.00918	0.02757	0.02065	0.01839	3.4866	0
	0.01006	0.02445	0.02684	0.01439	2.2021	0
	0.00816	0.01393	0.01654	0.00577	0.1835	0
	0.00728	0.01142	0.01747	0.00414	0.1835	0
	0.00932	0.02099	0.01484	0.01167	1.101	0
	0.00945	0.02167	0.01894	0.01222	1.101	0
	0.00966	0.01977	0.02196	0.01011	0.734	0
	0.00952	0.01665	0.02088	0.00713	0.734	0
	0.00966	0.01705	0.01887	0.00739	0.734	0
	0.00973	0.01692	0.01662	0.00719	0.9175	0
	0.00959	0.01787	0.01453	0.00828	0.5505	0
	0.01	0.01814	0.01414	0.00814	0.5505	0
	0.00979	0.01759	0.01654	0.0078	0.734	0
	0.00945	0.01868	0.01825	0.00923	0.5505	0
	0.00932	0.01746	0.01647	0.00814	0.5505	0
RB50_WL_0567_H08_T120_1	0.0081	0.03313	0.02111	0.02503	8.2579	0
	0.01183	0.04378	0.02018	0.03195	10.46	0
	0.01339	0.04371	0.03598	0.03032	9.359	0
	0.01237	0.02485	0.0311	0.01248	1.468	0
	0.00979	0.01977	0.02514	0.00998	2.2021	0
	0.01244	0.03944	0.03544	0.027	4.4042	0
	0.01325	0.03774	0.02855	0.02449	6.0558	0
	0.01271	0.03123	0.03745	0.01852	2.5691	0
	0.01101	0.02553	0.02646	0.01452	2.3856	0
	0.01291	0.03062	0.02738	0.01771	5.8723	0
	0.01325	0.03374	0.02429	0.02049	5.6888	0
	0.01196	0.02865	0.0184	0.01669	3.6702	0
	0.01115	0.02655	0.02049	0.0154	2.7526	0
	0.01047	0.0311	0.02824	0.02063	3.1196	0
	0.01298	0.03008	0.02839	0.0171	3.8537	0
	0.01407	0.03259	0.0215	0.01852	3.8537	0
	0.01081	0.0273	0.02467	0.01649	3.8537	0
RB50_WL_0567_H08_T120_2	0.0081	0.03272	0.01949	0.02462	8.625	0
	0.01156	0.04236	0.02119	0.0308	8.0745	0
	0.01251	0.04236	0.03637	0.02985	9.3591	0.1836
	0.0123	0.02811	0.027	0.01581	2.5692	0
	0.01156	0.02357	0.02266	0.01201	3.1197	0
	0.01271	0.03225	0.0328	0.01954	4.4043	0
	0.01169	0.03903	0.02855	0.02734	7.3405	0.1836
	0.01162	0.02804	0.0232	0.01642	2.3857	0
	0.01115	0.02472	0.02924	0.01357	2.5692	0

Continue from previous page

	0.01244	0.03252	0.03048	0.02008	6.6064	0
	0.01244	0.03408	0.02467	0.02164	4.9548	0
	0.01101	0.03008	0.02498	0.01907	5.5053	0
	0.0104	0.02621	0.02243	0.01581	2.7527	0
	0.01244	0.02987	0.02344	0.01743	3.6702	0
	0.01298	0.03435	0.02824	0.02137	3.1197	0.1836
	0.01237	0.03218	0.03102	0.01981	3.4867	0
	0.0121	0.03069	0.02436	0.01859	4.4043	0
RB50_WL_0567_H065_T120_1	0.00328	0.02112	0.01515	0.01784	2.9362	0
	0.00728	0.03205	0.01894	0.02477	6.0559	0
	0.01068	0.03286	0.01747	0.02218	5.5053	0
	0.01	0.02221	0.02576	0.01221	1.4681	0
	0.00755	0.01841	0.01523	0.01086	0.5506	0
	0.00966	0.02282	0.01941	0.01316	0.9176	0
	0.01006	0.02485	0.01987	0.01479	3.4867	0
	0.00925	0.01746	0.02096	0.00821	3.4867	0
	0.00932	0.0157	0.01995	0.00638	1.4681	0
	0.0104	0.02112	0.01577	0.01072	2.2022	0
	0.00952	0.02262	0.02042	0.0131	2.5692	0
	0.0102	0.01936	0.02104	0.00916	2.5692	0
	0.00966	0.01983	0.02398	0.01017	1.6516	0
	0.00959	0.02017	0.02282	0.01058	2.5692	0
	0.01034	0.01936	0.02204	0.00902	3.1197	0
	0.01054	0.02044	0.01987	0.0099	2.3857	0
	0.00993	0.01936	0.01709	0.00943	2.5692	0
RB50_WL_0567_H065_T120_2	0.00396	0.02207	0.01724	0.01811	3.4867	0
	0.00722	0.03211	0.01871	0.02489	6.6064	0
	0.01013	0.03496	0.01995	0.02483	5.6889	0
	0.00966	0.02105	0.02065	0.01139	1.4681	0
	0.00708	0.02031	0.0143	0.01323	0.5506	0
	0.00932	0.02268	0.02235	0.01336	0.9176	0
	0.01027	0.02472	0.01864	0.01445	3.3032	0
	0.00918	0.01848	0.02057	0.0093	4.0373	0
	0.0102	0.0178	0.0143	0.0076	1.4681	0
	0.01095	0.02167	0.01871	0.01072	3.1197	0
	0.00939	0.02194	0.02227	0.01255	3.1197	0
	0.0104	0.01997	0.02243	0.00957	2.0187	0
	0.0104	0.02024	0.02173	0.00984	2.3857	0
	0.01006	0.02248	0.02258	0.01242	2.5692	0
	0.00952	0.01936	0.02274	0.00984	3.1197	0
	0.01074	0.01909	0.02359	0.00835	2.2022	0
	0.01088	0.02099	0.01732	0.01011	2.3857	0

Table A.6 Individual event of a wave train for the dike side case, T=1.54s

Test code	h1	Fmax	Test code	h1	Fmax
RB00_WL06_H08_T154_1	0.10845	46.6117	RB00_WL06_H065_T154_1	0.07981	28.2605
	0.1216	51.3829		0.09036	30.2792
	0.12578	48.9973		0.0892	27.5265
	0.12338	45.1436		0.08605	28.6276
	0.12441	54.1356		0.08858	28.9946
	0.12708	50.8324		0.08605	28.8111
	0.13612	48.0797		0.08934	30.2792
	0.1277	50.2819		0.08673	29.9121
	0.12585	48.6303		0.08625	28.6276
	0.12605	56.5212		0.09043	29.1781
	0.11715	52.484		0.08625	27.8935
	0.1116	43.6755		0.08488	25.3244
	0.11879	48.0797		0.09221	30.6462
RB00_WL06_H08_T154_2	0.10783	45.5106	RB00_WL06_H065_T154_2	0.0842	27.3431
	0.12242	51.1994		0.09173	29.3617
	0.12181	45.5106		0.08981	26.9761
	0.11722	44.0425		0.08742	29.1782
	0.12345	50.2819		0.08749	30.0957
	0.11838	46.9787		0.08516	28.2606
	0.11886	52.117		0.08769	29.5452
	0.12016	50.2819		0.0894	30.6463
	0.12626	48.6303		0.08495	30.6463
	0.13112	48.6303		0.08721	31.1968
	0.12749	51.9335		0.08365	28.0771
	0.11167	44.593		0.08653	25.6915
	0.12879	46.6117		0.09098	28.2606
RB00_WL06_H08_T154_3	0.10639	44.96	RB00_WL06_H065_T154_3	0.08214	25.3245
	0.12605	48.6302		0.08776	30.4628
	0.12653	45.8775		0.08872	26.7925
	0.12318	46.6116		0.08687	27.5266
	0.12057	53.2179		0.09427	28.2606
	0.12235	50.0983		0.08461	28.9947
	0.1314	48.2632		0.08851	29.1782
	0.11982	49.7312		0.09242	28.6276
	0.12153	48.0796		0.09023	26.7925
	0.12228	51.9334		0.09221	30.0957
	0.12263	54.686		0.08755	28.8112
	0.11406	49.3642		0.08146	24.5904
	0.12208	49.1807		0.08865	29.3617
RB00_WL06_H05_T154_1	0.05693	12.6622	RB00_WL06_H035_T154_1	0.03268	4.2207
	0.06372	16.3324		0.03453	5.6888

Continue from previous page

	0.0618	14.6808		0.03426	5.3218
	0.06091	14.4973		0.03419	5.1382
	0.06187	15.5984		0.03508	5.5053
	0.06118	16.1489		0.03453	5.3218
	0.06159	15.7819		0.03481	5.3218
	0.06221	15.4148		0.03584	5.6888
	0.06214	15.5984		0.03508	5.3218
	0.06262	16.3324		0.037	5.5053
	0.06015	15.0478		0.0357	5.1382
	0.05639	13.5797		0.03371	4.4042
	0.06235	16.3324		0.03659	5.6888
RB00_WL06_H05_T154_2	0.05728	13.5798	RB00_WL06_H035_T154_2	0.03296	4.2207
	0.06433	16.883		0.0344	5.6888
	0.05961	15.9654		0.03371	5.3217
	0.05974	15.2314		0.03453	5.3217
	0.06166	16.1489		0.03433	5.5053
	0.05988	16.1489		0.03508	5.1382
	0.06036	16.1489		0.03536	5.5053
	0.06111	15.9654		0.03638	5.5053
	0.06173	15.9654		0.0359	5.5053
	0.06269	17.25		0.03673	5.6888
	0.06036	15.9654		0.03536	5.3217
	0.05632	13.5798		0.03337	4.4042
	0.06324	16.6995		0.03611	5.6888
RB00_WL06_H05_T154_3	0.05707	13.5797	RB00_WL06_H035_T154_3	0.03262	3.8537
	0.06419	16.5159		0.03467	5.5053
	0.06111	15.5983		0.03364	5.1382
	0.05919	15.0478		0.03426	4.9547
	0.06337	15.7818		0.03467	5.3218
	0.06077	15.5983		0.03494	5.1382
	0.05988	15.9653		0.03529	5.1382
	0.06125	15.7818		0.03584	5.5053
	0.0607	15.5983		0.03611	5.3218
	0.06221	16.5159		0.03631	5.6888
	0.05947	15.9653		0.0357	5.3218
	0.05536	13.7632		0.03316	4.2207
	0.06193	16.5159		0.03611	5.5053
RB00_WL0583_H08_T154_1	0.09831	35.4175	RB00_WL0583_H065_T154_1	0.07125	17.984
	0.09872	39.8218		0.07865	23.8564
	0.10002	35.9681		0.07474	21.2872
	0.09605	37.2526		0.07817	21.8378
	0.09899	36.8856		0.07625	22.5718
	0.09756	40.0053		0.07735	23.3058
	0.10427	38.5372		0.07248	22.7553

Continue from previous page

	0.10297	37.4361		0.07673	22.3883
	0.10838	39.4548		0.07392	22.3883
	0.10256	39.4548		0.07769	24.2234
	0.10084	37.2526		0.07289	22.3883
	0.09728	34.6835		0.06803	18.7181
	0.11406	39.2712		0.07666	24.9574
RB00_WL0583_H08_T154_2	0.09851	33.9494	RB00_WL0583_H065_T154_2	0.04056	8.258
	0.11187	43.125		0.04474	11.0107
	0.10756	36.1516		0.04289	10.2766
	0.09653	35.9681		0.0446	9.9096
	0.10591	37.4361		0.04453	10.6436
	0.1053	36.7021		0.0459	10.4601
	0.10441	35.9681		0.04618	10.6436
	0.10509	39.0877		0.04632	10.4601
	0.10893	37.4361		0.04659	10.4601
	0.10701	39.0877		0.04789	11.3777
	0.10804	38.1702		0.04364	9.9096
	0.09475	33.5824		0.04344	9.1756
	0.10934	42.2074		0.05276	12.1117
RB00_WL0583_H08_T154_3	0.09988	36.5186	RB00_WL0583_H05_T154_1	0.0172	1.2845
	0.11105	39.2712		0.02015	2.0186
	0.10735	35.9681		0.01796	1.6515
	0.10002	37.8032		0.01823	1.6515
	0.10283	36.8856		0.02015	2.0186
	0.10208	38.1702		0.01919	2.0186
	0.1042	34.3165		0.01802	2.2021
	0.10653	36.5186		0.01665	2.0186
	0.1092	37.0691		0.01741	2.2021
	0.10995	37.8032		0.0183	2.3856
	0.10317	37.9867		0.01679	1.8351
	0.10482	33.3989		0.01522	1.6515
	0.10995	40.9228		0.01933	2.5691
RB00_WL0583_H05_T154_2	0.01782	1.4681	RB00_WL0567_H08_T154_1	0.08687	26.4255
	0.02015	2.2022		0.09687	33.0319
	0.01885	2.0187		0.10187	26.9761
	0.0196	2.0187		0.08605	26.9761
	0.01823	2.2022		0.0894	28.4441
	0.01878	2.2022		0.08906	35.601
	0.01864	2.2022		0.0931	28.0771
	0.01672	2.0187		0.10324	29.7287
	0.01734	2.2022		0.09105	30.6463
	0.01775	2.3857		0.10269	34.133
	0.01624	1.8351		0.08879	27.7101
	0.01556	2.0187		0.08687	27.8936

Continue from previous page

	0.02111	2.9362		0.09365	32.1143
RB00_WL0567_H08_T154_2	0.08365	25.6915	RB00_WL0567_H065_T154_1	0.05303	12.4787
	0.09413	35.234		0.05734	18.1676
	0.08502	28.9947		0.05988	15.7819
	0.08988	29.9122		0.06091	14.8644
	0.09112	30.8298		0.05906	16.516
	0.08906	31.9308		0.05995	17.25
	0.10221	30.6463		0.06358	16.1489
	0.08838	29.3617		0.06008	15.9654
	0.09961	33.7659		0.0631	17.25
	0.09886	31.0133		0.06207	17.8005
	0.08865	27.1596		0.05481	15.4149
	0.08981	24.5904		0.05508	14.8644
	0.09434	36.1516		0.06193	18.7181
RB00_WL0567_H065_T154_2	0.05632	13.2128	RB00_WL0567_H05_T154_1	0.02775	4.0373
	0.0581	18.3511		0.02953	6.0559
	0.05906	14.8644		0.02755	5.1383
	0.06008	14.6809		0.02768	4.9548
	0.062	16.516		0.02905	5.1383
	0.05618	17.25		0.03029	5.5053
	0.05885	16.6995		0.03022	5.1383
	0.0581	16.516		0.02974	5.1383
	0.06015	17.617		0.03159	5.5053
	0.06084	18.3511		0.03241	5.8724
	0.0557	16.3325		0.02953	4.7713
	0.05645	15.0479		0.02953	5.3218
	0.0644	19.2686		0.03645	6.6064
RB00_WL0567_H05_T154_2	0.02659	4.2208	RB00_WL055_H08_T154_1	0.06556	18.5345
	0.02919	6.0559		0.07372	21.8377
	0.02741	5.1383		0.07858	21.2871
	0.02892	4.9548		0.08029	21.2871
	0.02871	5.3218		0.07625	24.4068
	0.03029	5.6889		0.07605	23.1222
	0.02816	5.3218		0.07851	23.1222
	0.02988	5.1383		0.07769	22.2047
	0.03022	5.6889		0.0794	24.7738
	0.03097	5.6889		0.0831	23.3058
	0.02803	4.7713		0.07933	21.8377
	0.02857	5.1383		0.0792	21.4707
	0.03631	6.6064		0.08207	24.5903
RB00_WL055_H08_T154_2	0.0718	19.2686	RB00_WL055_H065_T154_1	0.03864	8.4415
	0.07262	22.5718		0.04269	10.4601
	0.07844	21.6543		0.04207	9.3591
	0.08427	20.1862		0.04289	9.3591

Continue from previous page

	0.07728	23.1223		0.04207	9.7261
	0.08057	22.9388		0.0433	10.8271
	0.08207	22.2048		0.0431	10.2766
	0.07591	22.5718		0.04385	9.9096
	0.08523	22.2048		0.04467	10.8271
	0.08276	26.7925		0.0444	10.8271
	0.07687	21.8378		0.04227	9.3591
	0.08372	22.7553		0.04241	10.6436
	0.08344	24.2234		0.0483	11.9282
RB00_WL055_H065_T154_2	0.03899	8.2579	RB00_WL055_H05_T154_1	0.01248	1.2846
	0.04241	10.46		0.01083	2.0187
	0.04118	8.992		0.00953	1.4681
	0.04289	9.359		0.00974	1.4681
	0.04159	9.359		0.00885	1.4681
	0.04275	10.6435		0.01111	1.8351
	0.04412	10.2765		0.01111	1.4681
	0.04433	9.9095		0.01035	1.4681
	0.04522	11.1941		0.01001	1.6516
	0.04433	11.0106		0.01131	1.4681
	0.04042	9.1755		0.00891	1.1011
	0.04316	10.8271		0.01049	1.6516
	0.04447	11.5611		0.01515	1.8351

Table A.7 Individual event of a wave train for the dike side case, T=1.8s

Test code	h1	Fmax	Test code	h1	Fmax
RB00_WL0567_H08_T180_1	0.12133	40.189	RB00_WL0567_H08_T180_3	0.10947	36.702
	0.11098	33.949		0.10112	34.5
	0.10852	37.987		0.10434	36.152
	0.11132	38.721		0.10591	39.088
	0.11174	38.721		0.11468	37.62
	0.12044	40.923		0.11941	47.529
	0.12044	43.125		0.11653	45.694
	0.11742	44.593		0.12037	47.346
	0.13694	44.41		0.12694	42.942
	0.1103	35.234		0.10434	36.519
RB00_WL0567_H08_T180_2	0.1018	38.537	RB00_WL0567_H08_T180_4	0.10927	38.721
	0.10235	35.234		0.10304	34.867
	0.1092	37.62		0.1029	40.189
	0.10776	36.702		0.1116	38.721
	0.11845	38.17		0.11393	38.721
	0.11722	41.106		0.11358	41.657
	0.11776	42.942		0.12413	42.391
	0.1216	44.226		0.12249	43.675
	0.13722	41.29		0.12961	44.043
	0.10776	35.234		0.10995	34.684
RB00_WL0567_H065_T180_1	0.0768	22.5718	RB00_WL0567_H065_T180_3	0.07762	22.9388
	0.08077	20.9202		0.07735	20.7367
	0.07769	21.2872		0.08194	22.2048
	0.08523	22.9388		0.08351	23.1223
	0.08022	24.5904		0.08173	23.8564
	0.0805	26.609		0.08516	25.3245
	0.08262	26.7925		0.08392	26.609
	0.09029	28.8112		0.08324	28.6276
	0.09235	28.0771		0.08975	28.4441
	0.07885	21.6543		0.07831	22.0213
RB00_WL0567_H065_T180_2	0.0781	22.2048	RB00_WL0567_H065_T180_4	0.07748	21.6543
	0.07392	20.7367		0.07913	20.7367
	0.07906	21.8378		0.08454	22.0213
	0.08488	23.1223		0.07865	23.6729
	0.08146	24.2234		0.08303	23.3058
	0.08036	25.3245		0.08173	24.9574
	0.08111	27.1596		0.08303	26.0585
	0.08523	28.9947		0.0829	28.8112
	0.09098	27.3431		0.09331	27.1596
	0.07714	21.6543		0.08221	21.4707
RB00_WL0567_H05_T180_1	0.04269	8.992	RB00_WL0567_H05_T180_3	0.04262	9.1756
	0.04084	8.258		0.04234	8.4415

Continue from previous page

	0.04186	9.1756		0.04166	8.992
	0.0433	9.9096		0.04316	9.3591
	0.04392	9.9096		0.04275	9.7261
	0.04426	10.4601		0.04358	10.6436
	0.04351	10.4601		0.0444	10.4601
	0.04632	11.3777		0.04577	11.3777
	0.05186	12.1117		0.04775	11.7447
RB00_WL0567_H05_T180_2	0.04173	9.1756		0.04138	8.4415
	0.04289	9.1756	RB00_WL0567_H05_T180_4	0.042	9.5426
	0.04207	8.4415		0.04221	8.625
	0.04138	9.1756		0.04227	9.3591
	0.04316	9.3591		0.04358	10.2766
	0.04351	9.7261		0.04248	10.0931
	0.04351	10.6436		0.04474	10.6436
	0.0431	10.6436		0.0433	10.8271
	0.04536	11.1942		0.04577	11.3777
	0.04782	11.3777		0.05029	11.9282
	0.04132	8.4415		0.04179	8.4415

Appendix 2 Irregular wave test analysis

Due to time and test facilities constraint, irregular wave test was just executed several times. As mentioned in Chapter 3&4, there is no Active Reflection Compensation (ARC) system on the wave paddle, if a test lasting long time, water in the flume might be reflected.

For one regular test, it lasts for about half an hour, the incident wave will be influenced by the re-reflection wave from the wave paddle. The best way to analysis irregular wave is using the same data window (45~65 s) such as the regular waves (refer to Section 4.2), this means that only about 15 waves will be analyzed, and this few number waves might cause only 1~2 overtopping events on the dike crest for inland case. The sample capacity is too limited to analysis, therefore,

However, for zone 5 (see Figure 5.9), the overtopping wave load is just directly influenced by the highest surface elevation in front of the building, so in this section, firstly, the comparison results of measured overtopping wave load and calculated load using Equation 5.7 (C_1 equals 0.33) for inland case was given, then gives a estimation method for irregular waves using the Equations obtained in Section 4.1, here omit the influence of re-reflection waves from the wave paddle.

A2.1   Comparison regular tests result and irregular test

An important thing should be noted that, for irregular test in the present study, due to there is no Active Reflection Compensation (ARC) system on the wave paddle, one test lasts for about half an hour, the incident wave will be influenced by the re-reflection wave from the wave paddle, if using the same time window (45~65 s) such as the regular wave rest for irregular wave, this means that only nearly 20 waves will be analyzed and this few number waves will lose the statistical significance for irregular waves, and for inland case, only 1~2 overtopping waves in 20 waves during the time window would reach the building. However, for zone 5 (see Figure 5.9), the overtopping wave load is just directly influenced by the highest surface elevation in front of the building, so in this section, firstly, the comparison results of measured overtopping wave load and calculated load using Equation 5.7 (C_1 equals 0.33) for inland case was given, then gives a estimation method for irregular waves using the Equations obtained in Section 4.1, here omit the influence of re-reflection waves from the wave paddle.

Figure A.1 shows the raw time series plots for irregular test. Blue line is the time series obtained from the force gauge directly, while the red lines obtained from wave probe 2 which is fixed on the face of building using Equation 5.7 with C1 equaling 0.33. It appears that there is a good correlation between the measured and calculated load, though some peaks show that the Equation 5.7 under estimate the real load. There are some reasons which can be explained these peaks differences.

- The threshold value was not subtracted from the raw force data which cause measured force larger.
- The variation of force signals
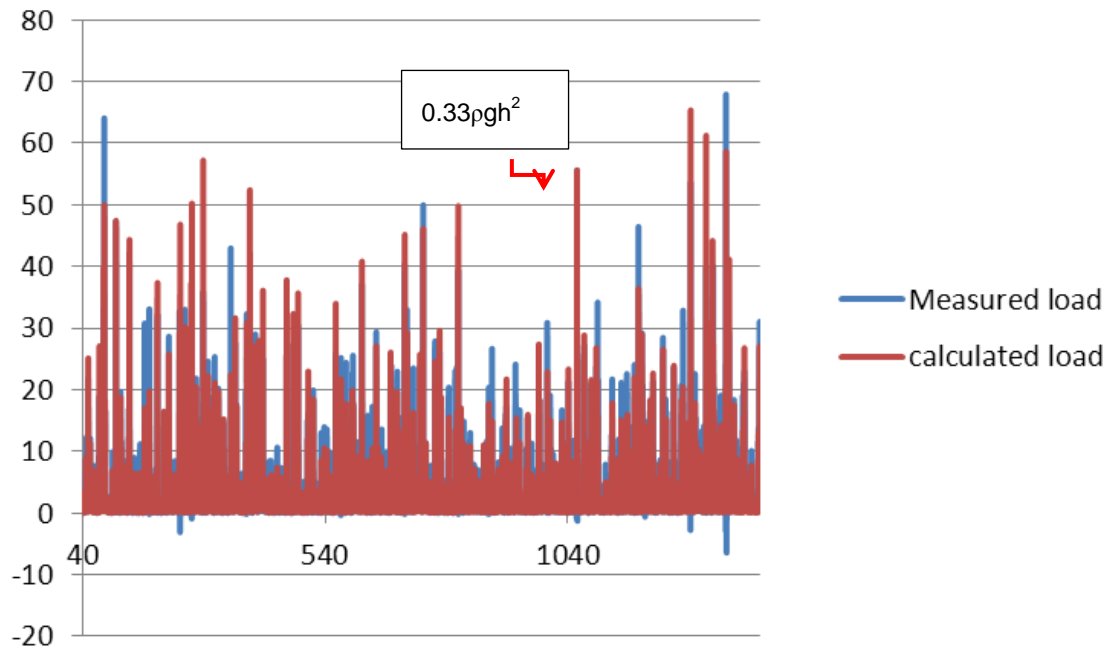
Figure A.1   Comparison of measured and calculated load time series for inland case

A2.2   Proposed application method for irregular wave

In irregular wave test, more than 1100 waves were generated, for dike side case, the number of overtopping wave events equals that of the incident waves, while for the inland case, due to the effect of wide crest, nearly 90% overtopping waves were reduced and only 10% remained (or 110 overtopping waves reach the building). Therefore, the number of overtopping wave events and two peaks of overtopping wave force (220 peaks totally) should be considered for irregular wave tests. This is the main difference of analysis method between regular and irregular tests.

In order to apply the regular test results into the irregular test, the number of overtopping waves and force should be the same. Therefore, for inland case with crest width=0.5m, Equation 5.11 can be rewritten as Equation 01, while for dike side case with crest width=0m, Equation 5.12 can be rewritten as Equation 02, where the subscript x% of incident wave height and maximum run-up means the exceedance level based on the total incident waves, while 5x% and 0.5x% mean the exceedance level based on the total number of overtopping wave force during one test.   .

$$F_{5x\%\,inland} = 0.51\rho g (H_{x\%})^2 (1 - \frac{R_c}{R_{ux\%}})^2 \qquad \textbf{0.1}$$

$$F_{0.5x\%\,dikeside} = 1.48\rho g (H_{x\%})^2 (1 - \frac{R_c}{R_{ux\%}})^2 \qquad \textbf{0.2}$$

For irregular wave, wave run-up height is given as 2% exceedence level, $R_{u2\%}$ by EurOtop Manual, and see Equation 03. Therefore, Equation 01 and Equation 02 can be rewritten as Equation 04 and Equation 05.

$$R_{u2\%} = H_{m0}(4 - \frac{1.5}{\sqrt{\xi_0}}) \qquad \textbf{0.3}$$

$$F_{10\%\,inland} = 0.51\rho g (H_{2\%})^2 (1 - \frac{R_c}{R_{u2\%}})^2 \qquad \textbf{0.4}$$

$$F_{1\% \, dikeside} = 1.48 \rho g (H_{2\%})^2 (1 - \frac{R_c}{R_{u2\%}})^2 \qquad \textbf{0.5}$$

The calculation report for irregular tests can be found in Appendix.5.Figure A2 shows the comparison results between the measured average overtopping wave force with a 2% exceedance during 1100 waves and the calculated results by Equation 05 for dike side case. It appears that it can give a good estimation. Due to the time limit, irregular tests for inland case (with crest width =0.5m) were just run with four conditions, with the same wave height, wave periods but four different freeboard.

The calculated value for these four tests were just using the calculated value of dike side case with the same test condition and divided the ratio between Equation 05 and Equation 04. Then compare these values with the measured force value. The results are shown in Figure A2 with the Red Cross. There is a scatter within the red crosses; this scatter with a circle is the data point which only has 113 overtopping wave events occur in front of the wall, so 10% exceedance level for the overtopping force is not suitable for this case anymore. If using 20% exceedance level for this case, the Red Cross will be on the straight line. The similar reason can be explained for the scatters in dike side case.

Overall, though there is very limit test data for irregular test for both the cases and there is no Active Reflection Compensation (ARC) system in the flume, the results of irregular wave test can be applied into the regular wave test results very well. The method of using different exceedance level for different parameters is suitable for analysis irregular wave conditions for this study.
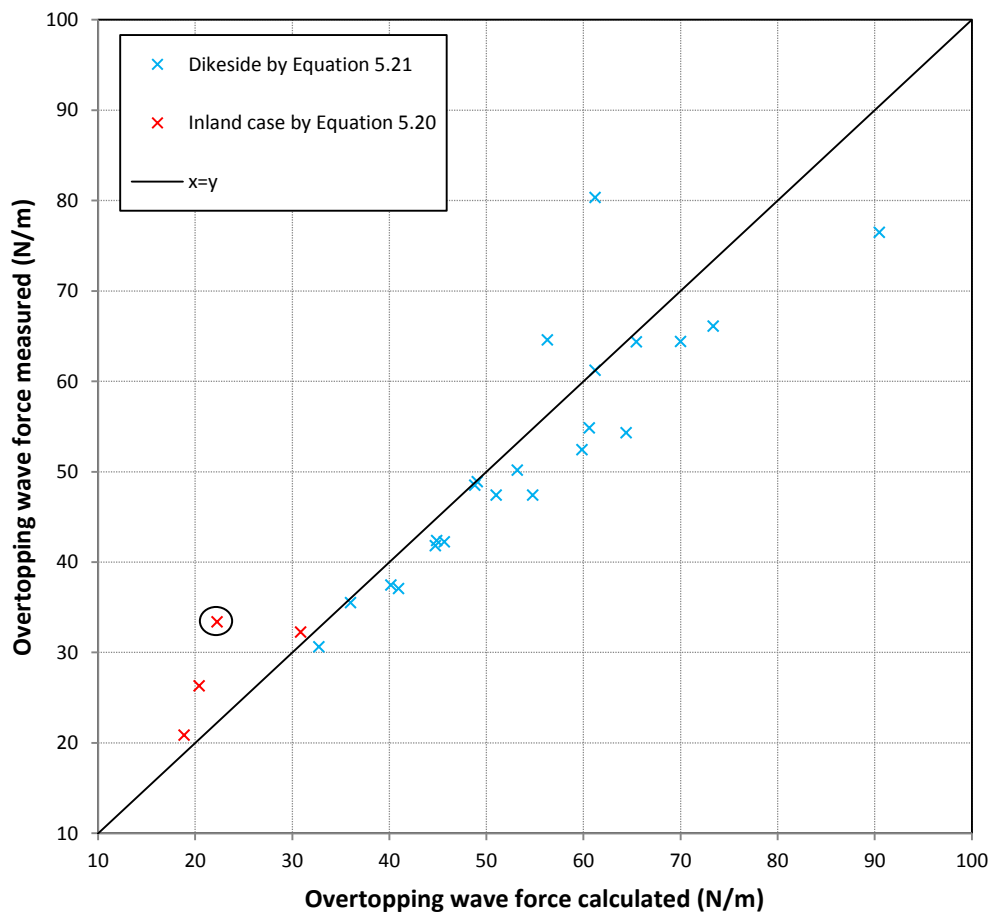
Figure A.2   Measured versus predicted overtopping wave force by Equation 5.11 and Equation 5.12

A2.3   Application into other experiment data

Equation 05 is has a good validity for irregular wave condition tested in present study. In this section, the extension of findings has applied into the irregular test results in this study. The configuration of dike side case with 0 m wide crest is more like the breakwater with high crown wall. Jensen (1984) as mentioned also in Martin and Losada (1999) show a full distribution of forces which makes a comparison possible to present study. Figure A.4 shows the calculation results using Equation 05.

Though it is checked with the data of *Jensen (1984)* and shows a relative good validity for breakwater with smaller wave height with 8 m, it overestimates the horizontal wave force under the significant wave height with 14m. The reason of overestimation in details maybe roughness of the structure is not considered in Equation 05 or the type of wave height distribution is not the same with *Jensen (1984).*

In the future, this study can be focus on irregular tests with AWAS in the flume, and the relationship of the overtopping wave events and the exceedance level can be explored more in detail.
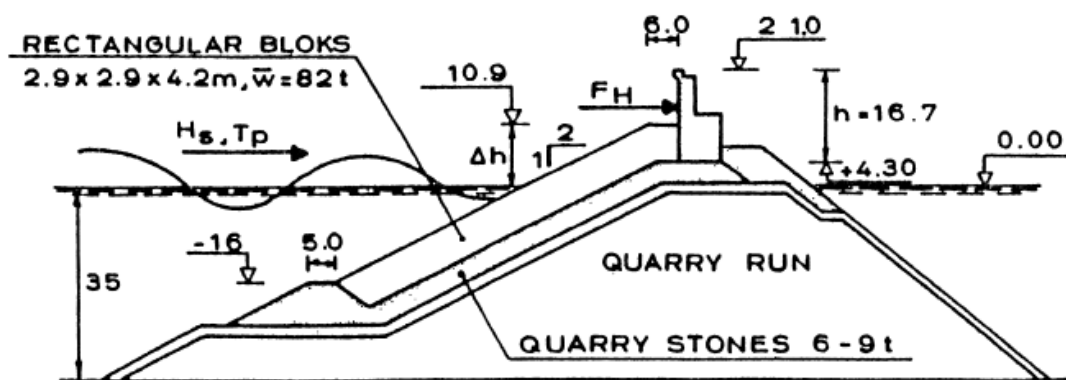
Fig. 16. Cross-section of breakwater tested by Jensen (1984).

Figure A.3   Cross section of breakwater tested by Jensen (1984) as mentioned in Martin and Losada (1999)
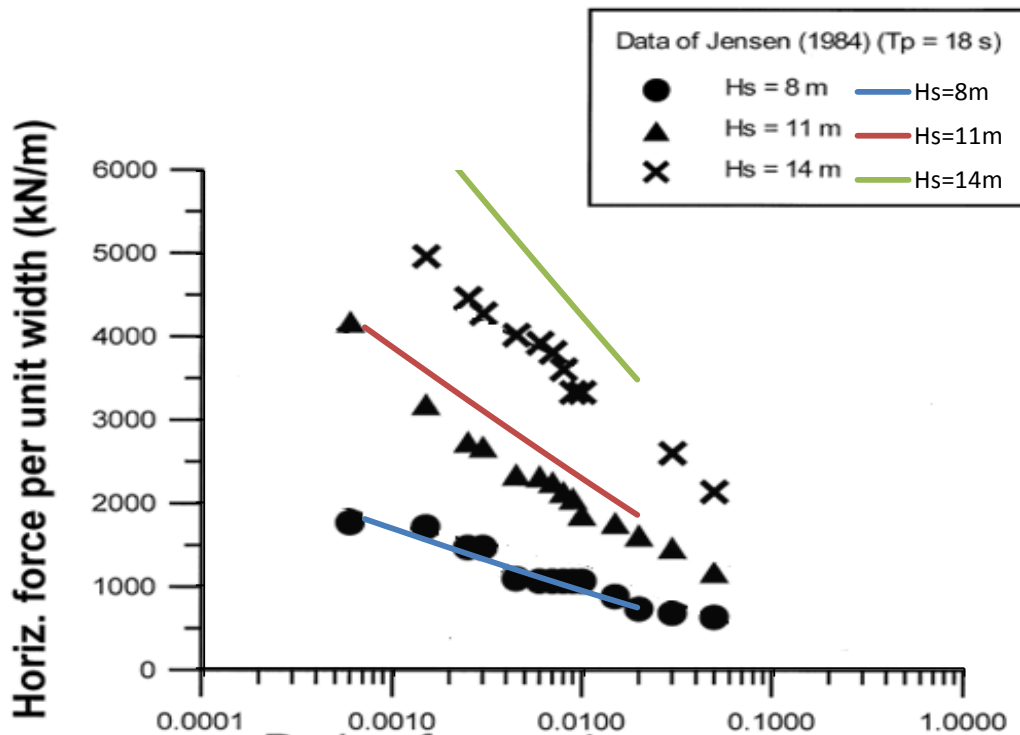
Figure A.4   Compared Estimated force with Jensen (1984) tested data.

Appendix 3 Force data and Pressure data

In the section, the force data tested by load cell are compared with that tested by pressure sensors using rectangular integral method. Figure A.5 shows the sketch of pressure integrated method. Then Figure A.6 gives the comparison between these two force result obtained by two instruments.

It appears that the peak value obtained by pressure sensors is bigger than load cell. The reason is that the spacing between each tow pressure sensors is 6 cm which leads the real pressure distribution information lost. So the real pressure distribution is unlike the one showed in Figure A.5. Another reason is that the variations of the pressure signal is so much that even there is no wave pressure, when integrated the pressure data, the final integrated force should be overestimated.

Therefore, in the present study, all the force data are using the ones obtained by load cell.
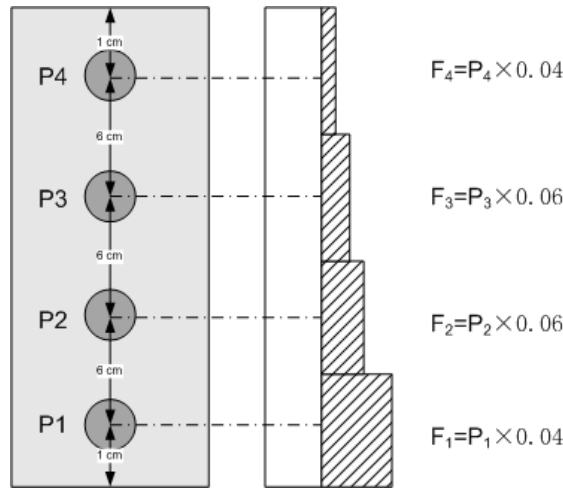
Figure A.5   Sketch of rectangular integrated method for force by using pressure data
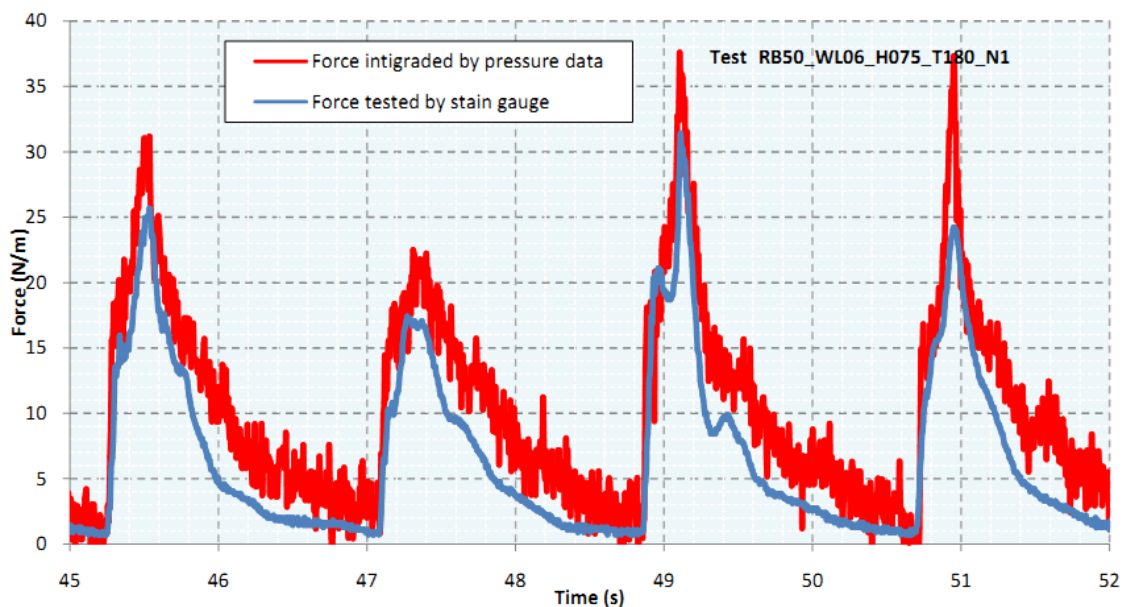
Figure A.6   Time series of integrated force by pressure data and force test by load cell.

Appendix 4 Test instruments

Load cell

Model 1042   **Single Point Load Cells**   ENHANCED

Features

- Capacities: 1 - 100 kg (2.20 - 220.46 lbs)
- Anodized aluminum construction
- 6 wire (sense) circuit
- Single point 400 x 400 mm platform
- IP66 protection
- NTEP approved 5000 divisions
- OIML approved 6000 divisions

Model 1042 is a low profile, two -beam single point load cell designed for direct mounting of low cost weighing platforms, ideally suited for retail, bench and counting scales.

Available in anodized aluminum, this high-accuracy load cell is approved to NTEP 5000 divisions and other stringent approval standards, including OIML R60 C4 and OIML R60 C3, 30% utilization.

A special humidity - resistant, IP66, protective coating assures long term stability over the entire compensated temperature range. Interchangeable, replacement to industry standard models 1040, 1041, 1140 (stainless).

Tedea-Huntleigh, with models ranging from 1 to 50,000 kg capacities, is the world's largest manufacturer of precision load cells.

The two additional sense wires feed back the excitation voltage reaching the load cell. Complete compensation of changes in lead resistance due to temperature changes and/or cable length changes, is achieved by feeding this voltage into the appropriate electronics.

Also Available from Tedea-Huntleigh
Also in this range, a stainless steel, bolt hole compatible version designated model 1140 and 1142 are available for applications unsuitable for load cells of aluminum construction.

For further details please contact the factory or your local distributor.

TEDEA th,
HUNTLEIGH
EXCELLENCE IN LOAD CELLS

Contact Info
E-mail
sales@tedea-huntleigh.com
Website
www.tedea-huntleigh.com

Europe	International	China	Germany	France	
Tedea-Huntleigh Europe Ltd.	Tedea-Huntleigh International Ltd.	Beijing Tedea-Huntleigh No. 16 Hong Da Bei Lu	Tedea-Huntleigh GmbH.	SEEA sa	20630 PLUMMER ST CHATSWORTH CA 91311 USA
37 Portmanmoor Road Cardiff	5 Hozoran St. New Industrial Zone	Da Xing County, Beijing Economic & Technology Develop-	Mumlingweg 18 D-64297	16 Rue Francis Vovelle 28000 Chartres	
CF24 5HE United Kingdom	P.O. Box 8381, Netanya 42506 Israel	ment Area, Beijing 100176	Darmstadt-Eberstadt Germany	France	TEL: 800.626-2616 FAX: 818.701.2799
Tel:+44(0)29-20460231 Fax:+44(0)29-20462173	Tel: +972-9-863-8888 Fax: +972-9-863-8800	Tel:+86-10-67881604-09 Fax:+86-10-67881576	Tel:+49-6151-94460 Fax:+49-6151-944640	Tel: +33-237-33-3120 Fax:+33-237-3129	

Model 1042

Single Point Load Cells

Parameters	Z	M	E	F	G	G5	G3	I*	I5**	Units
OIML ACCURACY CLASS			C1	C2	C3	C3 / 50	C3 / 30			
NTEP ACCURACY CLASS/NMAX			III / 1500	III / 2000	III / 3000				III / 5000	
Rated Capacity (R.C.)		1, 3, 5, 7, 10, 15, 20, 30, 50, 75, 100								kg
Rated Output (R.O.)				2						mV/V
Rated Output Tolerance				0.2						±mV/V
Zero Balance				0.2						±mV/V
Total Error Per OIML R60	0.075	0.05	0.03	0.02	0.02	0.02	0.02			± % of R.O.
Total Error Per NIST Handbook 44			0.03	0.02	0.02				0.02	± % of R.O.
Creep and Zero Return (30 min.)	0.07	0.07	0.05	0.025	0.017	0.017	0.017		0.033	± % of load
Temperature Effect: On Output	0.07	0.005	0.003	0.0014	0.001	0.001	0.001		0.001	± % of load / °C
Temperature Effect: On Zero	0.025	0.025	0.01	0.006	0.004	0.0023	0.0014	0.0023	0.0014	± % of R.O. / °C
Temperature Range: Safe				-30 to +70						°C
Temperature Range: Compensated				-10 to +40						°C
NTEP V min.					RC/3500			RC/6000	RC/10000	kg
Eccentric Loading Error	0.015	0.015	0.0074	0.0074	0.0049	0.0049	0.0049		0.0049	± % of load / cm
Maximum Recommended Platform Size				40 x 40						cm
Maximum Safe Static Overload (central loading)				150						% of R.C.
Ultimate Static Overload (central loading)				300						% of R.C.
Deflection				< 0.4						mm
Excitation: Recommended				10						Volts AC or DC
Excitation: Maximum				15						Volts AC or DC
Input Impedance				415 ± 15						Ohms
Output Impedance				350 ± 3						Ohms
Insulation Resistance				> 2000						MegaOhms
Weight (nominal)				0.30						kg
Cable Type				6 conductors, 26 AWG, shielded, PVC jacket, 1 meter						
Cable Code				+exc - green, +sig - red, +sen - blue -exc - black, -sig - white, -sen - brown						
Construction				anodized aluminum, except 1 and 3 kg capacities						
Circuit Type				Unbalanced						
Environmental Protection				IP 66						
Approvals				NTEP (5000 divisions) and OIML (4000 divisions)						

NOTES : Balanced span temperature compensation optional. * 85% Utilization standard, other utilization available on request . ** 50% Utilization standard, other utilization available on request

Wiring Schematic Diagram
Unbalanced Bridge Configuration
(Balanced option available)

+Input (Green)
+Sense (Blue)
+Output (Red)
-Input (Black)
-Sense (Brown)
-Output (White)
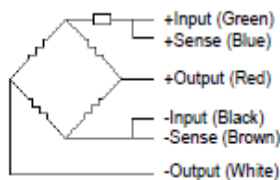
The two "sense" wires sample the bridge supply voltage at the load cell. Complete compensation of change in the lead wire resistance, due to temperature change and/or cable extension, is achieved by feeding this voltage into appropriate electronics.

Mounting
4 Mounting holes
M6

Outline Dimensions All Capacities (in inches)

Capacities kg	A
1-30	.787
50-100	.992

Pressure sensors

Druck
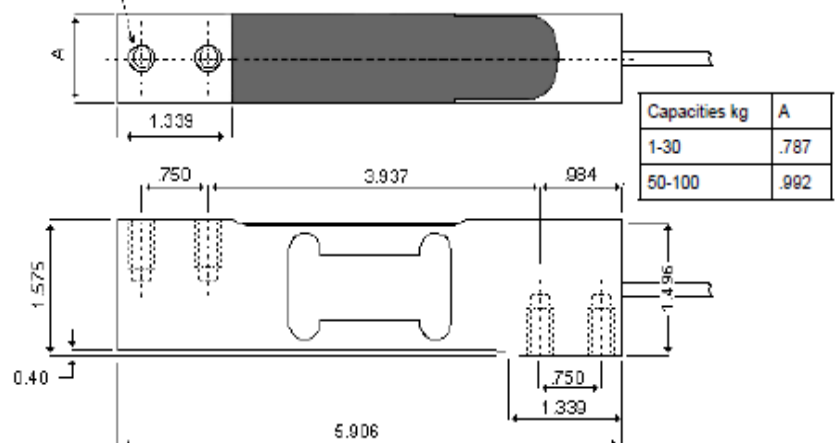
MINIATURE SERIES

High Performance Pressure Transducers

· High technology, micro machined silicon sensor
· Excellent linearity and hysteresis
· High overload capability
· Fast response
· Pore water
· Scanivalve operation
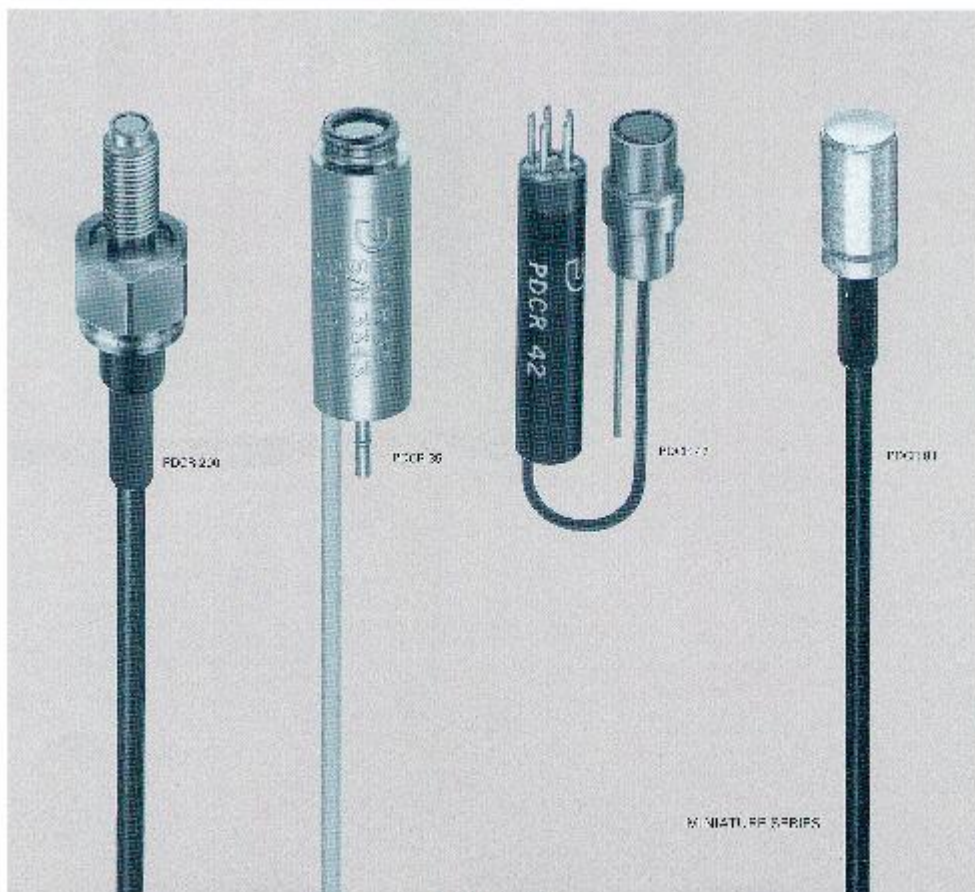
Miniature Series - 06/99

1

MINIATURE SERIES: High Performance Transducers

INTRODUCTION

Druck's experience with silicon diaphragm micro machining technology is considerable.

For more than 15 years a commitment to continuous research and development in this field using the very latest techniques and equipment has culminated in some remarkable achievements in pressure transducer design and performance.

The miniature series is a typical example of the benefits of such work. A range of high accuracy sensors complete with thermal compensation in a miniature package providing maximum performance with minimal size and weight.

The silicon diaphragm is intricately micro machined, and semi-conductor strain gauges are diffused into the substrate to become an atomic part of the diaphragm. Each gauge is connected to form a wheatstone bridge configuration, which is subsequently terminated to offset and thermal compensation circuitry.

High signal outputs, excellent linearity, negligible hysteresis and good repeatability performance with considerable improvements in long term stability are the benefits of using Druck miniature pressure transducers.

Your Specific Requirements

In addition to the sensors show, Druck have the engineering capability to design pressure transducers to specific individual requirements. By careful consideration of the configuration, environments, compatibility and other important performance characteristics, our engineering team can design, build and exhaustively test instruments for your needs.

Please contact our Sales Office for further information.

GENERAL PURPOSE		SCANIVALVE	PORE WATER
PDCR 200	PDCR 35	PDCR 42	PDCR 81

Scale: 2:1
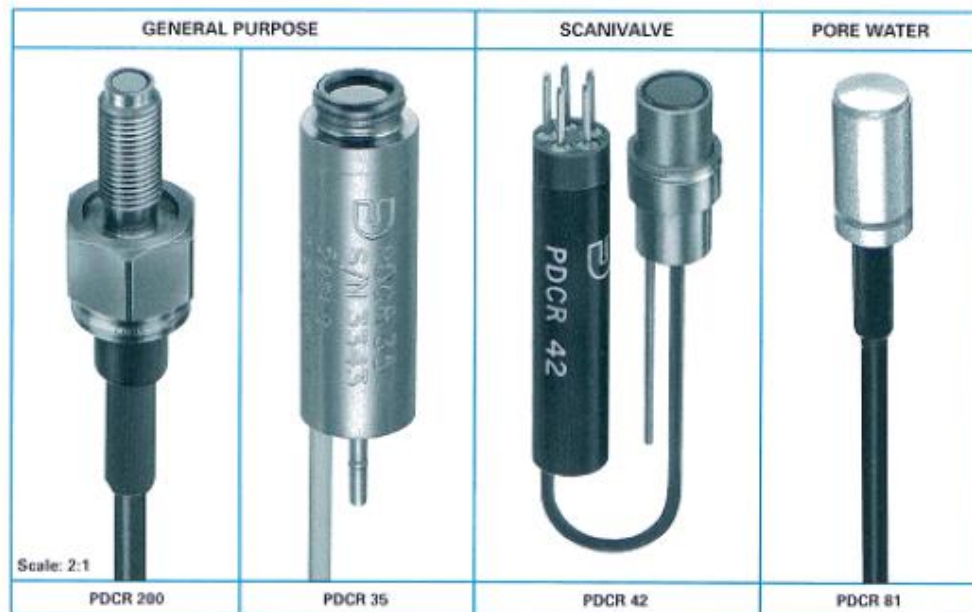
PDCR 200 Pressure units and range identification

Significant figures
Black - 0
Brown - 1
Red - 2
Orange - 3
Yellow - 4
Green - 5
Blue - 6
Violet - 7
Grey - 8
White - 9

Multiplier
Silver - x 0.01
Gold - x 0.1
Black - x 1
Brown - x 10
Red - x 100
Orange - x 1000
Yellow - x 10000

Engineering Unit
White - psi
Red - bar
Blue - insH2O
Black - kPa

Example:
● ● ● ● x 100 psi
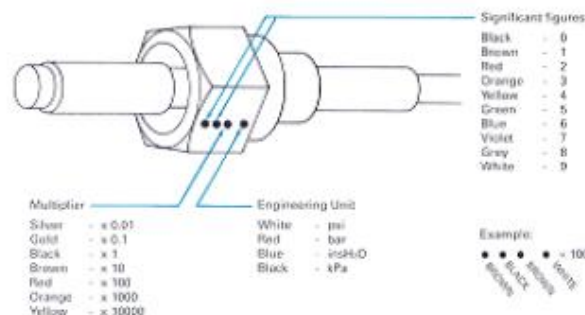
INTRODUCTION

Please state the following:-
(1) Type number
(2) Pressure range
(3) Gauge or differential
(4) Temperature range
(5) Pressure connection
(6) Pressure media

For non-standard requirements please specify in detail.

Continuing development sometimes necessitates specification changes without notice.

2

MINIATURE SERIES: Specification

TYPE	GENERAL PURPOSE		SCANIVALVE	PORE WATER
	PDCR 200	**PDCR 35**	**PDCR 42**	**PDCR 81**
FEATURES	FLUSH MOUNTING CHOICE OF MOUNTING THREADS HIGH OUTPUT	RUGGED CONSTRUCTION	HIGH ACCURACY HIGH OVERLOAD CAPABILITY	CERAMIC FILTER RUGGED CONSTRUCTION LONG TERM SURVIVABILITY
Standard Specification Operating pressure ranges (1)	1, 2, 3, 6, 15, 30 and 60 bar gauge or differential (2)	700 mbar, 1, 1.5, 2, 3.5, 5, 7, 10, 15, 20 and 35 bar gauge (2)	75 mbar, 175 mbar, 350 mbar, 700 mbar, 1, 3, 5, 7, 14, 20 and 35 bar gauge or differential (2)	75 mbar, 350 mbar, 1, 3, 7, 15 and 35 bar gauge
Overpressure (with negligible effect on calibration)	3 x for all ranges (3) (2 x for 1 and 2 bar range on reference side)	4 x for all ranges (3)	10 x for 75 and 175 mbar range (3) 6 x for 350 mbar range 4 x for 700 mbar range and above	20 x for 75 mbar range 10 x for 350 mbar range 5 x for 1 bar range 3 x for 3 bar range and above
Positive pressure media	Fluids compatible with silicon, titanium and epoxy adhesive (and ceramic porous plate for PDCR 81)			
Reference pressure media	Dry, non-conducting gases			
Transduction principle	Integrated silicon strain gauge bridge			
Excitation voltage	10 Volts 6mA nominal	10 Volts 5mA nominal	12 Volts 8mA nominal	5 Volts 6mA nominal (10 volts max.)
Output voltage (nominal) at stated excitation	150 mV for all ranges	100 mV for all ranges	15 mV for 75 mbar range, 25 mV for 175 mbar range, 50 mV for 350 mbar and 700 mbar range, 75 mV for 1 bar range and above	15 mV for 75 mbar range, 35 mV for 350 mbar range, 50 mV for 1 bar range, 75 mV for 3 bar range and above
Zero offset (4)	±15 mV maximum	±5 mV maximum	±3 mV maximum	±10 mV maximum
Span setting	±30% of nominal output	±3 mV maximum (4)		±20% of nominal output
Output impedance (nominal)	1500 ohms	2000 ohms	1000 ohms	
Load impedance	Greater than 100 kohms for quoted performance			
Resolution	Infinite			
Combined non-linearity and hysteresis	±0.3% B.S.L.	±0.1% B.S.L.	±0.06% B.S.L. (5)	±0.2% B.S.L.
Operating temperature range	-20° to +120°C (6)	-20° to +80°C (6)	-40° to +80°C (6)	-20° to +120°C (6)
Temperature effects	±1.5% total error band 10° to 60°C (7)	±1.0% total error band 0° to 50°C (7)	Thermal zero shift ±0.02% F.S./°C 175 mbar range ±0.06% F.S./°C Thermal sensitivity shift ±0.02% of reading/°C 10° to 40°C (7)	Thermal zero shift ±0.06% F.S./°C Thermal sensitivity shift ±0.2% of reading/°C (7) (8)
Natural frequency (mechanical)	75 kHz for 1 bar range increasing to 580 kHz for 60 bar range	56 kHz for 350 mbar range increasing to 360 kHz for 35 bar range		
Acceleration sensitivity	0.002% F.S./g for 1 bar decreasing to 0.0005% F.S./g for 60 bar range	0.003% F.S./g for 350 mbar decreasing to 0.0002% F.S./g for 35 bar range		0.006% F.S./g for 350 mbar decreasing to 0.0003% F.S./g for 35 bar range
Mechanical shock	1000g for 1ms in each of three mutually perpendicular axis will not effect calibration			
Weight (nominal)	12 grams	12 grams	10 grams	30 grams with 5 metres cable
Electrical connection	1 metre shielded integral cable (9)		20 cm integral cable connects transducer and compensation package. Free socket supplied	5 metres integral Teflon vented cable

Key to table above

(1) Other pressure units can be specified, e.g. psi, kPa, etc.
(2) For absolute pressures a vacuum can be pumped on the reference side.
(3) The transducers can be used in a bi-directional differential mode up to ±1 bar.
(4) More accurate settings available.

(5) ±0.04% B.S.L. available.
(6) Temperature range can be extended.
(7) For special applications it is possible to give improved temperature effects over a wider temperature range.

(8) Constant current operation ±0.05% of reading/°C typical.
(9) Longer lengths available.

Miniature Series - 06/99

INSTALLATION DRAWINGS Dimensions: mm

PDCR 200

Mounting Torque
15±5 lbf. ins.

Pressure Connections
10-32 U.N.F.
M5 x 0.5

Thread Length-X
19 (0.750) standard
11 (0.438) optional

O Ring
Ø9.3 inside x 0.8 section
Material: Buna-N

Reference Tube
Ø1 x 13 long

Electrical Connection
4 core shielded cable
Red   Supply positive
Blue   Supply negative
Yellow   Output positive
Green   Output negative
Screen   N/C to transducer body

PDCR 35

Thread
M8 x 0.75

Electrical Connection
4 core shielded cable
Red   Supply positive
Blue   Supply negative
Yellow   Output positive
Green   Output negative
Screen   N/C to transducer body

PDCR 42

Pressure Connection
Fits Scanivalve Ø0.25 ins
cavity or adaptors

Reference Tube
Ø1 x 12.7 long

Compensation package

Miniature Connection
Pin 1   Supply positive
Pin 2   Output positive
Pin 3   Output negative
Pin 4   Supply negative

PDCR 81

Filter
(ceramic)

Teflon tube Ø2.3

Electrical Connection
Red   Supply positive
Blue   Supply negative
Yellow   Output positive
Green   Output negative

Wave gauges

Waterbouwkundig Laboratorium en Hydrologisch Onderzoek
Berchemlei 115 – 2140 Antwerpen

Cel Instrumentatie

Handleiding

GOLF 3-B

W L H   Borgerhout

311_handleiding_golf-3b

1 van 8

Waterbouwkundig Laboratorium en Hydrologisch Onderzoek
Berchemlei 115 – 2140 Antwerpen

Cel Instrumentatie

GOLF-3B

INHOUD

311_handleiding_golf-3b

2 van 8

Waterbouwkundig Laboratorium en Hydrologisch Onderzoek
Berchemlei 115 – 2140 Antwerpen

Cel Instrumentatie

GOLF 3B

1. Doel

Het bouwen van een kleinere golvenmeter voor gebruik op scheepsmodellen en in het sleepkanaal . Deze zal dienen ter vervanging van de bestaande GOLF-3 golvenmeters. Het elektronische gedeelte moet bruikbaar zijn zowel met probes van 1200 mm als met probes van 300 mm en 150 mm .

2. Principe

2.1 Opstelling

In figuur 1 ziet men een samenstelling van een probe voor een golvenmeter.
Een weerstandsdraad is de eerste elektrode. Hij is gespannen tussen twee punten. Een inox-buis dient als tweede elektrode en isoleert de twee draden die aan het uiteinde van de weerstandsdraad zijn aangesloten (onderaan isoleren).
Figuren 2 en 3 geven details van het onderstuk en het bovenstuk weer van een probe van 150 mm.. Figuur 4 geeft de samenstelling weer van een probe van 1200 mm.

Voorwaarden:
- De weerstandsdraad moet corrosievrij zijn en een constante weerstand per lopende meter hebben. Gebruikte draad : AISI316L RVS. d.w.z. 18% Cr ; 12% Ni ; 2% Mo en met een specifieke weerstand van $2\Omega/ft$. Deze kan vervangen worden door RVS met dezelfde afmetingen en specificaties.
- De inwendige weerstand van het voltmetergedeelte moet oneindig groot zijn.
- De samenstelling van het water moet homogeen zijn.
- De verbreidingsweerstand van het water moet constant zijn over de ganse indompeldiepte. Conductiviteit beter dan 0.4-$20*10^{-3}$ mho.

2.2 Principe

Door een homogene weerstandsdraad wordt een constante stroom gestuurd.
De spanningsverdeling langs de draad is dus constant Een tweede elektrode, zijnde de inox-buis, zal nu als loper van een potentiometer fungeren en een spanning in de voltmeter sturen evenredig met de indompeldiepte van de weerstandsdraad.

3.Uitvoering

3.1 Elektronisch schema

In figuur 5 is het schema weergegeven. De op-amp U1A , U1B , en U3 vormen een kanteelspanningsgenerator. Gegevens aangaande U3 , zie bijlage 3.

311_handleiding_golf-3b

3 van 8

Waterbouwkundig Laboratorium en Hydrologisch Onderzoek   Cel Instrumentatie
Berchemlei 115 – 2140 Antwerpen

De symmetrie wordt geregeld door VR1. Het vermogen wordt geleverd door U3 als stroombron voor de weerstandsdraad tussen de punten 2 en 1.

De inox-buis, aangesloten aan het punt 4 van de sonde, levert de kanteelspanning evenredig met de indompeldiepte aan de buffer U1C. U1D versterkt het signaal. (R11 aanpassen in functie van de lengte van de probe)

De op-amp U2C en U2D werken als piekgelijkrichter en filter. Met U2B en met VR2 kan men de nulinstelling regelen. U2A versterkt het signaal nog meer en met VR3 kan men de versterking instellen voor een uitgangsspanning van +/- 5V / 75 mm. indompeldiepte voor probe 150 mm.

(+/-5V / 600 mm voor probe 1200 mm en +/-5V / 150 mm voor probe 300 mm)

U4 is een isolatieversterker die het signaal isoleert van de modellen en van het water waarin de probe staat. Gegevens aangaande U4 , zie bijlage 1.

De geïsoleerde DC - DC-voedingen U5 en U6 verzorgen de voeding van de verschillende op-amps. Gegevens aangaande U5 , U6 , zie bijlage 2.

U4 genereert zijn eigen secundaire voeding .

Als optie kan op de -15V van U6 een weerstand met LED aangesloten worden , dit als "IN werking"-verklikker.

3.2 Gedrukte schakeling

In figuur 6 kan men de PCB zien van de Golf-3B.

Het componenten- en bedradingschema ziet men in figuur 7.

Aan de punten 1, 2, 3 en 4 kan men de meetprobe aansluiten.

"Out +/-" is de uitgangsspanning.

"24 +/-" is de aansluiting van de voeding. (24VDC van het model of van de sleepwagen)

Als optie kan op de -15V van U6 een weestand met LED aangesloten worden, dit als "IN werking"-verklikker, de LED zal oplichten indien de voeding van 24VDC aanwezig is.

Bij gebruik van probe 1200 mm : R11 = 330K en R9 = 22R1
Bij gebruik van probe 300 mm   : R11 = 680K en R9 = 22R1
Bij gebruik van probe 150 mm   : R11 = 1M2 en R9 = 22R1

3.3 Opbouw

De pcb wordt gemonteerd in een spatwaterdichte aluminium doos.
De gegevens aangaande aluminium dozen zijn te vinden in bijlage 4.(RS-nr. 507-056)
Bovenaan komt de aansluitkabel binnen via een wartel, zie figuur 1 en 5.

Aansluitgegevens voor probe 150 mm: plug 5FX &5MX

    OUT +/- 5V .....pin 2 .... wit   2
    OUT gnd ....pin 3 ....bruin   1
     +24VDC ....pin 7 ....rood   5
    GND 24V ....pin 6 ....zwart   4
    afscherming .....doos ....scherm   scherm

Onder aan de aluminiumdoos wordt de probe van 150 mm gemonteerd met een wartel PG9 in metaal. Fig. 1.

Voor de montage van de probe 1200 mm gebruiken wij een aluminiumdoos (RS-nr.507-056).
Aan de zijkant komt de aansluitkabel via een 7-pins Socapex-plug.
De tweede elektrode van deze probe bestaat uit twee aan elkaar gelaste inox-buizen van 8mm.

311_handleiding_golf-3b   4 van 8

Waterbouwkundig Laboratorium en Hydrologisch Onderzoek
Berchemlei 115 – 2140 Antwerpen   Cel Instrumentatie

De weerstandsdraad wordt hier tussen de boutjes onder en boven gespannen en binnen de pvc-blokjes worden de verbindingsdraden aangesloten. Deze moeten opzij uit het bovenste blokje komen. Alle openingen uitgezonderd de zijopening opgieten met epoxiehars.
Met twee inox bouten M6 monteren wij de aluminiumdoos aan de probe en laten de vier aansluitdraden door de boring in de aluminiumdoos komen. Zie figuur 4.
De pcb monteren in de aluminiumdoos op pvc hoogtebussen.

Aansluitgegevens voor probe 1200 mm:

    soc 2 .... out +/- 5V
    soc 3 .... GND out
    soc 6 .... GND 24V
    soc 7 .... +24VDC sleepwagen of model.

4. Afregeling

De pulsvorm van de oscillator symmetrisch regelen:
Sluit een oscilloscoop aan op de uitgang punt 4 van de op-amp U3=L165V
Regel met trimmer VR1 de pulsvorm symmetrisch.

4.1 In water

Zet de probe tot het midden in water, regel met de trimmer VR2 (zie figuur 7, ZERO) de uitgangsspanning op 0 Volt.
Trek de probe 75 mm uit het water (150 mm voor 300 mm-probe, 600 mm voor de 1200 mm-probe) en regel met VR3 (zie figuur 7, GAIN) de uitgangsspanning op -5Volt.
Dompel nu de probe 150 mm in het water (300 mm voor 300 mm-probe, 1200 mm voor de 1200 mm-probe) de uitgangsspanning is nu +5Volt.

4.2 Op het droge

Sluit de weerstandsdraad kort aan de inox-buis op een afstand van 37.5 mm van de onderkant. (75 mm voor 300 mm-probe, 300 mm voor de 1200 mm-probe) en regel met de ZERO-trimmer de uitgang op 0Volt.
Maak nu de kortsluiting 37.5 mm lager (75 mm voor 300 mm-probe, 300 mm voor de 1200 mm-probe) en regel met de GAIN-trimmer de uitgang op -5Volt.
Maak nu de kortsluiting op 75 mm hoogte (150 mm voor 300 mm-probe, 600 mm voor de 1200 mm-probe) en nu moet de uitgang +5Volt zijn.

5. Storingen

Bij het gebruik van lange aansluitdraden en bij het aansluiten aan een AD-ingangskaart is het mogelijk dat oscillaties optreden. Plaats een weerstand van 4R7 in serie met de uitgang en een weerstand van 4K7 parallel aan de ingang van de meetkaart. Zie figuur 5.
Om de opgevangen ruis bij kleine indompeldiepten te onderdrukken, gaat men een weerstand van 10K in serie met de ingang van U1C zetten samen met een $1M\Omega$ naar de GND. (aan ingang 10 van U1C in figuur 5). Ontkoppelen van de $1M\Omega$ met een 2K2 capaciteit geeft het een aanvaardbare oplossing.

311_handleiding_golf-3b   5 van 8

6. Onderhoud

Om de verbreidingsweerstand over de ganse indompeldiepte constant te houden moet men zorgen dat de meetdraad en de meetbuis van de probe overal zuiver zijn.
Kalkafzetting en het aanklitten van oppervlaktestof en van vetten moeten vermeden worden. Daarom zal men iedere week de probes kuisen met een reinigingsmiddel dat de inox-draad en inox-buis niet kan aantasten. Let op dat het isolatieblokje onder aan de probe goed zuiver is, zoniet gaat de lineariteit van de meting verloren.

7. Gebruik op model

Sluit de golvenmeter volgens §3.3 aan op een voeding van 24VDC @ 50mA.
De uitgang (out +/-5V en GND out) verbinden met een voltmeter, schrijver of ander registratieapparaat.
De golvenmeter in het model monteren op ongeveer halve diepte, (volgens lengte van de probe)
Opmerking: De golvenmeters niet in de onmiddellijke omgeving van metalen voorwerpen opstellen.

8. Specificaties

8.1 Probe

Meetbereik : 150mm en 1200mm
Minimum afmetingen :   probe-150mm ; 160 x 15 x 10 (mm)
                       probe-1200mm ; 1275 x 40 x 20 (mm)
Meetdraad : inox-legering AISI 316L draad met weerstand 2Ω/ft. en diameter 0.4mm
Meetstaaf : inox AISI 304-buis gelast met zilversoldeersel
Bevestiging : inox-schroeven AISI 304
Opgietstof : Araldite & Rota Bond 2000 (34454)
Montagestukken : hard PVC - 411 van VINK nv. B-2220 Heist o/d Berg
                       tel : (0032) 15/25.97.11

8.2 Meetcircuit

Uitgangspanning : 150mm-probe ; +/- 5Volt voor +/- 75mm @ 4mA
                  300mm-probe ; +/- 5Volt voor +/- 150mm @ 4mA
                  1200mm-probe ; +/- 5Volt voor +/- 600mm @ 4mA
Voeding   : 24VDC @ 50mA Tol : 10%
Nauwkeurigheid : +/- 1%
Herhaalbaarheid : +/- 1%
Opwarmtijd   : 30 min.
Afmetingen   : probe-150 mm en 300 mm ; 150 x 64 x 34 (mm)
                 : probe-1200 mm ; 175 x 80 x 57 (mm)
Rise time   : 55 ms.

311_handleiding_golf-3b

Waterbouwkundig Laboratorium en Hydrologisch Onderzoek
Berchemlei 115 – 2140 Antwerpen

Cel Instrumentatie

9. IJking in model, in watervat of op het droge

Het is eenvoudiger de probes te laten bewegen in het water in plaats van het water in hoogte te regelen.
Men monteert de GOLF-3 met bijhorende klemmen (voor probe 150mm, klem van Φ18mm.) op een meetnaald met driepoot.

9.1 IJking nat

- Zet de golvenmeter in het water op half de meetdraadlengte.
- Lees op het gebruikte meettoestel de gemeten waterstand af (ongeveer 0V) (Vo).
- Laat de golvenmeter X mm dalen en noteer de gemeten waterstand (Vx).
- Draai de golvenmeter omlaag over Y mm en noteer de gemeten waterstand (Vy).
- (Vx-Vy)/(Y-X) geeft de gevoeligheid in "Volt/mm" weer.

9.2 IJking droog

- Sluit de weerstandsdraad kort naar de inox-buis op een afstand van 40 mm van de onderkant (80 mm voor 300 mm-probe, 305 mm voor de 1200 mm-probe).
- Lees de gemeten waterstand af (V_{40}),(V_{80}),(V_{305}).
- Maak nu een kortsluiting 37,5 mm lager (75 mm voor 300 mm-probe, 300 mm voor de 1200 mm-probe).
- Lees de gemeten waterstand af ($V_{2,5}$),(V_5),(V_5).
- (V_{40} - $V_{2,5}$)/ 150 geeft de gevoeligheid in "Volt/mm" voor 150 mm-probe.
- (V_{80} - V_5)/ 300 geeft de gevoeligheid in "Volt/mm" voor 300 mm-probe.
- (V_{305} - V_5)/1200 geeft de gevoeligheid in "Volt/mm" voor 1200 mm-probe.

Opmerkingen :

Indien de golvenmeter ver van de meet-PC staat (grotere lijncapaciteit dan 270pF) en men een PC30-meetkaart gebruikt, moet men aan de PC in serie met de meetlijn een weerstand van 4R7 plaatsen en daarna afsluiten met een capaciteit van 0.1 à 2 mF.
Daar de PC30-meetkaart voorzien is voor ingangsspanningen tot +/- 5Volt DC, zijn alle golvenmeters geijkt op +/- 5Volt DC volle indompeling.

Op de pcb-golf3 is reeds een weerstand van 4R7 met een belasting van 4K7 aangebracht.
De golvenmeters moeten per meetsonde worden aangepast:

Bij gebruik van probe 1200 mm : R11 = 330K en R9 = 22R1
Bij gebruik van probe 300 mm : R11 = 680K en R9 = 22R1
Bij gebruik van probe 150 mm : R11 = 1M2 en R9 = 22R1

311_handleiding_golf-3b

7 van 8

Waterbouwkundig Laboratorium en Hydrologisch Onderzoek
Berchemlei 115 – 2140 Antwerpen   Cel Instrumentatie

10.Komponentenlijst

Weerstanden

R1 , R2 ....8K2
R3 ....18K
R4 , R5 , R6 , R7 , R10 ....47K
R8 ....39K
R9 ....22.1R
R11 ....probe 1200 ....330K
............probe 300 ....680K
............probe 150 ....1M3
R12 , R14 , R15 , R18 , R27 , R28 ....20K metaal film 1%
R13 ....15K
R16 , R33...10K metaal film 1%
R17 ....6K8
R19 ....2K2
R20 , R21 , R23 , R25 ....22K
R22 ....68K
R26 ....27K
R29 ....1K5 (optie)
R30 ....4R7
R31 ....4K7
R32 ....1M

Capaciteiten

C1 ....82nF   poly met
C2 ....220nF poly met
C3 ....10pF   cer
C4 , C10 ....1µF   poly met
C5 ....100pF polystyreen
C6 , C8 , C9 , C12 ....1µF   tan
C11 ....10µF   tan
C13 ....2.2nF

Trimmers

VR1 .... 10K .. 12 tr verticaal 10mm. 3296W top adjust
VR2 .... 5K .. 12 tr verticaal 10mm. 3296W top adjust
VR3 .... 50K ..12 tr verticaal 10mm. 3296W top adjust

IC'S

U1 , U2 ....LM324 of AD713J Lemaire , Analog devices
U3 ....L165V RS nr. 301-599 data : 232-2677, zie bijlage 3
                                        RS Tel : +32 (0) 2 544 15 62
U4 ....AD203SN   ACAL nv/sa   Lozenberg 4 , B-1932 Zaventem
                                        Tel: +32 (0)2 720 59 83 Gegevens U4 , zie bijlage 1.
U5 ....TET 4821   TME Trade Mark Electronics BVBA
                                        Merksemsteenweg 194, B-2100 Deurne
                                        Tel: +32 (0)3 325 19 10
U6 ....TET 4823   idem . Gegevens aangaande U(, U6 , zie bijlage 2.

Diodes

D1 , D2 ....1N914
D3 ....LRC41

Aluminiumdoos

RS grey painted diecast box IP65 , Nr. 501-840 (150mm) , Nr. 507-056 (1200mm)
Gegevens aangaande aluminiumdozen , zie bijlage 4.
Cable gland 4-6mm , M12 ....RS Nr. 614-025 .

311_handleiding_golf-3b   8 van 8